Investigation of Form Effect on Ballast Mechanical Behavior Based on Discrete Element Modeling

Von der Fakultät Bau- und Umweltingenieurwissenschaften
der Universität Stuttgart zur Erlangung der Würde eines
Doktor-Ingenieurs (Dr.-Ing.) genehmigte Abhandlung

Vorgelegt von

Bo Wang

aus Shihezi, VR China

Hauptberichter:	Prof. Dr.-Ing. Ullrich Martin
Mitberichter:	Prof. Dr.-Ing. Harald Garrecht

Tag der mündlichen Prüfung: 25.10.2018

Institut für Eisenbahn- und Verkehrswesen der Universität Stuttgart

2018

Ehrenwörtliche Erklärung

Hiermit erkläre ich, dass ich diese Arbeit selbständig verfasst und keine anderen als die von mir angegebenen Quellen und Hilfsmittel verwendet habe.

Stuttgart, den 21.06.2018 Bo Wang

Acknowledgement

This dissertation would not be completed without support of many people. First, I sincerely appreciate the help from my supervisor, Prof. Ullrich Martin, for his excellent academic guidance, suggestion, and supervision on my topic through all the years. At the same time, I would like to thank him for the encouragement he gave and his faith in me. They spurred me to overcome the difficulties and helped me through these challenging and meaningful years.

Second, I would like to express my gratitude to my second supervisor, Prof. Harald Garrecht, for offering valuable suggestions on my dissertation. As the leader of Material Testing Institute at University of Stuttgart, he also gave me a precious opportunity to perform the box test, which was the essential calibration tool for the model I proposed. The dissertation would not be finished without this test.

Many thanks to my colleagues at Institute of Railway and Transportation Engineering. Dr. Sebastian Rapp and Mr. David Camacho, the constructive team of our institute, thanks for hearing my problems out and giving valuable opinions. I would also like to thank Dr. Yong Cui, Dr. Xiaojun Li, Dr. Fabian Hantsch and Dr. Jiajian Liang, for their long standing support and friendship. I appreciate all the fun we had together.

Finally, special thanks to my family, for the care and love without hesitation.

Table of contents

List of figures

List of tables

Abstract

As an essential component of the ballast track, the ballast layer provides functionalities such as drainage, load distribution, as well as strength and stability for the railway track. The mechanical behaviors of ballast track such as its permanent settlement, breakage, force propagation and void ratio are in a great extent influenced by the form distribution of ballast stones. Its reasonable design will greatly improve the mechanical behaviors, and thus prolong the maintenance cycle of ballast track, or reduce the number of ballast stones needed for construction.

This dissertation focuses on proposing optimized ballast stones in the ballast aggregate in regard to their geometrical forms. As the first step, a ballast random form generator, which is designed to generate ballast form databases with different form distributions, is proposed. 15 databases are created for further usage. Afterwards, Discrete Element Method (DEM) based simulations are performed to investigate the mechanical behaviors of ballast aggregates. The simulation model is established based on a box test, whose result is presented firstly. Establishment and calibration process of the model are expatiated afterwards. A parameter study regarding to crucial modeling parameters is also performed. Using the validated parameters and the 15 generated form databases, DEM simulation models with different form distributions of ballast stones in the ballast aggregate are proposed. Simulative methods to quantify the mechanical behaviors are elaborated. Based on the obtained results, the interrelation between mechanical behaviors of ballast aggregate and the form effect on mechanical behavior of the ballast aggregates are studied. The optimized ballast aggregate is proposed based on the findings stated above.

The proposed optimized ballast aggregate is expected to be a reference for construction of ballast track in real world. The modeling technic and the calibrated modeling parameters can be used for optimization for different railway operating programs.

Kurzfassung

Als wesentlicher Bestandteil des Schotteroberbaus erfüllt die Schotterschicht wichtige Funktionen wie die Entwässerung, die Lastverteilung und garantiert zudem Festigkeit und Stabilität der Bahnanlage. Das mechanische Verhalten des Schotteroberbaus, wie die Kraftausbreitung, die Porenzahl und -größe sowie das Bruch- und Setzungsverhalten, wird in hohem Maße durch die Formverteilung der Schottersteine beeinflusst. Eine ideale Kornzusammensetzung verbessert das mechanische Verhalten erheblich und ermöglicht so, eine deutliche Verlängerung der Instandhaltungszyklen, oder eine Verringerung der Schottermenge.

Der Schwerpunkt der Dissertation liegt auf der Optimierung der Schottersteine im Schottergefüge hinsichtlich ihrer geometrischen Formen. Es wird zunächst ein Zufallsgenerator zur Generierung von Schottersteinformen vorgestellt, der es ermöglicht, Datenbanken der Schotterformen mit verschiedenen Formverteilungen zu erzeugen. Dabei werden beispielhaft 15 Datenbanken für die weitere Verwendung erstellt. Anschließend werden zur Untersuchung des mechanischen Verhaltens von Schottergefügen mittels der Diskreten-Elemente-Methode (DEM) Simulationen durchgeführt. Das Simulationsmodell wird auf Basis eines Box-Tests erstellt, dessen Ergebnis eingangs dargestellt wird. Weiterhin wird der Aufbau und Kalibrierungsprozess des Modells erläutert sowie eine Parameterstudie bezüglich entscheidender Modellierungsparameter durchgeführt. Unter Verwendung der validierten Parameter und der 15 generierten Formdatenbanken werden anschließend DEM-Simulationsmodelle mit verschiedenen Formverteilungen von Schottersteinen im Schottergefüge vorgeschlagen und simulative Methoden zur Quantifizierung des mechanischen Verhaltens erarbeitet. Basierend auf den gewonnenen Ergebnissen wird der Zusammenhang zwischen dem mechanischen Verhalten des Schottergefüges in Abhängigkeit von der Formverteilung der Schottersteine dargestellt. Die diesbezügliche Optimierung des Schottergefüges hinsichtlich der Schotterform bildet ein Ergebnis der im Zuge der Dissertation entwickelten Methode.

Das optimierte Schottergefüge bildet eine Empfehlung für die Erstellung des Schotteroberbaus in den real existierenden Systemen. Die Modellierungstechnik und die kalibrierten Modellierungsparameter können zudem für eine Optimierung verschiedener Verkehrsbelastungen verwendet werden.

1 Introduction

Railway is often considered as the most economical and convenient one of all kinds of overland transportations. In spite of the growth of other kinds of transports, railway continues to be the backbone of transportation industry in most industrialized countries. Regarding to railway infrastructure, railway tracks can be roughly divided into ballasted tracks and slab tracks, where the ballasted tracks own dominant position of the railway network worldwide due to their low construction cost and easy maintainability [1–3].

The ballasted track is a fundamental part of railway infrastructure. It can be classified as superstructure and substructure, where the superstructure is consisted of rails, rail pads, sleepers (ties) and rail fastening systems (fastenings), while the substructure is a geotechnical layer consisting of ballast, sub-ballast and subgrade (formation and base, see Fig. 1-1). As an essential component of the ballast track, the ballast layer provides functionalities such as drainage, load distribution, as well as strength and stability for the railway track. It is made up of angular shaped granular stones, which have a variety of geometrical, physical and chemical properties such as form, resistance to fragmentation and corrosion [4]. This study focuses on the ballast layer, which is one of the research directions at Institute of Railway and Transportation Engineering (IEV). For research framework at IEV on railway constructive direction please refer to Appendix I.

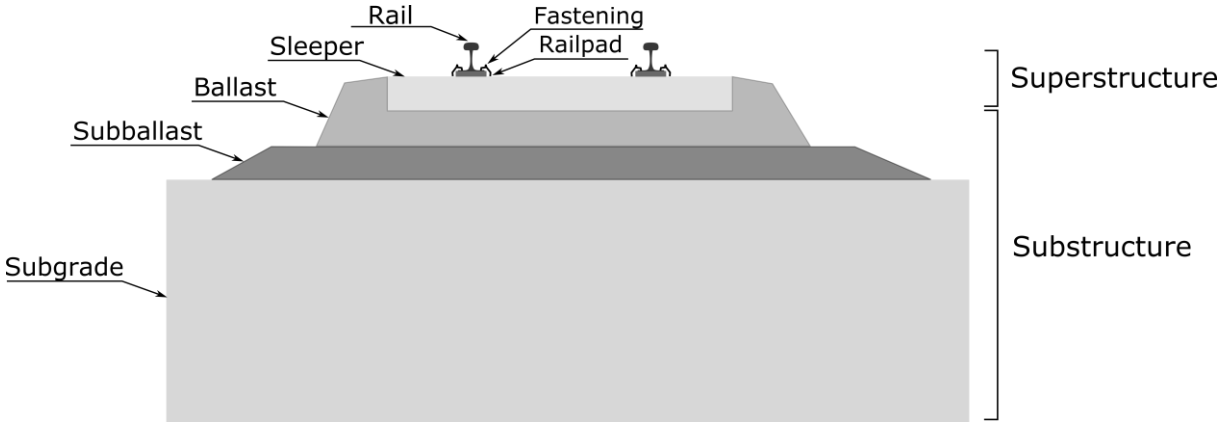

Fig. 1-1: Schematic of a typical railway ballasted track

1.1 Problem statement

The ballasted track has obvious advantages such as low one-off construction cost and easy maintainability. However, comparing to the slab track, the ballasted track

has a shorter maintenance cycle, which causes a much higher maintenance workload and cost. Prolonging the maintenance cycle of ballast track is obviously economically beneficial for its long-term application [5].

Two typical railway defects requiring maintenance are, first, unevenness of rail, which endangers safety of railway operation and enlarges dynamical rail-wheel force; second, mud pumping, which causes a loss of track elasticity. The unevenness of rail is a result of permanent settlement of the ballast layer, while the mud pumping can be aroused by the breakage of ballast stones. These defects of ballasted track are strongly linked to the properties of ballast stones. Therefore, it is essential to design the ballast stones wisely, so that the track defects, which will reduce the maintenance cycle and increase the cost, can be prevented as much as possible.

Among all the ballast stone properties to be determined, the geometrical property, i.e., the form distribution, has the biggest impact on the functionality of ballasted track. The form of a ballast stone includes its size and shape. For a ballast aggregate, the size and shape distributions of the ballasts are obviously influential to its mechanical behavior such as settlement, breakage, force propagation, etc. Using Discrete Element Method (DEM) based simulations, the forms of ballast stones can be depicted and the mechanical behavior can be studied. However, former researches were mainly focusing on only one or two aspects of mechanical behavior. The interrelationship between mechanical behaviors, which is an essential foundation for proposing the geometrically optimized ballast stones and improving the functionality of ballast track, has not been fully studied. Furthermore, in former DEM simulations, the form distributions of ballast stones are acquired from reality. For an optimization study, the realistic distributions are not adequate, because the optimal distribution may not exist in reality. A wide spectrum of form distributions should be investigated.

1.2 Research objective

The final objective of this study is to propose optimized ballast stones in regard to their geometrical forms. These ballasts constitute an aggregate, which will be structurally more stable, and at the same time maintains other merits of ballast track such as hydraulic conductivity. Using these optimized ballast stones, maintenance cycle and cost of ballast tracks can be reduced.

The final objective is broken down to sub-objectives and realized step by step in this study. The sub-objectives to be accomplished are listed as follows:

a. Propose ballast form databases with different form distributions
b. Establish and calibrate DEM simulation model
c. Investigate the effect of ballast form distribution on mechanical behavior of ballast aggregate
d. Investigate the interrelation between mechanical behaviors of ballast aggregate
e. Propose the optimized ballast aggregate in regard to ballast forms

1.3 Research scope

A ballast random form generator is developed and implemented to generate ballast form databases with different form distributions of ballast stones. The generator uses geometrical specifications from European railway standards to, first, generate the databases; second, quantify the geometrical properties of generated ballast forms. Five databases with changing mean sizes, five databases with changing size distributions and five databases with changing shape distributions (15 databases in total) are created for future usage in DEM simulations. The reliability of the generator is checked by comparing the geometrical properties of desired ballast aggregate and generated ballast aggregate.

The DEM based simulation software Particle Flow Code (PFC) is employed to establish the DEM calibration model. Model related parameters are calibrated by a box test, which is performed by Material Testing Institute (MPA) and Institute of Railway and Transportation Engineering (IEV) at University of Stuttgart. Procedure of the test is introduced and results are presented. Establishment and calibration process of the DEM calibration model are expatiated. A parameter study regarding to two crucial modeling parameters is performed.

Using the validated parameters and the 15 generated form databases, DEM simulation models with different form distributions of ballast stones are proposed. Based on the obtained results, the interrelation between mechanical behaviors of ballast aggregate and the form effect on mechanical behavior of the ballast aggregates are studied. The optimized ballast aggregate is proposed based on the findings stated above.

1.4 Thesis outline

In chapter 2, research background and recent studies regarding to topic related aspects, including ballast geometrical specification, methods of capturing forms of ballast stones, discrete element method and modeling, and mechanical properties of ballast aggregate, are proposed. In chapter 3, the ballast random form generator is introduced and its functionalities are explained in detail. The validation of the generator is performed. In chapter 4, procedure and result of the box test, which is used for calibration of the DEM calibration model, are presented. The establishment and the calibration process of the DEM calibration model are expatiated. A parameter study regarding to two crucial modeling parameters is performed. In chapter 5, the influence of size and shape distribution of ballast stones on mechanical behavior of ballast aggregates are investigated respectively. The interrelations of mechanical behaviors are discussed in detail. Ballast aggregate with optimized form distribution is proposed. In chapter 6, major conclusions of this study are summarized. Recommendations for future works are provided.

2 Research background and recent studies of ballast mechanical behavior using Discrete Element Method (DEM) based simulation

In this chapter, research background and recent studies of ballast mechanical behavior using Discrete Element Method (DEM) based simulation are presented. Topics such as ballast geometrical specifications in standards, methods of capturing the forms of ballast stones, DEM and modeling, as well as mechanical properties of ballast aggregate are covered.

2.1 Ballast geometrical specifications in standards

The geometrical property of ballast aggregate can be divided into its size distribution and shape distribution. In this section, standardized testing procedures for capturing the geometrical property of ballast aggregate, which are determined by railway standards [6–10], are briefly introduced. These procedures are used to quantify the ballast forms and their distributions in engineering practices, they are the theoretical foundation of the ballast random form generator expatiated in chapter 3, which is the crucial first step for the DEM simulations performed in this dissertation.

2.1.1 Ballast size

In Europe, the gradation of ballast aggregate is determined by a standardized sieving method, whose testing procedures and requirements are regulated in detail in [8]. The minimal mass of the testing sample M (in kg) is determined by equation (2.1):

$$M = (D/10)^2 \tag{2.1}$$

where D is the maximal size of the particles (in mm) in the sample. The sample will be firstly washed and dried out, then placed on the top of a sieve tower, which is consisted of quadrate-meshed sieves with different meshing sizes. The sieves are arranged with decreasing mesh sizes from top to bottom. The mesh sizes are regulated in [6] and part of them are chosen for determination of ballast aggregate gradation (see Table 2-1). The sample and the sieve tower are shaken afterwards, so that the smaller particles will go through the sieve with bigger mesh size and land on the sieve with smaller one. Afterwards, the particles on the sieve with the biggest mesh size will be weighed, and their total mass will be recorded as R_1. The same procedure will be performed to the rest sieves and the masses on these sieves will be rec-

orded as $R_2, \dots, R_i, \dots, R_n$. The mass of the particles, which go through all the sieves, will be recorded as P. The percentage passing by mass PM_i is:

$$PM_i = 100 - \sum(100 * R_i/M_1) \tag{2.2}$$

where M_1 is the mass of the testing sample after drying.

The tested ballast aggregate is afterwards graded into 5 categories according to [10] (see Table 2-1). The test acquired ballast size distribution line should be in between of the upper and lower boundaries of a certain category (see Fig. 2-1).

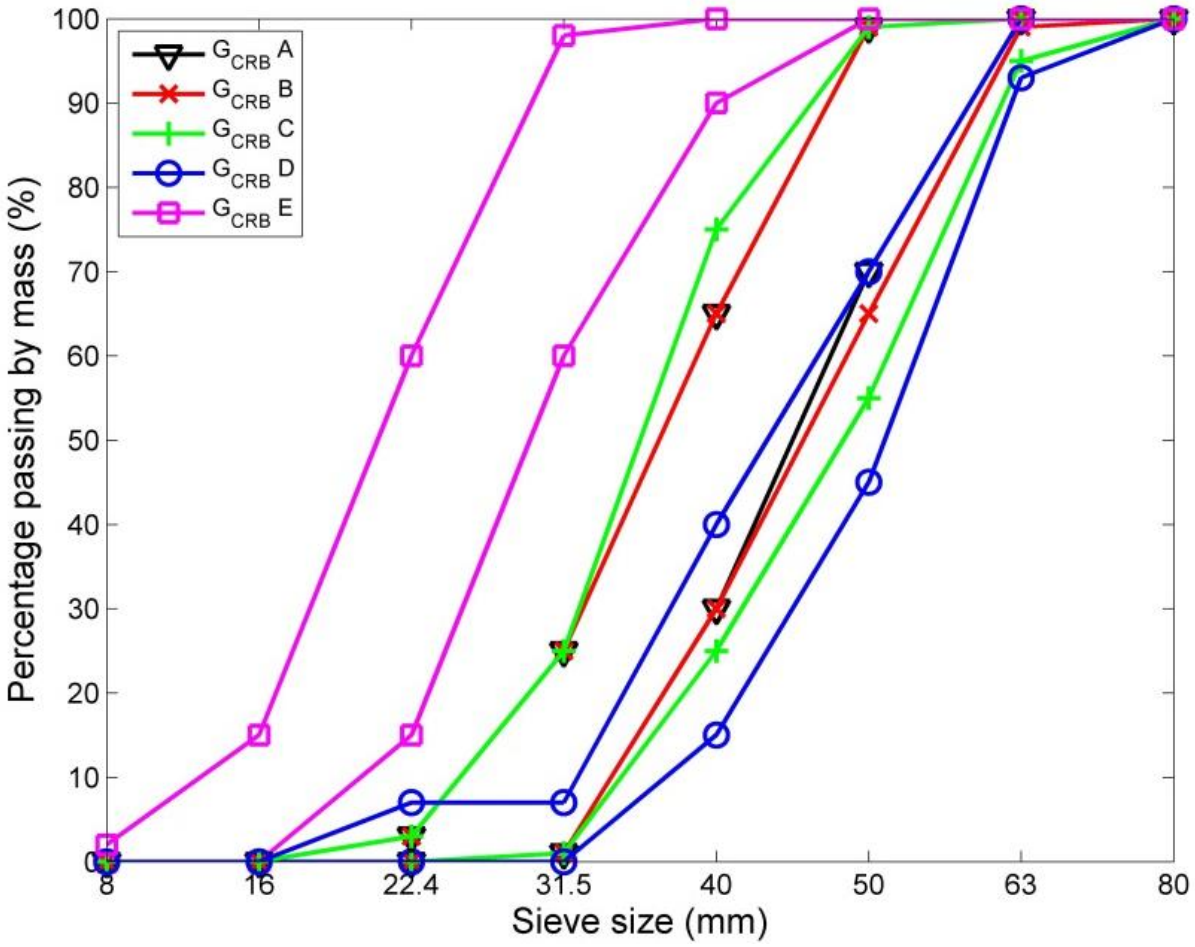

Fig. 2-1: Categories for grading

Table 2-1: Categories for grading [10]

Sieve size in mm	Railway ballast size 31.5 mm to 50 mm	Railway ballast size 31.5 mm to 63 mm		Railway ballast size 22 mm to 40 mm	
	Percentage passing by mass				
	Grading category G_{CRB}				
	$G_{CRB}\ A$	$G_{CRB}\ B$	$G_{CRB}\ C$	$G_{CRB}\ D$	$G_{CRB}\ E$
80	100	100	100	100	-
63	100	95 to 100	95 to 100	93 to 100	-
50	70 to 99	65 to 99	55 to 99	45 to 70	100
40	30 to 65	30 to 65	25 to 75	15 to 40	90 to 100
31.5	1 to 25	1 to 25	1 to 25	0 to 7	60 to 98
22.4	0 to 3	0 to 3	0 to 3	0 to 7	15 to 60
16	-	-	-	-	0 to 15
8	-	-	-	-	0 to 2

2.1.2 Ballast shape

According to [10], ballast shape are quantified by three parameters: flakiness index, shape index and particle length.

The flakiness index describes the mass proportion of flat ballast stones in a ballast aggregate. To calculate the flakiness index, the testing sample is firstly divided into particle groups according to the particle sizes, i.e., between which two sieves these particles stay. The smaller and bigger meshing size of the two sieves (d_i/D_i) are used to identify the particle group. Grid sieve tests will be performed on each group, where the slot width of the grid sieve is the half of D_i (see Table 2-2). For particle group d_i/D_i, the mass of this group is denoted as R_i, while the mass of the particles, which go through the corresponding grid sieve of this group is denoted as m_i. The flakiness index FI_i of the group d_i/D_i and the flakiness index of the whole sample FI are:

$$FI_i = (m_i/R_i) * 100 \tag{2.3}$$

$$FI = (M_2/M_1) * 100 \tag{2.4}$$

where M_1 is the mass of the testing sample after drying, i.e., the summed mass of each particle group. M_2 is the summed mass of particles, which go through the grid

sieves. The sample is then classified into different categories according to its flakiness index (see Table 2-3).

Table 2-2: Grid sieves [9]

Particle Groups d_i/D_i	slot widths of the grid sieves mm
80/100	50 ± 0.5
63/80	40 ± 0.5
50/63	31.5 ± 0.5
40/50	25 ± 0.4
31.5/40	20 ± 0.4
25/31.5	16 ± 0.4
20/25	12.5 ± 0.4
16/20	10 ± 0.2
12.5/16	8 ± 0.2
10/12.5	6.3 ± 0.2
8/10	5 ± 0.2
6.3/8	4 ± 0.15
5/6.3	3.15 ± 0.15
4/5	2.5 ± 0.15

Table 2-3: Categories for maximum values of flakiness index [10]

Flakiness Index	Category FI_{RB}
≤15	FI_{RB} 15
≤20	FI_{RB} 20
≤25	FI_{RB} 25
4 to 25	FI_{RB} 4/25
>25	$FI_{RBDeclared}$

The calculation of the shape index is regulated by [7], where the particles of every particle group are classified as cubic or non-cubic shaped. A non-cubic shaped particle is the particle, whose ratio of length and thickness is bigger than three (i.e., $L/E > 3$). The length and thickness of the particles will be measured by an appropriate gauge or caliper. The shape index of the whole sample is:

$$SI = \left(\frac{\sum M_{2i}}{\sum M_{1i}}\right) * 100 \tag{2.5}$$

where $\sum M_{1i}$ is the sum of mass of all the particle groups. $\sum M_{2i}$ is the sum of mass of the non-cubic particles in each particle group. According to the shape index, the testing sample is further classified to different categories (see Table 2-4).

Table 2-4: Categories for maximum values of shape index [10]

Shape Index	Category SI_{RB}
≤10	SI_{RB} 10
≤20	SI_{RB} 20
≤30	SI_{RB} 30
5 to 30	SI_{RB} 5/30
>30	$SI_{RBDeclared}$

The particle length L is defined as the longest dimension of a ballast stone, which is measured by an appropriate gauge or caliper. The ballast stones with a particle length bigger than 100mm will be classified as long ballast. The ratio of the mass between long ballast and the whole sample will be calculated and categorized to the relevant category specified in Table 2-5.

Table 2-5: Categories for maximum values of particle length [10]

Percentage by mass with length = 100 mm in a greater than 40 kg sample				
Particle length category L_{RB}				
L_{RB} A	L_{RB} B	L_{RB} C	L_{RB} D	$L_{RBDeclared}$
≤ 4	≤ 6	≤ 8	≤ 12	≥ 12

2.2 Discrete element modeling

The mechanical behavior of ballast aggregates with different form distributions are investigated in this dissertation by DEM based simulations. In this section, the theoretical method is firstly introduced. Afterwards, a modeling tool based on this method, e.g., DEM software Particle Flow Code (PFC), is introduced. Its basic theory, material modeling support and constitutive models are explained in detail.

2.2.1 Discrete element method

DEM is a mesh-free method (comparing to mesh-based methods like Finite Element Method, Rand Element Method or Volume Element Method), which focuses on dealing with discontinuous mechanics issues. It treats each particle (in railway engineering, ballast stone) as an independent element, relative motions such as translation

and rotation of each element are allowed. When simulating ballast stones, the obvious advantage of DEM is that it can easily and intuitively simulate their important geometrical parameters such as shapes and sizes. To this end, the interlocking effect, which is a notable characteristic of a ballast aggregate, can be represented. Besides, DEM can simply and clearly define the interaction between ballast stones by simplifying it as a spring-damper system and extract the contact force, which enables the study of the force propagation angle inside ballast aggregate under loading. Furthermore, DEM avoids the unrealistic tensile forces between particles when mesh-based methods are used, because the simulated particles are independent with each other in DEM. Additionally, using the Bonded Particle Model (BPM) of DEM to represent a single ballast stones allows the simulation of its breakage under loading, and thus the breakage rate of ballast aggregate can be studied. Other mechanical properties of a ballast aggregate such as void ratio, settlement and particle coordination number can also be investigated by DEM simulations. For these reasons, in the past few years, the usage of DEM in ballast track research becomes more and more comprehensive.

DEM derived from Molecular Dynamics (MD), which was proposed by Alder and Wainwright in 1957 [11]. Both of these methods have identical spirit. However, the difference is the relationship of the elements. MD is mainly applied for researching the microscopic interactions between atoms or molecules, interaction force between objective element and all the other elements need to be considered. Meanwhile, DEM is mainly used for studying the macroscopic phenomenon, only the force between the objective element and its contacted element is considered.

DEM was firstly proposed by Cundall [12]. At that time it was applied to rock mechanics, the originate research object was the mechanical behavior of rocks. After this, Cundall and Strack proposed DEM which applied to soil mechanics [13,14], it is known as soft particle approach afterwards. Based on this method, they developed the software BALL using 2D disc and software TRUBAL using 3D sphere for simulating the particles. TRUBAL was afterwards developed to commercial software PFC-2D/3D. Since then, the application of this method was to study the behavior of granular materials. An assembly which consists of thousands of particles can be examined numerically.

Other researchers continuously developed DEM on the basis of Cundall's theory. In 1980, Walton [15] made some development of DEM by using it to research on the flowing of the discrete material. In 1985, Campbell [16,17] proposed hard particle approach and used it to analyze shear flow. Both hard particle approach and soft particle approach can be classified as rigid particle. Correspondingly, in 2004, Munjiza [18] presented a Finite-Discrete Element Method (deformable particle), which meshes every particles with FEM and allows deformation in them.

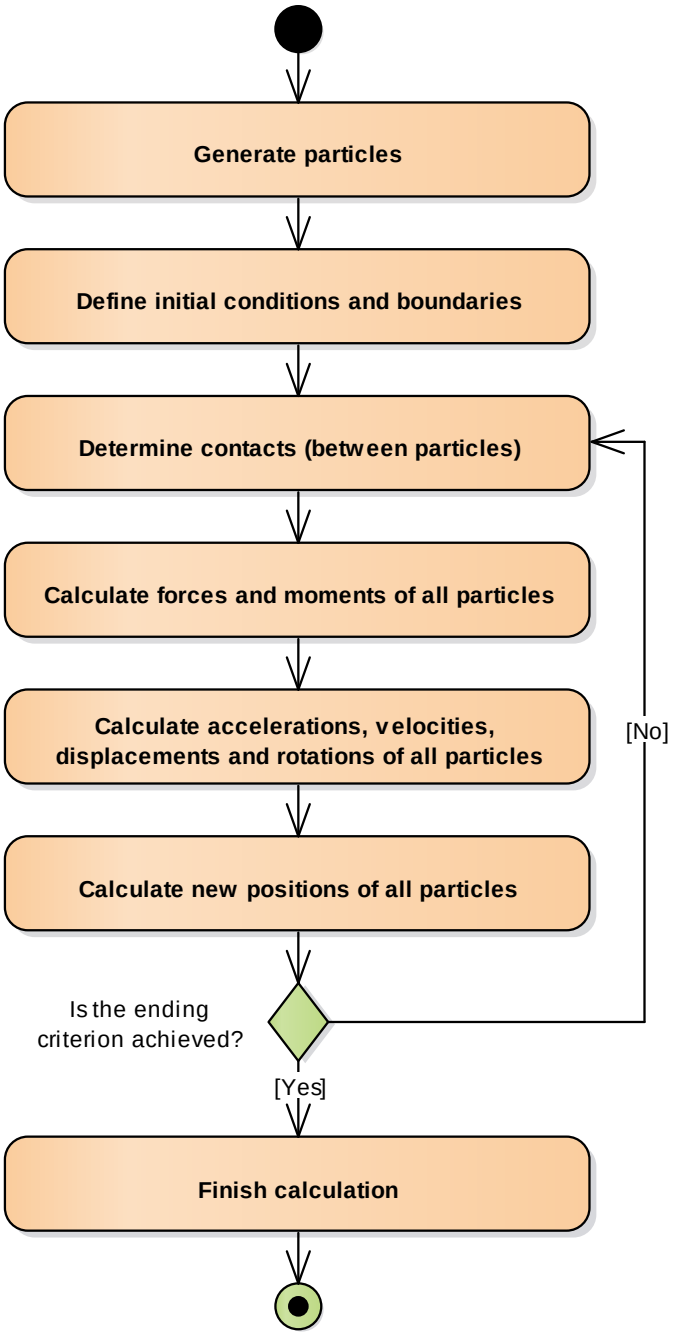

Fig. 2-2. Calculation process of DEM

DEM is a numerical calculation method based on Newton's laws of Motion. It treats each particle as an individual element, which could have six degrees of freedom. The basic variable in DEM is the overlap of contacted particles u_n. Based on this, the force between particles, which deduces acceleration, angular acceleration, velocity angular velocity of the particles, can be calculated. Thus, the renewed positions of particles in the next time step can be obtained. The calculation process of DEM is shown in Fig. 2-2.

2.2.2 Discrete element modeling

2.2.2.1 Particle Flow Code

Based on DEM, numerous of software applications are developed and used for engineering purposes, among which the PFC is the most well-known and widely used one. PFC was firstly proposed by Cundall and Stack and further developed by Itasca [13,19]. In this section, basic modeling components (i.e., balls, clumps, walls, contacts, PFC commands and FISH, see Fig. 2-3) and cycling of PFC (see Fig. 2-5 and Table 2-6) are introduced.

PFC model components

A ball is a rigid disk with unit thickness in 2D, or a rigid sphere in 3D. It is with properties such as radius and density, and can translate and rotate in the simulation. Ball motion obeys the equations of motion, while the loading conditions are defined by the force and moment resulting from interactions with other pieces, gravity, and an externally applied force and moment.

A clump is a rigid collection of n rigid spherical pebbles. A pebble is in great extent very similar to a ball. However, unlike a collection of balls, there is no interaction between pebbles inside of a clump, meaning relative motions and forces between pebbles do not exist in the simulation, and thus, big overlaps can exist.

A wall is a manifold surface composed of line segments in 2D, or triangular facets in 3D. It can translate and rotate, but its motion does not obey the equations of motion, because it does not have mass. This indicates that a wall cannot be pushed by balls or clumps.

Particles in the PFC model interact at contacts by means of a generalized internal force. Contact mechanics is embodied in particle-interaction laws that employ a soft-contact approach, for which all deformation occurs at the contacts between the rigid bodies. The particle-interaction laws are referred to as contact models, each contact is assigned a single contact model.

PFC utilizes a command-driven format. Word commands control the operation of the program. By using the commands, the users can establish simple models in PFC.

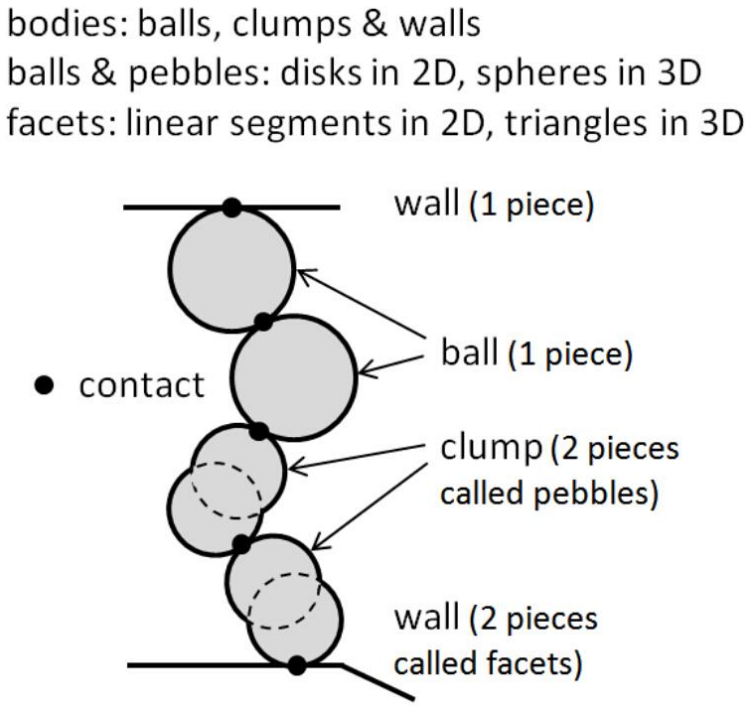

Fig. 2-3. Sketch of a PFC model showing bodies, pieces, and contacts [19]

FISH is an embedded programming language that enables the user to interact with and manipulate PFC models, defining new variables and functions as needed. These functions may be used to extend PFC's usefulness or add user-defined features. FISH was developed in response to users who wanted to do things with Itasca software that were either difficult or impossible with existing program structures. Rather than incorporate many new and specialized features into PFC, FISH was provided so that users could write functions to perform custom analyses.

Cycling of PFC

The DEM formulation is an explicit, time-stepping solution to Newton's laws of motion. The model state is advanced in time by executing a series of calculation cycles. Cy-

cling continues until one or more solve limits are reached. In addition, one or more FISH functions can be specified as solve limits, allowing for custom cycling termination criteria. Fig. 2-4 presents a schematic of the process of executing a series of cycles.

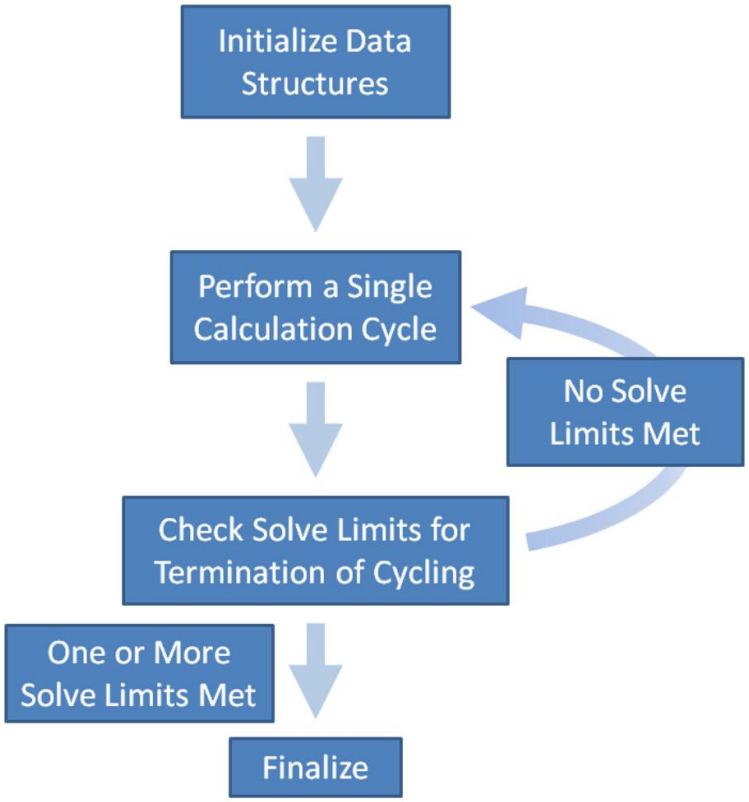

Fig. 2-4. Schematic of a series of calculation cycles [19]

The sequence of operations executed during one calculation cycle is termed the cycle sequence (see Fig. 2-5 and Table 2-6). The cycle sequence consists of an ordered set of operations where each operation has a floating point number assigned to it, termed a cycle point. Table 2-6 lists the specific operations and associated cycle points.

This system was introduced so that additional operations could easily be added to the cycle sequence. In addition, the cycle points allow for the simple identification of cycle sequence operations so that FISH callback functions can be inserted at various points during a cycle in a strict order for execution.

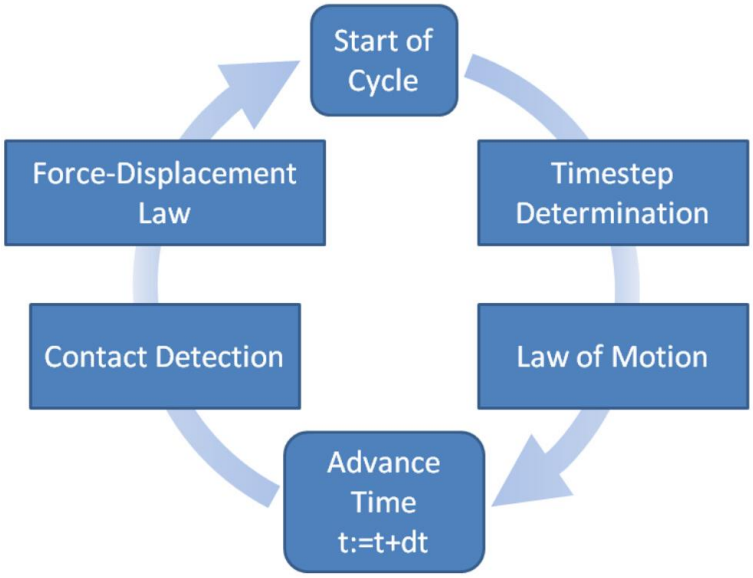

Fig. 2-5. Sequence of primary operations that occur during each calculation cycle, termed the calculation cycle sequence [19]

Table 2-6: Calculation cycle operations and associated cycle points [19]

Cycle point	Cycle operation
-10.0	Validate data structures
0.0	Timestep determination
10.0	Law of motion (or update thermal bodies)
15.0	Body coupling between processes
20.0	Advance time
30.0	Update spatial searching data structures
35.0	Create/delete contacts
40.0	Force-displacement law (or thermal contact update)
42.0	Accumulate deterministic quantities
45.0	Contact coupling between processes

2.2.2.2 The material-modeling support

The material-modeling support in PFC, which is provided in the form of a consistent set of FISH functions (i.e. the FISHTank), supports material genesis and testing of PFC materials with microstructural monitoring. A PFC material is made of rigid grains (can either be balls or clumps, which follow a general gain-size distribution) with interaction at contacts, which can be described by different contact models. Simula-

tions of compression, diametral-compression and direct tension tests can be performed with the PFC material to support practical applications and scientific inquiries.

The BPM in PFC is a material with balls as the rigid grains. The microstructural monitoring of the material-modeling support is able to visualize fragments caused by external forces by painting them with different colors. The breakages between the particles can be shown by generating small discs between them. These two features facilitate the observation and research of the ballast stone breakage behavior.

A shortcoming of the current version of the FISHTank (version 20) is that it only supports the generation of regular shaped BPM, which is obviously not the case of irregularly shaped ballast stones. Improvements should be made based on the current version.

2.2.2.3 The constitutive models for bonding materials in PFC

The particles of BPM are bonded by applying the contact model for bonding materials. The PFC provides three choices for generating a BPM: Contact Bond (CB), linear Parallel Bond (PB) or Flat Joint (FJ) models. The bond in the CB model can be seen as a couple of elastic springs (or a point of glue) with constant normal and shear stiffness acting at the contact point. The bond in the PB model can be envisioned as a set of elastic springs, which are distributed over a cross-section lying on the contact plane and centered at the contact point. These springs are of the parallel-bond component, resist rotation between particles and can carry a moment. They act parallel to the springs of the linear component of PB model. The bond break is embodied by deleting the parallel-bond component. If the two pieces are once again in contact, the interaction will be determined by the remaining linear component. The FJ model describes the bond as an interface, which exists between the bonded notional surfaces of the contacting particles and is discretized into elements, with each element being either bonded or unbonded. If all the elements are unbonded, the bond will be considered as broken and the interface is removed. If the two particles come back in contact, the interaction will be depended on the unbonded notional surfaces [20].

If the contact of particles remains after the breakage of the bond, the normal and shear stiffness of the CB model remain the same. This indicates that in the CB model, the bond breakage, which mimics the tiny crack inside a rock specimen, may not in-

fluence the macro-stiffness of a BPM as significant as it is in the reality [21]. The PB model solves this problem by using both the parallel-bond and linear component for the bonded state. The removal of the parallel-bond component to simulate the bond breakage will directly reduce the stiffness of two contact particles, thus affect the macro-behavior of the BPM. However, the removal also eliminates the moment between particles, which means that the relative rotations between two broken particles can no longer be resisted. This results in a much lower estimation of unconfined compressive strength (q_u) of the BPM, when the tensile strength of the bond is chosen to match the Brazilian strength (σ_t). In the FJ model, since the notional surfaces will not be deleted even though a fully broken state is reached (only the interface for bonding will be deleted), the notionally polygonal particles can still carry a moment. With a reasonable choice of the tensile and shear strength of the bond, q_u and σ_t can be simultaneously matched [22].

Researchers have been using BPMs with FJ model to simulate different rocks and study different research objectives. Wu and Xu [23] calibrated FJ model with test results of Jinping marble. The test and simulation results matched well with each other. The authors indicated that other than reproducing proper rotational resistance, FJ model can also, firstly, provide enough particles interlocking to ensure necessary strength of the material; secondly, implement pressure-dependent shear strength; thirdly, mimic the pre-existing cracks of rock. Xu *et al.* [24] used FJ model to investigate Brazilian tensile strength (BTS) of Birsbane tuff. The effects of micro-structures and micro-parameters on BTS were studied. Failure mechanism was investigated. It was proved by the authors that FJ model was reliable for research of BTS and failure mechanism of the BPM. Vallejos *et al.* [25] compared the enhanced bonded-particle model (EBPM) and FJ model by simulating the intact rock behavior of Westerly granite. Elastic parameters, peak and threshold envelopes, and post peak behavior were discussed in detail. It was concluded that the FJ model better represented the mechanical behavior of the specimen. Especially, the post peak behavior of the FJ model was in good agreement of those of the specimen for low and intermediate levels of confining pressure. Cheng *et al.* [26] studied the interaction between en-echelon fractures and a fault of rock specimen. FJ model parameters are chosen in accordance with macro-behavior of Carrara marble from uniaxial compression test,

Brazilian test and direct tension test. FJ model was used to check the contact force around en-echelon flaws.

From the above-mentioned researches, it can be concluded that FJ model is reliable for simulating breakage behavior of rock. However, in all these papers, since standardized tests were used for calibration of the FJ parameters, the shapes of BPMs are geometrically regular. It is obviously not the case of ballast stones. It is necessary to assure that the modeling method is still valid for the irregular shaped BPMs, thus can be used for investigating ballast aggregates.

2.2.2.4 The FJ model

In this study, the ballast stones are simulated by BPM using the FJ model. Since the FJ model discretizes the interface between two contacted particles into elements, the total contact force F_c and moment M_c are respectively the sum of every element force $F^{(e)}$ and moment $M^{(e)}$ at the center of the interface x_c (see Fig. 2-6). The number of FJ elements is the product of which in radial direction N_r and in circumferential direction N_a (see Fig. 2-7).

The element force $F^{(e)}$ is resolved into a normal and shear force. The element moment $M^{(e)}$ is resolved into a twisting and bending moment:

$$F^{(e)} = -F_n^{(e)}\hat{n}_c + F_s^{(e)} \tag{2.6}$$

$$M^{(e)} = M_t^{(e)}\hat{n}_c + M_b^{(e)} \tag{2.7}$$

where $F_n^{(e)} > 0$ is tension, $\hat{n}_c$ is the normal direction of the element plane, $F_s^{(e)}$ is the shear force, $M_t^{(e)}$ and $M_b^{(e)}$ are the resolved twisting and bending moment. The normal stiffness k_n is used for updating $F_n^{(e)}$ and $M_b^{(e)}$, and the shear stiffness k_s is used for updating $F_s^{(e)}$. An assumption is made that the shear stress, arising from relative twist rotation, is constant over the element and equal to its value at the element's centroid. It is then concluded that $M_t^{(e)}$ is zero w.r.t. the element's centroid. For a detailed explanation of the FJ model please see [19,22].

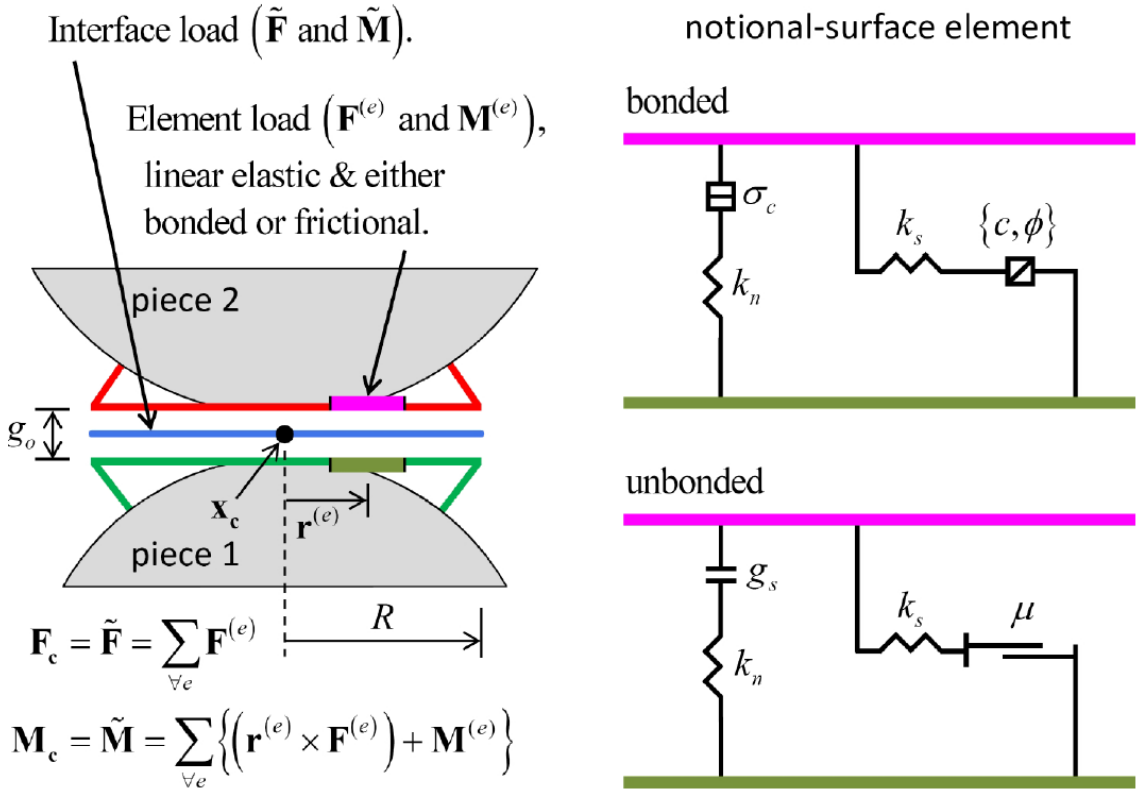

Fig. 2-6. Behavior and rheological components of FJ model [27]

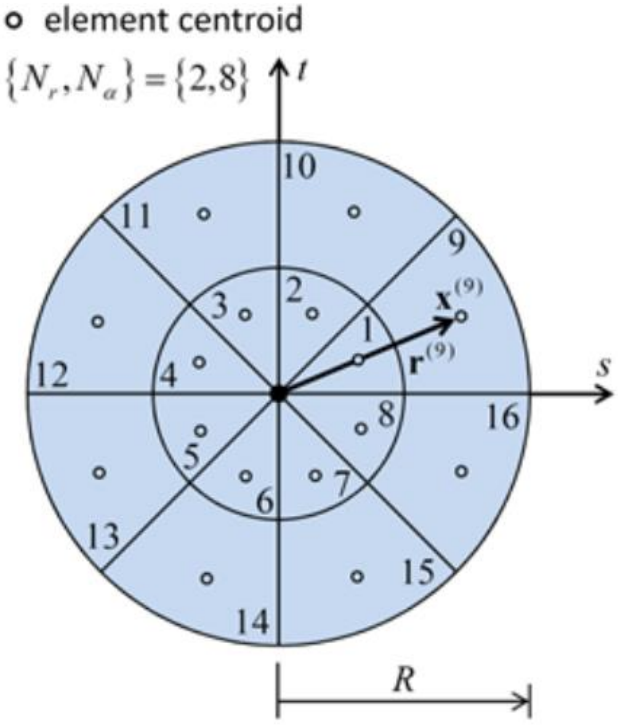

Fig. 2-7. Element-numbering convention of interface discretization of the FJ model [19]

The element force $F^{(e)}$ is resolved into a normal and shear force. The element moment $M^{(e)}$ is resolved into a twisting and bending moment:

$$F^{(e)} = -F_n^{(e)}\hat{n}_c + F_s^{(e)} \tag{2.8}$$

$$M^{(e)} = M_t^{(e)}\hat{n}_c + M_b^{(e)} \tag{2.9}$$

where $F_n^{(e)} > 0$ is tension, $\hat{n}_c$ is the normal direction of the element plane, $F_s^{(e)}$ is the shear force, $M_t^{(e)}$ and $M_b^{(e)}$ are the resolved twisting and bending moment. The normal stiffness k_n is used for updating $F_n^{(e)}$ and $M_b^{(e)}$, and the shear stiffness k_s is used for updating $F_s^{(e)}$. An assumption is made that the shear stress, arising from relative twist rotation, is constant over the element and equal to its value at the element's centroid. It is then concluded that $M_t^{(e)}$ is zero w.r.t. the element's centroid. For a detailed explanation of the FJ model please see [19,22].

2.3 Methods of capturing the forms of ballast stones

When DEM simulation is performed, it is the first task to simulate the forms of ballast stones. In the past, researcher tended to use regular and similar-sized geometrical forms to represent ballast particles [28–30]. However, this method ignores the important angular property of ballast stones, which provides the stability of the ballast layer with interlocking effect between them. According to the European standards of ballast aggregates, the form of ballast stones should be quantified in aspects of size and shape, where the size should follow a certain grading distribution and the shape should obey requirements with regard to flakiness index, shape index, and particle length [10]. Using regular and similar-sized forms in the simulation will certainly deprive the possibility of researching on the influence of mechanical behavior of a ballasted track provided by the changing of form. Capturing the realistic geometrical forms of ballast stones becomes the crucial first step for researchers.

In general, there are two ways to fulfill the task. The first one is to use digital image devices to capture the forms. Tutumluer and Huang [31–33] proposed a digital image-aided DEM particle shape generation method. This method creates a 3D image of a single ballast stone by using three 2D orthogonal views. It uses a flat and elongated ratio, angularity index, and surface texture to quantify the ballast's geometrical form. Anochie-Boateng et al. and Latham et al. [34,35] used a laser scanning technique. After scanning, the result would be outputted as a digital scan file with a mesh

of triangular elements. The volume, width, height, and thickness would be obtained and used to define the shapes and sizes of the particles.

The other way of capturing the form is to use algorithms. In general, as ballast stones usually feature quite planar faces, these algorithms create randomly shaped polyhedrons as representations of ballast particles. Ergenzinger [36] proposed an algorithm based on tangent planes on ellipsoids. The tangent planes were generated by intersection points, which were firstly the intersection between the ellipsoid and its axes, then the randomly moved points on the surface of the ellipsoid and in normal direction. The geometrical form of a ballast stone was represented by the volume with the random intersection planes as surfaces. Eliáš [37] proposed an algorithm based on Voronoi tessellation. The vertices of ballast geometrical forms were firstly generated in a given volume with the restriction that the minimum distance between two vertices was larger than the restricting distance l_{min}. Afterwards, polyhedrons were created by means of connecting the generated vertices.

The obvious advantage of image aided method is that it can easily obtain realistic forms of ballast stones. However, the process is time consuming and expensive. In addition, a completely comprehensive database cannot be obtained, for the simple fact that each ballast stone is different. On the other hand, algorithmic approaches are much quicker, and they always contain random processes during the creation of the forms, which means that every simulated ballast stone will be different. Besides, the generated form can improve the computing efficiency in further DEM simulations, since there are much fewer elements (e.g., triangular walls in DEM software PFC) due to a simplified representation of the geometrical profile of ballast stone, and thus less calculation load in every iteration during, e.g., the packing process of BPM, where the ballast stone is embodied by bonded balls; or during the contact detection process, if the ballast stone is represented directly by the geometrical form. Furthermore, the algorithmic approach can generate a nonexistent distribution of ballast forms in reality, which enables the investigation of mechanical behavior of such ballast aggregate, and then benefits the optimization of conventional ballast track, under the assumption that the currently used standardized ballast form distributions are not yet fully optimized. However, this advantage of the algorithmic approach is not yet fully developed. The former algorithms mainly focused on generating one single bal-

last stone. The form distribution of ballast stones in an aggregate has not been considered.

2.4 Mechanical property of ballast aggregate

The mechanical property of ballast aggregate is strongly affected by the geometrical property of the ballast stones. In this section, the state of the arts of DEM modeling of the ballast form affected mechanical properties of ballast aggregate, i.e., the settlement, the degradation, the force propagation angle and the void ratio are introduced.

2.4.1 Ballast settlement

Ballast settlement usually leads to track irregularity, which could cause excessive dynamic loading and decrease of train speed. A better understanding of ballast settlement behavior will be helpful for improving ballast track designs.

Tutumluer [38] created a DEM model with different ballast shape, angularities and rough surface textures in order to investigate ballast settlement under repeated wheel loading. The result showed that rounded aggregate particles usually lead to lower ballast settlements. Huang [39] simulated the settlement of ballast when the trains moved at critical speeds, which cause resonance effect (unfavorable track performance) of the wheel-rail interaction. Bian et al. used a DEM approach to evaluate the impacts of gradation on both ballast void space and load carrying performances [40]. On the other hand, DEM simulations were performed to predict the settlement of ballast layers with different gradations. It was shown that the aggregate with higher void tended to yield more settlement, since it is more structurally inadequate and contains fewer contacts between particles. Tutumluer et al. presented findings of a railroad ballast DEM modeling research study focused on investigating settlement of ballast aggregates with different shapes and angularities [32]. Three ballast aggregates with cubical-angular, cubical-rounded and elongated-rounded shaped ballast stones were investigated. The simulation results indicated that the elongated-rounded and the cubical-rounded ballast aggregates yielded smaller settlement than the cubical-angular one, which was in general against the common belief and what was normally expected. The reason could be that the cubical-angular ballast aggregate tended to generate a loose packing in the simulation, hence resulted a larger air void and a higher settlement under the same loading condition. Furthermore, even

though the elongated-rounded aggregate yielded lower settlement, it did not imply that this kind of shape outperformed the others, since it is known that the elongated ballast stones are easier to be broken, yet the breakage was not considered in the simulation.

2.4.2 Ballast degradation

Under the action of the long-term dynamic wheel-rail force, ballast particles can break into smaller pieces. Although most DEM implementations do not allow particle breakage since the original DEM considers unbreakable particles, a couple of methods have been found to consider breakage in DEM software when simulating ballast [28]. Depending on which kind of ballast particle generation method is used, two ways to simulate ballast degradation are proposed.

The first solution is to treat each particle as a porous agglomerate built by bonding smaller particles [41]. These agglomerates can disaggregate during the simulation by simply splitting the clump when breakage criterion is met. Ergenzinger [36,42] proposed a progressive failure model to simulate the singular stress concentrations near crack tips and instable crack propagation, which are common in real ballast stones yet not commonly existed in BPMs. This failure model accumulated local damage by reducing the strength R_m of a bond between two spheres i and j and was calculated by

$$R_m(t) = \hat{R}_m \left(\frac{n_{c,i}(t) n_{c,j}(t)}{n_{c,i}(0) n_{c,j}(0)} \right)^{\beta} \tag{2.10}$$

where $\hat{R}_m$ is the bond strength in undamaged material; $n_{c,\iota}(t)$, $\iota = i, j$ is the number of a sphere's remanent bond; $n_{c,\iota}(0)$, $\iota = i, j$ is the coordination number of a sphere. The exponent β was chosen as the limited, weighted sum of the involved spheres' number of broken bonds

$$\beta = min\big(\alpha\big[n_{b,i}(t) + n_{b,j}(t)\big], b\big) \tag{2.11}$$

where α is a weighting factor, which can adjust the speed of damage accumulation; $n_{b,\iota}(t) = n_{c,\iota}(0) - n_{c,\iota}(t), \iota = i, j$ is the number of broken bonds; b denotes a maximal exponent.

The other solution for simulating the particle breakage is to replace the particles fulfilling a predefined failure criterion with an equivalent group of smaller particles. This solution is suitable when polyhedron is used. Lobo-Guerrero and Vallejo [28] compared the permanent settlement of two simulated ballast track section (only one of them allowed crushing). Since the simulation software (PFC2D) didn't allow particle breakage, they used the FISH language in PFC to program a subroutine to describe the failure criterion [43–45]. The simulation results showed that the permanent settlement increased strongly when particle breakage was considered. Hossain [46] also used the failure criterion programed by Lobo-Guerrero and Vallejo. He quantified breakage in relation to particles size distribution. The influence of confining pressure on both breakage and permanent deformation was studied. Eliáš [37] described the crushing of ballast by splitting the particles into smaller polyhedrons when a certain stress-based criterion is fulfilled. This criterion was based on the comparison of equivalent stress σ_e and particle strength f_t.

$$\sigma_e = \sqrt{\frac{(\sigma_1)^2+(\sigma_2)^2+(\sigma_3)^2}{2}} \tag{2.12}$$

$$f_t = f_0 \sqrt[3]{\frac{4\pi}{3V}} \tag{2.13}$$

where σ_1, σ_2, σ_3 are principal stresses, f_0 is a material parameter, V is the volume of the particle. When equivalent stress exceeds particle strength, particle breaks. The particle strength is inversely proportional to particle size.

2.4.3 Force propagation angle

One of the outstanding advantages of ballasted track is its ability to attenuate the rail-wheel force, which is propagated from top to bottom. Lichtberger indicated that the force propagation depends on the force propagation angle [1]. He also pointed out that the new angular ballast stones have a force propagation angle of 42°, while the used ballast stones of 39° and the soiled ballast stones of 30°. A bigger force propagation angle could maintain the elasticity of the ballast layer, lower the stress, and thus reduce the possibility of ballast degradation and settlement. It is also assumed that a bigger force propagation angle would ensure better energy dissipation.

Lichtberger only revealed the influence of ballast usage conditions on the force propagation angle. However, as an important parameter of ballast aggregate, the influ-

ence of ballast gradation is still unclear. Besides, the differences of the force propagation angles, which are yielded by different loading frequencies, should also be investigated.

Steiner et al. used a stress measuring platform under a ballast layer to detect the force propagation angle [47]. The angle in this study was defined as the 90% of the total force measured by the platform. Different material of ballast stones were used as the ballast layer, the caused difference was discussed. However, the effect of form distribution was not taken into consideration in the study.

2.4.4 Void ratio

The void ratio is the ratio of the void volume and the volume of a ballast aggregate. Bian et al. used a DEM approach to evaluate the impacts of gradation on both ballast void space and load carrying performances [40]. The ballast gradations differ from each other by uniformities, namely given a fixed maximal size of the ballast stone in a certain ballast aggregate, its uniformity increases with the decrease of the percentage of the smaller stones in the group. In other words, if there are not so many small stones, the ballast aggregate is more uniform, since the sizes of ballast stones are more or less the same, and vice versa. It is indicated by the authors that as the uniformity goes smaller, i.e. finer particles are gradually introduced, the void space firstly becomes smaller, due to the reason that the finer particles take the place between large particle; then the void space becomes bigger, since the contacts among larger particles are severed and those large particles are separated apart by finer particles filling the matrix thus causing an expansion.

3 The random form generator for ballast stones

The DEM based simulation is a proper approach for investigating mechanical behavior of granular matters such as ballast stones. In this study, DEM software PFC is implemented for simulation of ballast aggregates with different form distributions of ballast stones, where the ballast stones are represented by arbitrary shaped polyhedrons matching the geometrical specification of ballast stones in reality expatiated in railway standards [6–10].

In this chapter, to generate the forms of ballast stones for latter usage in DEM simulations, a ballast random form generator is developed using the Python programing language. The algorithm of the generator will be firstly introduced. The algorithm contains the form generation part, the form evaluation part and the belongingness judgement part (see Fig. 3-1). The evaluation of the form and its belongingness judgement are based on the specifications expatiated in standards [6–10], and calculated based on the three orthogonal dimensions of the generated ballast form a, b and c. The generator is designed to create ballast form databases, which are of different combinations of size and form distributions, so that the mechanical behavior of different ballast aggregates can be studied in the further DEM simulations. The generator requires input parameters, i.e., the mass, the grading, the flakiness index, the shape index and the particle length of a desired form database (the objective parameters). After generating the database, the generator calculates the same parameters of the actual generated form database as output parameters (the generated parameters). The result is checked by comparing the two sets of parameters.

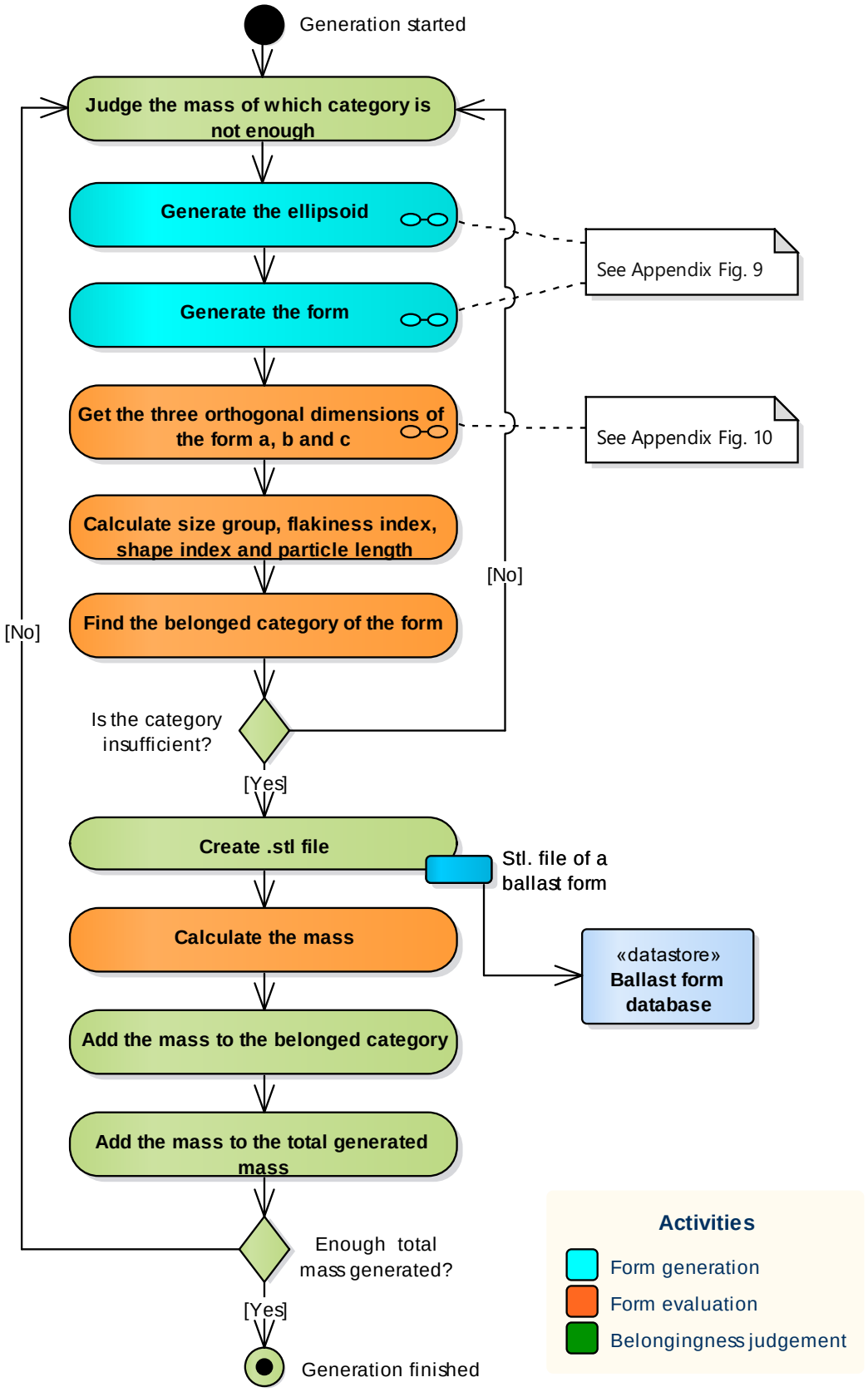

Fig. 3-1. Train of thoughts of the ballast random form generator

3.1 Form generation

The generation of the form is based on random shaped ellipsoids and random placed vertexes on the surface of the ellipsoids. The corresponding train of thought is illustrated in Fig. 3-2. For detailed steps please refer to Appendix Fig. 9.

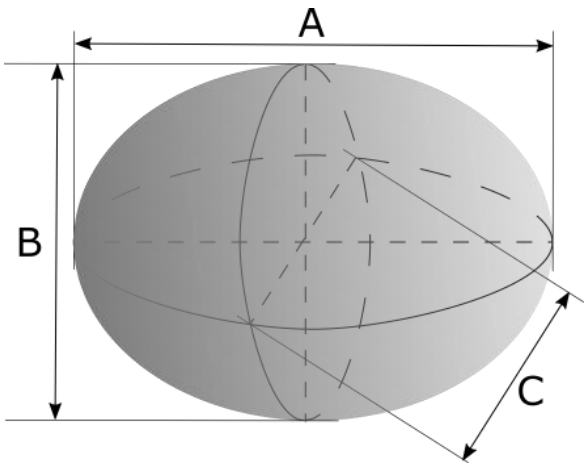

step 1: create an ellipsoid with random major axle A, middle axle B and minor axle C

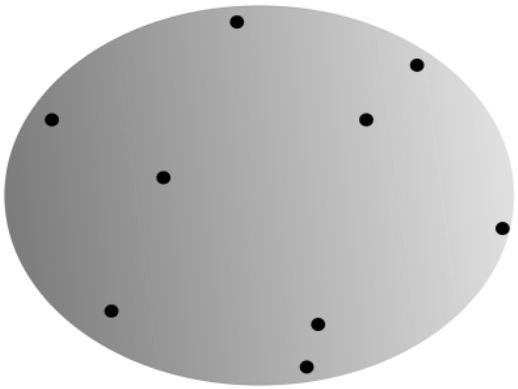

step 2: create n points randomly placed on the surface of the ellipsoid as vertexes of the polyhedron

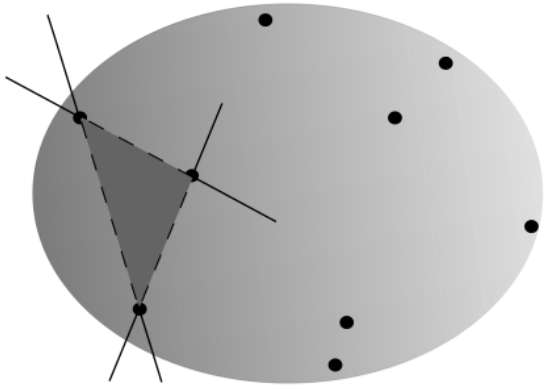

step 3: connect three points to create a facet, under the condition that all the other points are on the same side of the created facet

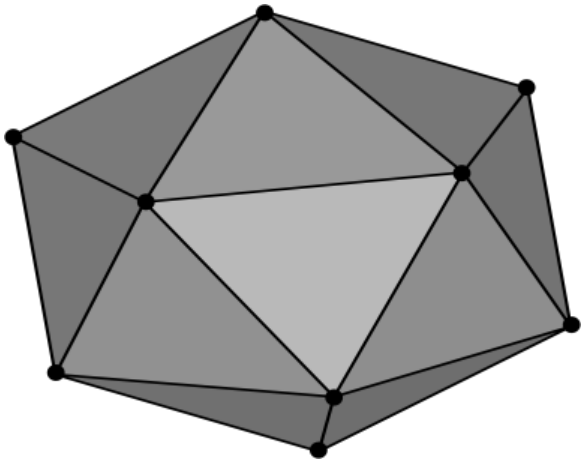

step 4: create all the facets

Fig. 3-2. Train of thought of generation of a ballast form

The geometrical information of the created vertexes, edges and facets will be saved as a .stl file, so that they can be used in the further DEM simulations. The creation of the form of the ballast stones is finished. However, the size and shape are still not known. Using the criterions from [6,9,10], a further algorithm is developed to judge the size and shape of the created ballast form.

3.2 Form evaluation

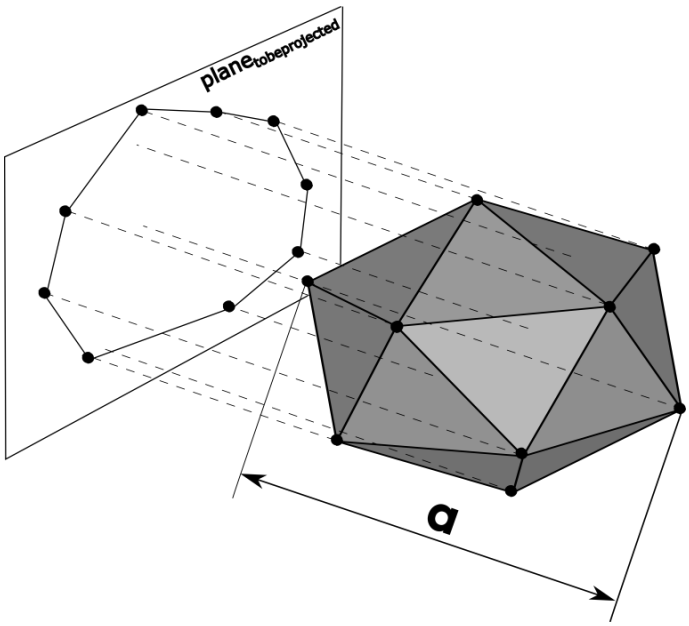

a: process of finding a

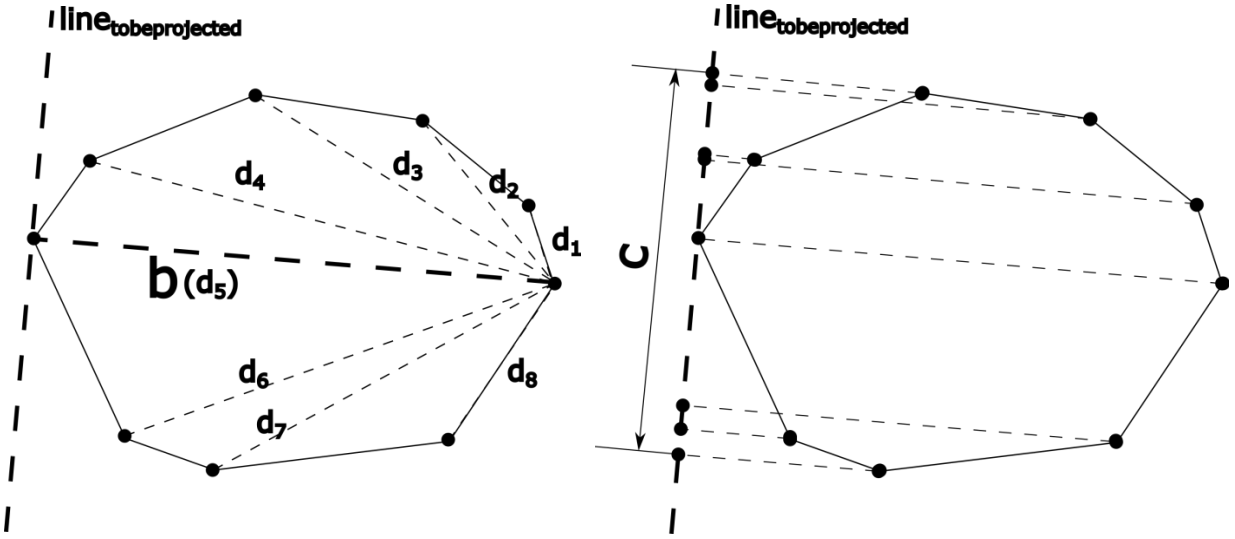

b: process of finding b c: process of finding c

Fig. 3-3. Form evaluation of the generated ballast form

To determine the form of the created ballast stone, the geometrical dimensions a, b and c (orthogonal with each other) should be firstly evaluated. The following steps are performed and illustrated in Fig. 3-3. For detailed steps please refer Appendix Fig. 10.

a. Calculate the distances between all the vertexes and record the maximum distance as a and its perpendicular plane as $plane_{tobeprojected}$ (see Fig. 3-3, a)

b. Project all the vertexes along the direction of the maximum distance a to the plane $plane_{tobeprojected}$. The vertexes are then all on the plane (see Fig. 3-3, a). These new vertexes constitute edges
c. Calculate the distances between all the new vertexes and record the maximum distance as b and its perpendicular line as $line_{tobeprojected}$ (see Fig. 3-3, b)
d. Project all the new vertexes along the direction of the maximum distance b, to the line $line_{tobeprojected}$. The vertexes are then all on the line (see Fig. 3-3, c)
e. Calculate the distance between two vertexes and record the maximum distance as c (see Fig. 3-3, c)

The maximal distances a, b and c are not necessarily in ascending and descending order. In the algorithm, a, b and c will be further rearranged to descending order, which is also assumed in the following sections for the sake of a clearer discussion.

3.2.1 Form size

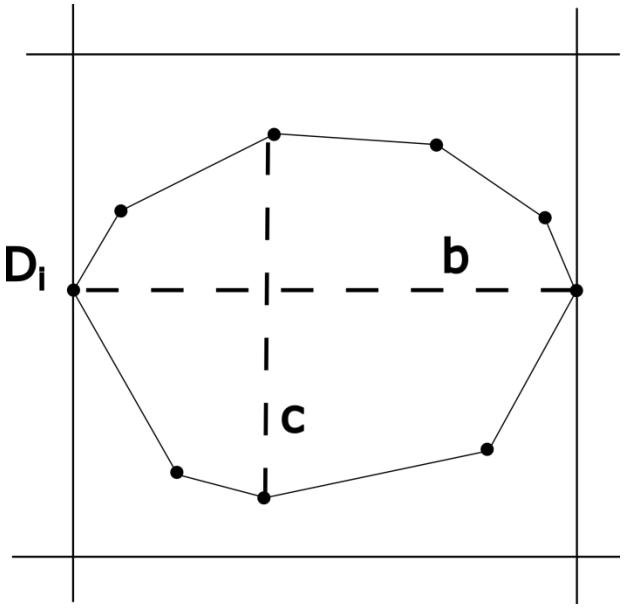

Fig. 3-4. Form size determination

In the European standard [8], the ballast size is quantified by categorizing it to certain particle group, which is denoted by the two meshing sizes of the two sieves (d_i/D_i), where the ballast stone stays after shaking. Since the meshing is quadrate-shaped, in the algorithm, if b is smaller than D_i (implying that c is also smaller than D_i), the generated form will certainly fall through the sieve with meshing size D_i. On the other hand, if b is bigger than d_i (implying that a is also bigger than d_i), the generated form will always stay on the sieve with meshing size d_i (see Fig. 3-4). In other words, in

the algorithm, a generated form will belong to the particle group d_i/D_i, if it meets the condition:

$$d_i \leq b < D_i \tag{3.1}$$

3.2.2 Form shape

According to [10], ballast shape are quantified by three parameters: flakiness index, shape index and particle length (see section 2.1). In this section, the algorithmic procedures to calculate these three parameters are presented.

For the calculation of the flakiness index, the particle groups in Table 2-2 should be treated respectively. Provided the generated form belongs to the particle group d_i/D_i, the slot width of the grid sieve should be $D_i/2$ (see Table 2-2). If the minimal width c is smaller than $D_i/2$, the generated form can pass the grid sieve. The generated form will be marked as flat.

To calculate the shape index, [10] indicates that the particles of every particle group have to be firstly classified as cubic or non-cubic shaped. A non-cubic shaped particle is the particle, whose ratio of length and thickness is bigger than three (i.e., $L/E > 3$). In the random form generator, it corresponds with $a/c > 3$. The generated form will be marked as non-cubic.

The particle length is demonstrated in [10] as percentage by mass with length ≥ 100 mm in a greater than 40 kg sample. The length corresponds with a in the random form generator. If $a \geq 100mm$, the generated form will be marked as long.

The ratio of the mass of marked forms (flat, non-cubic and long) and the mass of total generated forms will be respectively calculated and denoted as flakiness index, shape index and particle length.

3.2.3 Form mass

The distribution of ballast form is regulated by mass in the standards [6–10]. To calculate the mass of the generated ballast form, the volume has to be firstly calculated, provided that the density (i.e., the material type) of the ballast stone is known. Since the generated form is random shaped polyhedron, which cannot be calculated by simple equations, it is then divided into n tetrahedrons. The volume of the polyhedron V_{sum} is the sum of volume of each tetrahedron:

$$V_{sum} = \sum_{i=1}^{n} \left| \left(\overrightarrow{v_1^v} \times \overrightarrow{v_2^v} \right) \cdot \overrightarrow{v_3^v} \right| / 6 \tag{3.2}$$

where $\overrightarrow{v_1^v}$, $\overrightarrow{v_2^v}$ and $\overrightarrow{v_3^v}$ are respectively vectors from the three vertexes of a sharing facet on both the tetrahedron and the original polyhedron to the fourth point. The fourth point has to be inside of the polyhedron to assure a right calculation (see Fig. 3-5). The volume of a concave polyhedron cannot be calculated by this method. However, it is reasonable to exclude this case since the chance of a concave ballast stone is very low.

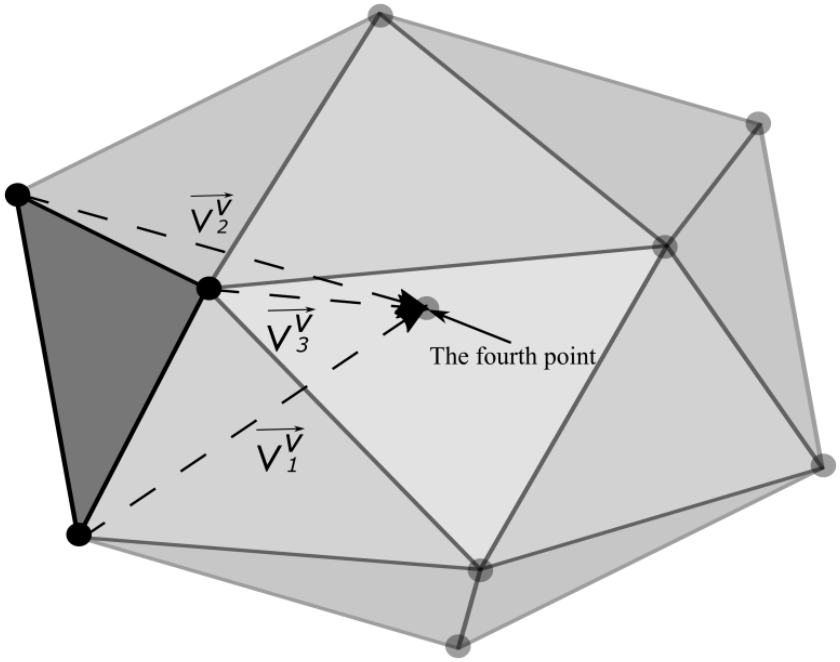

Fig. 3-5. Volume calculation

3.3 Belongingness judgement of the from in a ballast aggregate

In addition to the generation of a single form, the random form generator judges the belongingness of the form to a certain group. A group is a combination of the size and shape properties (e.g., particle group 80/100, flat, non-cubic, long). Each group will have an objective mass, which is calculated by multiplying the total mass to be generated with the mass percentage of the group; and an objective form, which is the combination of size and shape properties of the group. The algorithm starts with the generation of the first particle group. The axial lengths of the ellipsoid are adjusted to fit the generation of the objective form and efficiency of the generation will be increased. If the mass of the group is sufficient, the objective form to be generated will be altered to the next group. If the total generated mass exceeds the given objective mass, the generation terminates.

With given grading category, flakiness index, shape index and particle length, the ballast form generator is able to generate corresponding ballast form databases. It is important to notice that the above-mentioned four parameters are normally denoted as ranges (e.g., G_{CRB} A means particle grading between upper and lower limits, see Fig. 2-1 and Table 2-1). However, specific values are needed for the generator. Therefore, if ranges are given (e.g., category like G_{CRB} A), the generator will calculate the average value of the range and use it for the further calculation. Nevertheless, specific values are also allowed to be given.

In addition, conflictions have been noticed. Some of the combinations of the four parameters cannot exist. For example, shape index cannot be bigger than flakiness index, since the condition of being non-cubic is stricter than the one of being flat. Appropriate parameters should be given when using the generator.

3.4 Generating of ballast form databases using the generator

Table 3-1: Objective parameters of form aggregates to be generated

database index		mass (kg)	grading (-)	flakiness index (%)	shape index (%)	particle length (%)
changing mean sizes (database group 1)	G_1-1	50	G_1-1	not applicable	30	1
	G_1-2	50	G_1-2	not applicable	30	1
	G_1-3	50	G_1-3	not applicable	30	1
	G_1-4	50	G_1-4	not applicable	30	1
	G_1-5	50	G_1-5	not applicable	30	1
changing size distributions (database group 2)	G_2-1	50	G_2-1	not applicable	30	1
	G_2-2	50	G_2-2	not applicable	30	1
	G_2-3	50	G_2-3	not applicable	30	1
	G_2-4	50	G_2-4	not applicable	30	1
	G_2-5	50	G_2-5	not applicable	30	1
changing shape distributions (database group 3)	G_3-1	50	G_3-1	not applicable	10	1
	G_3-2	50	G_3-2	not applicable	20	1
	G_3-3	50	G_3-3	not applicable	30	1
	G_3-4	50	G_3-4	not applicable	40	1
	G_3-5	50	G_3-5	not applicable	50	1

In this study, 15 ballast form databases with different form distributions (different combinations of input parameters, i.e., the objective parameters) are established by

the generator for the further DEM simulations. Since the DEM models in this study will be in 2D (for the reasons please refer to section 4.3), the generator will also create 2D form databases. Detailed information of the desired databases is listed in Table 3-1 and Table 3-2.

Table 3-2: Gradings

sieve size (mm)		80	63	50	40	31.5	22.4	16	8
percentage passing by mass (%)	G_1-1	100	98	94	88.5	83	78	16	0
	G_1-2	100	95	88.5	83	78	16	4.5	0
	G_1-3	100	92	84	78	16	9.5	3.5	0
	G_1-4	100	89	78	16	9.5	6.5	2.5	0
	G_1-5	100	78	16	9.5	6.5	3.5	1.5	0
	G_2-1	100	99.5	97.5	90	4	1.5	0.5	0
	G_2-2	100	96.5	92.5	84	10	5.5	2.5	0
	G_2-3	100	93.5	87.5	78	16	9.5	4.5	0
	G_2-4	100	90.5	82.5	72	22	13.5	6.5	0
	G_2-5	100	87.5	77.5	66	28	17.5	8.5	0
	G_3-1	100	93.5	87.5	78	16	9.5	4.5	0
	G_3-2	100	93.5	87.5	78	16	9.5	4.5	0
	G_3-3	100	93.5	87.5	78	16	9.5	4.5	0
	G_3-4	100	93.5	87.5	78	16	9.5	4.5	0
	G_3-5	100	93.5	87.5	78	16	9.5	4.5	0

As shown in Table 3-1 and Table 3-2, according to the input parameters, the 15 form databases are categorized into three groups, i.e., the group with changing mean sizes, the group with changing size distributions and the group with changing shape distributions. The five databases of the first group differ with each other by different mean sizes of their belonging ballast stones (see Fig. 3-6), while the ones of the second group vary with the ballast stones' size distributions (see Fig. 3-7). The five databases of the third group have identical size distributions, but they vary with different shape indexes (see Fig. 3-8).

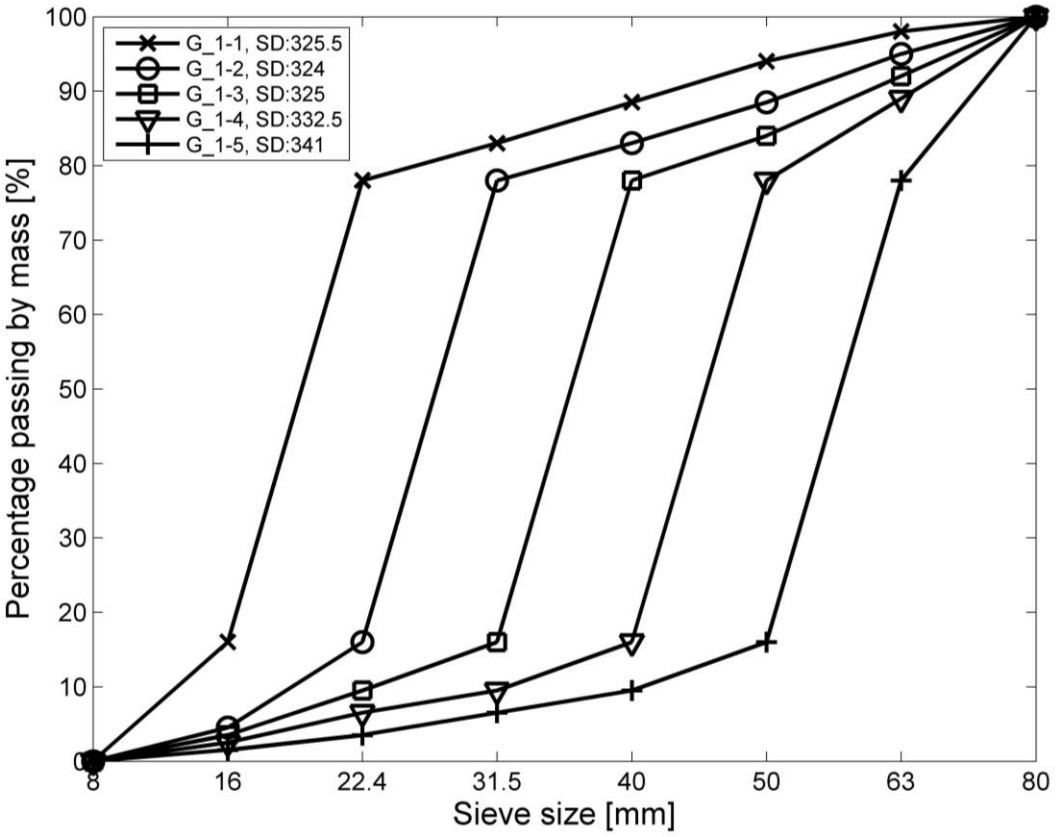

Fig. 3-6. Size distribution curves of database group one with changing mean sizes

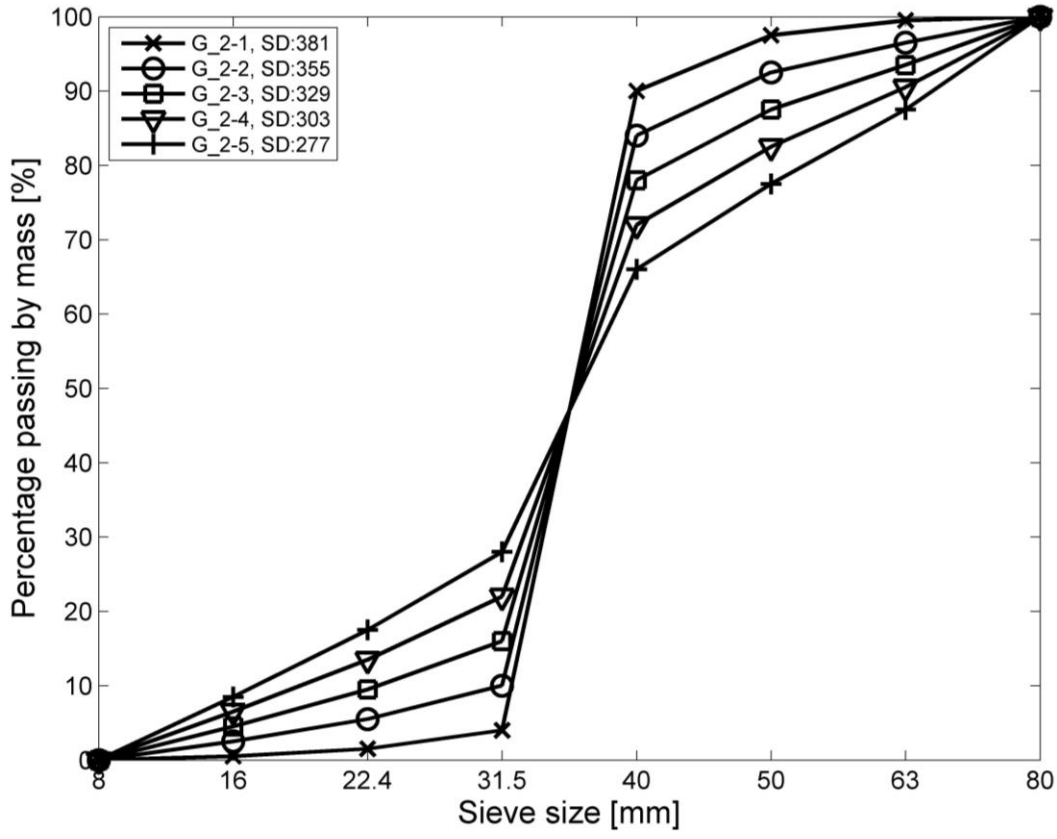

Fig. 3-7. Size distribution curves of database group two with changing size distributions

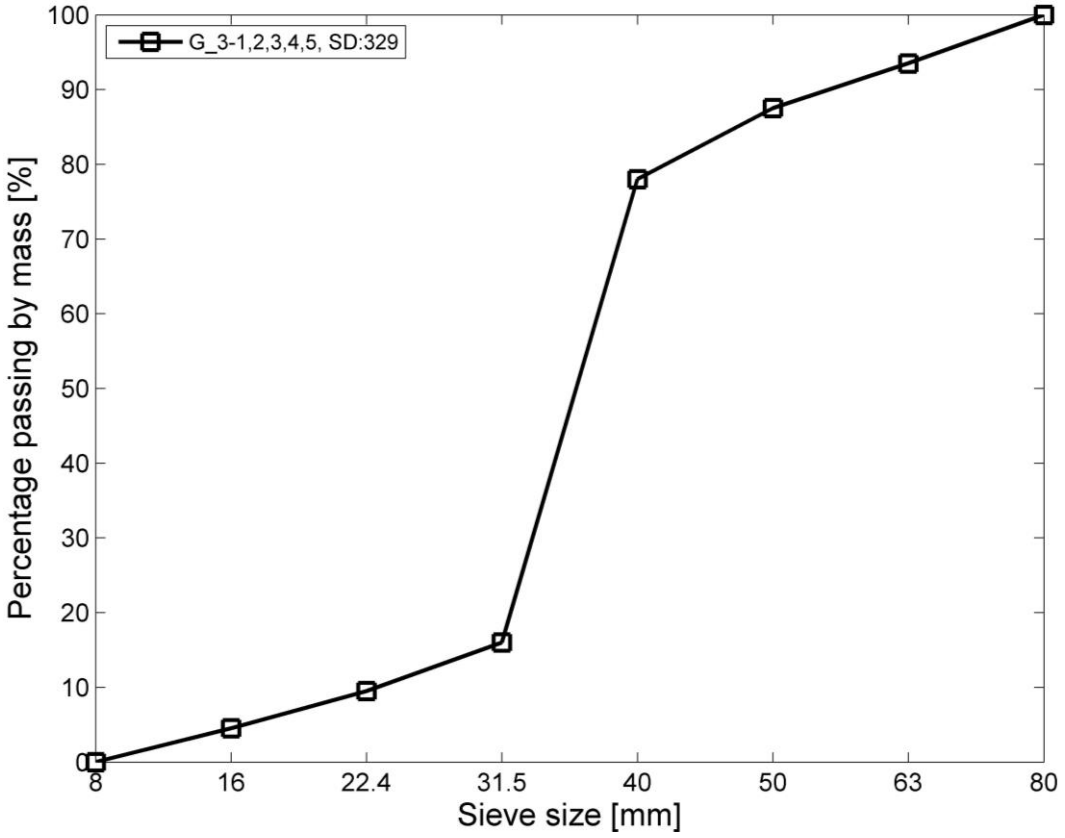

Fig. 3-8. Size distribution curves of database group three with changing shape indexes

Using these 15 form databases, the effect on mechanical behavior of ballast aggregate by changing mean size, size distribution and shape distribution can be studied in further DEM simulations. To quantify the degree of size distribution, e.g., the diversity of the sizes, the parameter Size Diversity (SD) is proposed and calculated as following:

$$SD = \sum_{i=1}^{8} |f(i) - 50| \tag{3.3}$$

where $f(i)$ is the percentage passing by mass of a certain sieve size of a certain ballast aggregate (e.g., for G_1_1, $f(2) = 16$, $f(3) = 78$, see Table 3-1 and Fig. 3-6). The SD values of the five form databases of group one stay almost the same (around 330) while the ones with the databases group two are changing from 227 to 381.

3.5 Validation of the generator by comparing the objective and generated parameters

In this section, validation of the ballast random form generator is performed. Form aggregates are generated. 9 randomly picked generated forms of each form database are illustrated in Fig. 3-9. The generated parameters, which are calculated based on the generated form aggregates, are compared to the objective ones.

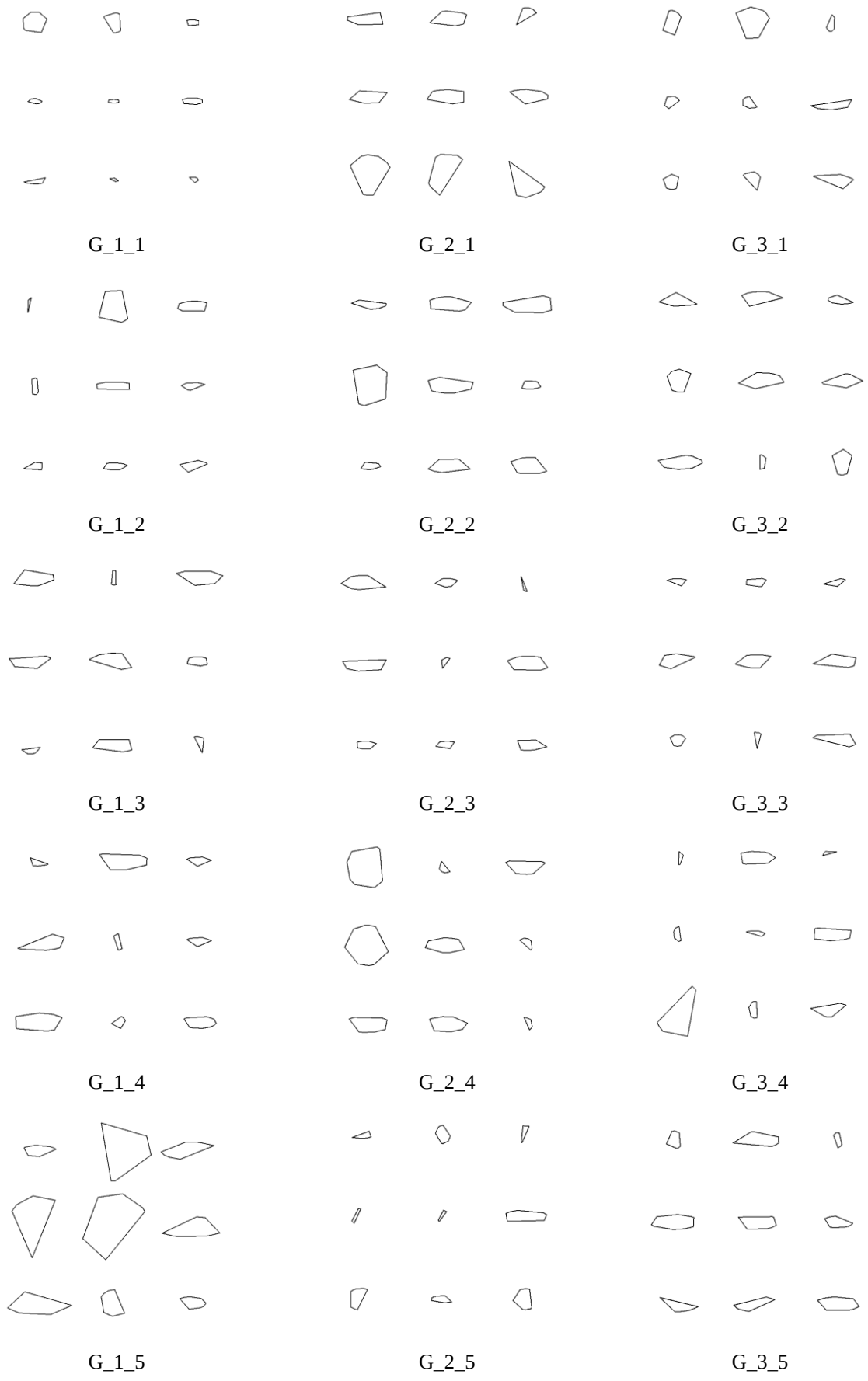

Fig. 3-9. The form databases (only 9 randomly picked particles from the aggregates are demonstrated)

Fig. 3-10, Fig. 3-11 and Fig. 3-12 demonstrate the objective and generated grading curves of the five form aggregates. It is shown in the figure that the grading curves of the generated form aggregates fit very well to the objective ones. Furthermore, some generated grading curves (e.g., G_1_1, G_2_5) fit better than others. It is because these form databases have more particles among other databases (see Fig. 3-13). Since the algorithm judges the mass adequacy by comparing the current generated mass to the objective mass of a certain form group, the final generated mass of this group will always exceed its objective mass because of the last generated particle in the group, which causes the difference. If an aggregate with more particles is being created, the difference will be attenuated.

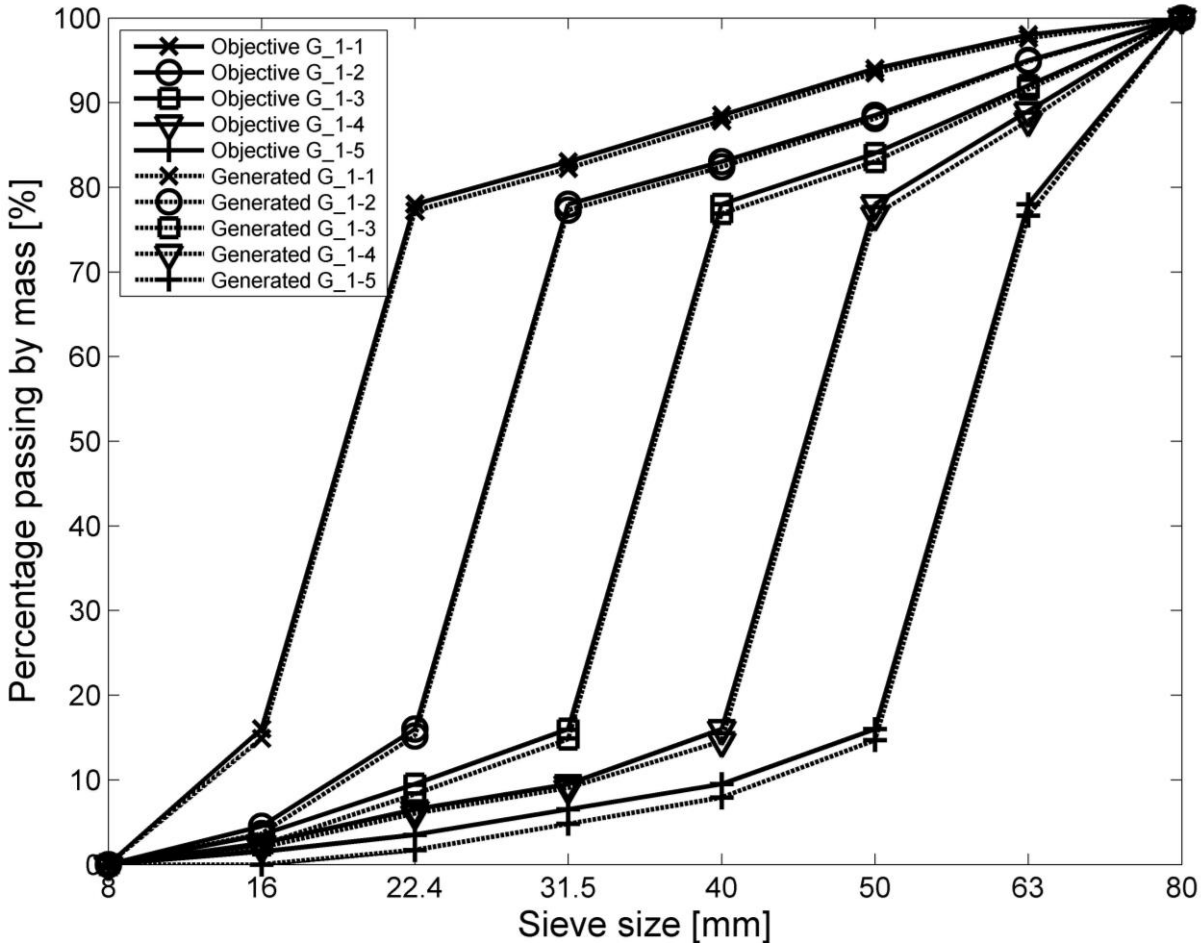

Fig. 3-10. Grading of the objective and generated aggregate (group 1: varying mean sizes)

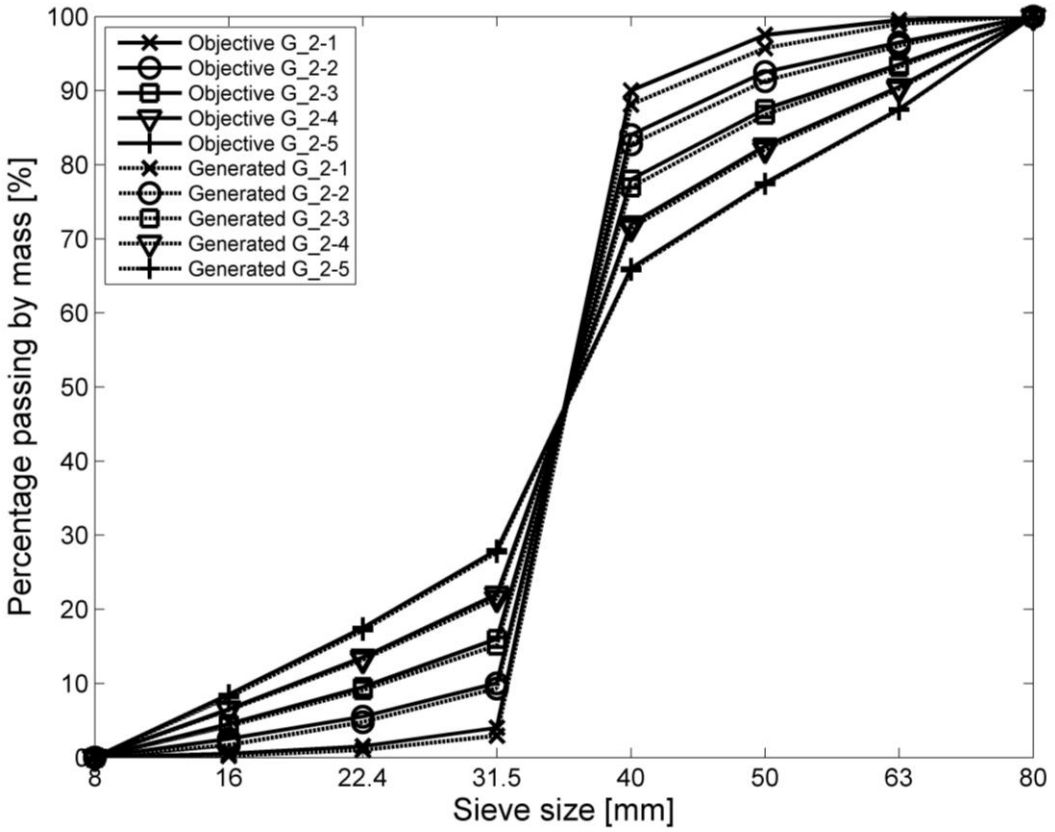

Fig. 3-11. Grading of the objective and generated aggregate (group 2: varying size distributions)

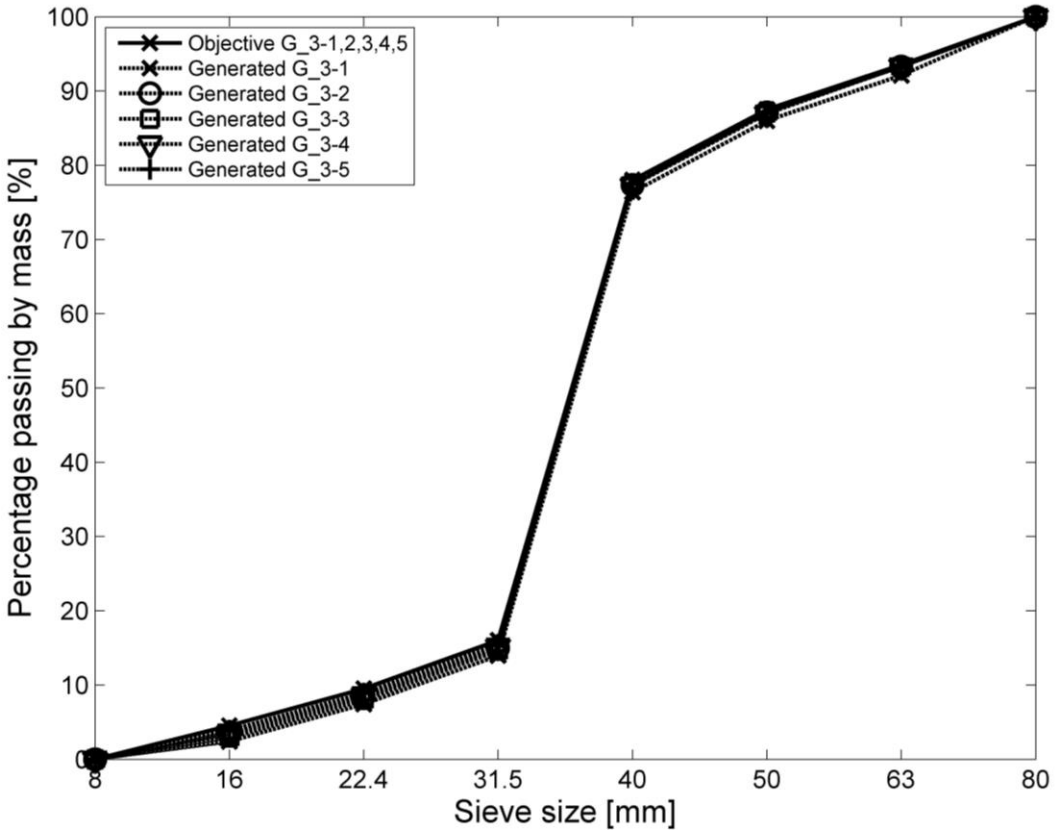

Fig. 3-12. Grading of the objective and generated aggregate (group 3: varying shape index)

Fig. 3-13 shows the generated number of particles of each form database. It can be seen in the figure that the form databases G_1_1, G_2_5 and G_3_5 have the most generated particles respectively in each database group. For G_1_1, its grading line is left most among other databases in the group (see Fig. 3-10), meaning the particle size of this grading is generally smaller. For G_2_5, its grading line is the most flattened (see Fig. 3-11), meaning there are the most number of small particles in this form database. The grading curve of G_3_5 is basically the same as other databases (see Fig. 3-12). However, the shape index of this database is the highest comparing to other databases in group 3 (see Table 3-1), meaning that there are less rounded ballast stones and more flat-shaped ballast stones in the database, which results in a higher number of particles.

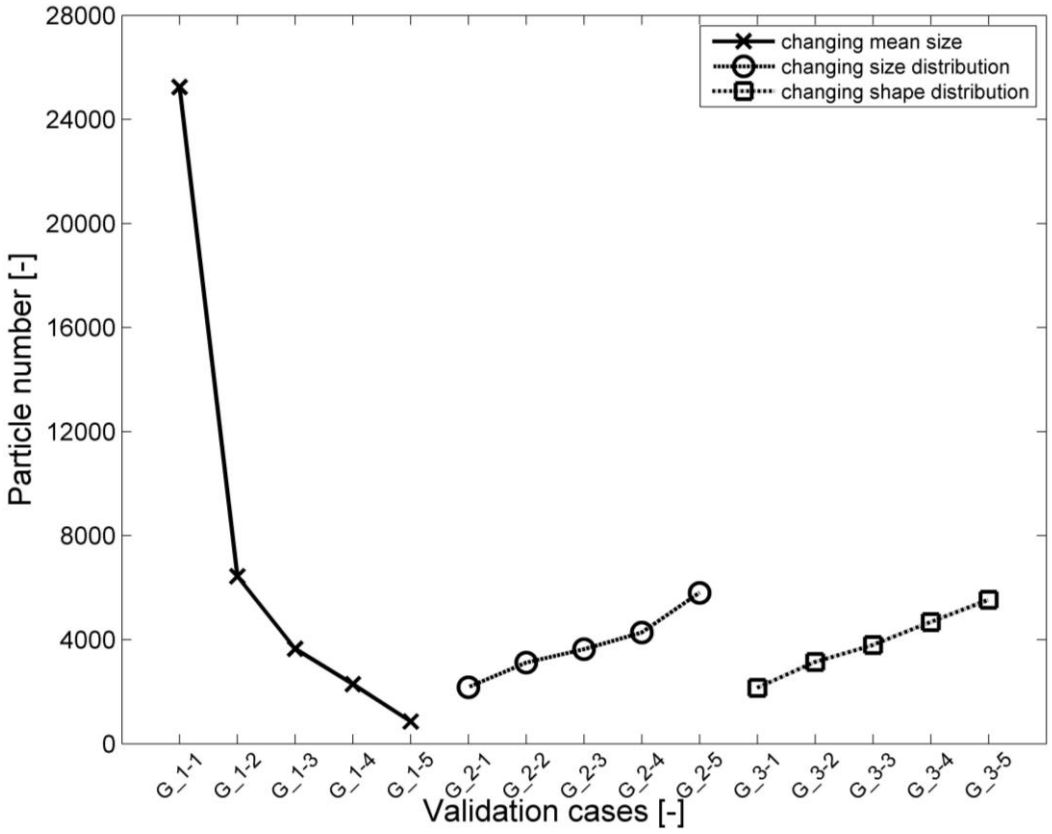

Fig. 3-13. Particle numbers

Fig. 3-14 and Fig. 3-15 illustrate the objective and generated shape and mass parameters of the form databases. Generally speaking, the more particles there are in an aggregate, the less difference it will cause between the objective and the generated parameters. The particle length results bigger difference than other parameters (see Fig. 3-16). The reason is that the long particles are normally proportionally small

in an aggregate (in this study, only 1% of the total mass), making this parameter more sensitive comparing to other ones.

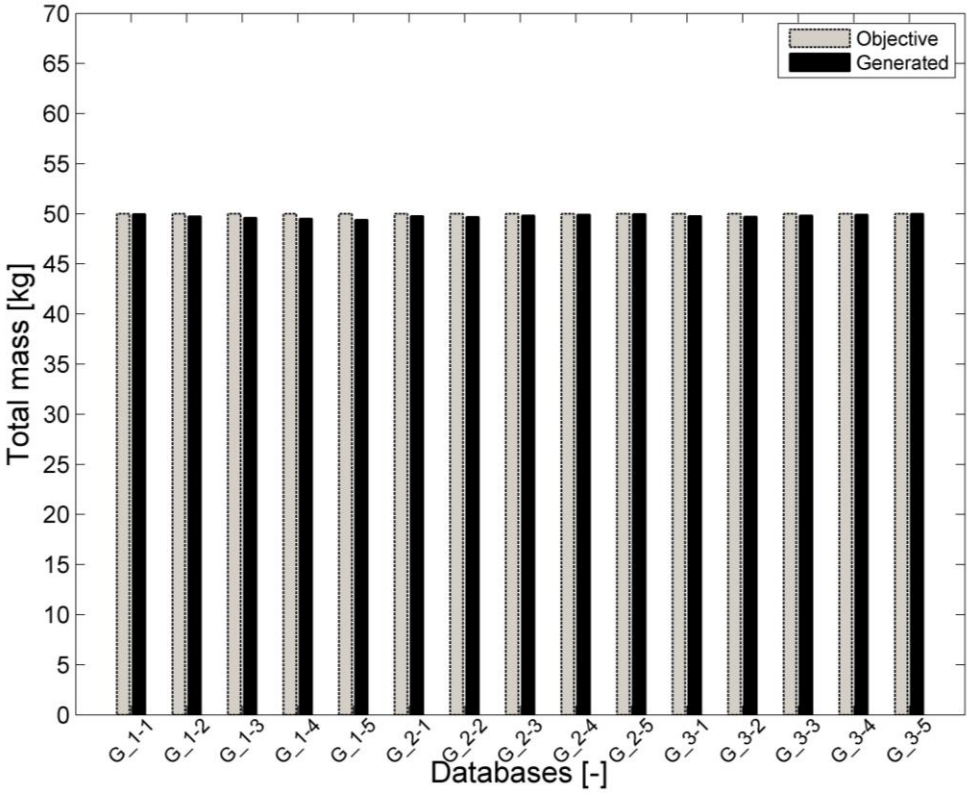

Fig. 3-14. Total mass

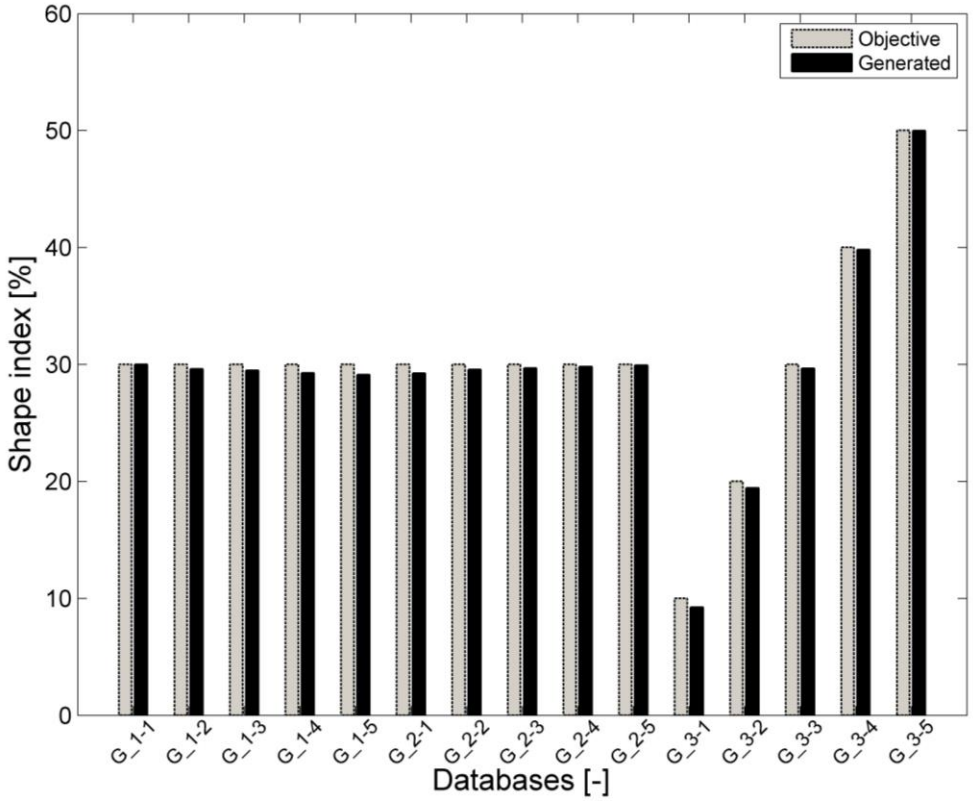

Fig. 3-15. Shape index

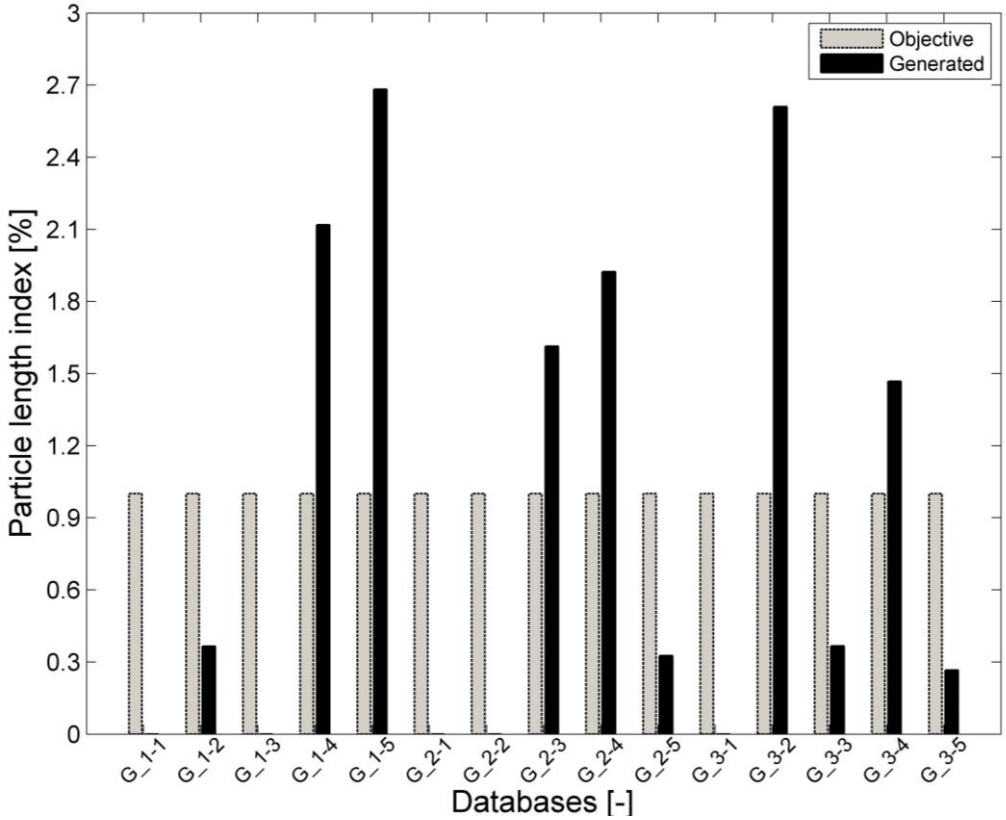

Fig. 3-16. Particle length index

4 Establishment, calibration and parametric study of the DEM calibration model

The DEM based simulation is a decent tool to investigate the mechanical behavior of ballast stone. In this chapter, the DEM calibration model is proposed. The modeling parameters are calibrated by the box test, which is firstly introduced in this chapter. Afterwards, the modeling process of the DEM calibration model, which serves for the purpose of the calibration of the DEM parameters, is expatiated in detail. Later on, a parametric study of two crucial DEM parameters using the calibration model is performed. At last, simulative quantification methods of the mechanical behavior are proposed, two simulation cases are performed to demonstrate the methods.

4.1 The box test

In this study, the simulation model is calibrated by the settlement of the ballast aggregate in a box test, which is performed by MPA and IEV at the University of Stuttgart [48,49]. The box test is a small-scaled test comparing to the full-scaled test for the investigation of the mechanical behavior of a ballast aggregate [50]. In the test, ballast stones are dumped into a container and acted upon by static or dynamic loading. The test is usually performed to investigate the change of the mechanical behavior of different ballast aggregates under the same loading pattern. It also serves as a calibration tool for simulation models due to its convenience and low cost.

In this study, a steel cylinder, which is with a height of 22 cm and a diameter of 34 cm, is manufactured and employed as the container (see Fig. 4-1, a). The ballast samples investigated in the test are obtained from the Stuttgart public transport operating company SSB AG. Based on the specifications of the European standards [7–10], several properties of a ballast aggregate should be tested and a report should be generated to identify the aggregate. The report contains information such as gradation, shape distribution, raw density, Los-Angeles coefficient of the ballast aggregate. However, for this study, only the research-related information, i.e., the geometrical categorizes and raw density, is taken into consideration (see Table 4.1, for more detailed explanations of the categories and the indexes see also [7–10]). This geometrical information will be also used for generating a ballast form database using the generator proposed in chapter 3, which is named as the database “the box test”, and will be used in the establishment of the DEM calibraion model later on. In

the test, 200 ballast stones are randomly selected as the test sample from the aggragation, and manually placed in the cylinder one by one in order to form a compacted packing. Some of the ballast stones are painted in yellow so that their breakage behavior such as abrasion and crushing can be studied after the loading process (see Fig. 4-1, b and c). The seleted ballast stones are composed roughly of 70% hard rock (e.g., basalt, granite) and 30% soft rock (e.g., limestone). To further compact the test sample, three pre-loading processes with the stactic loading of $10kN$, $20kN$ and $30kN$ are firstly performed. Afterwards, the test sample is acted upon by a sinusoidal dynamic force with a maximal value of $45kN$ and a minimal value of $15kN$ for 10,000 steps (see Fig. 4-2, a. Note that only 100 steps are demonstrated, otherwise the curve would be too crowded to be discerned). In order to better demonstrate the relationship between the settlement of the test sample and the loading steps, the position of the pressing plate by $30kN$ of every loading step was extracted (see Fig. 4-2, b). It is demonstrated in the figure that the settlement accumulates faster in the beginning than the latter loading steps. This settlement of ballast aggragation will be used for the calibraiton of the DEM model.

Note that the loading element and the pressing plate are not rigidly coupled in the test (see Fig. 4-1, c). It eables the pressing plate to rotate, so that a uniform contact between the plate and the ballast aggregate can be found during the loading process. In this way, the contact force is well distributed and the unrealistic exaggerated local stress of the ballast stones, which arouses extra breakages of them, can be avoided.

a: the empty cylinder b: without the pressing plate c: with the pressing plate

Fig. 4-1. The box test setup

Table 4.1: The geometrical categorizes and the raw density of the ballast test sample in the box test

Grading category (-)	Shape index (-)	Particle length category (-)	Flakiness index (-)	Raw density (kg/m^3, soft / hard)
G_{CRB} B	SI_{RB} 5/30	L_{RB} B	FI_{RB}35	2620 / 2850

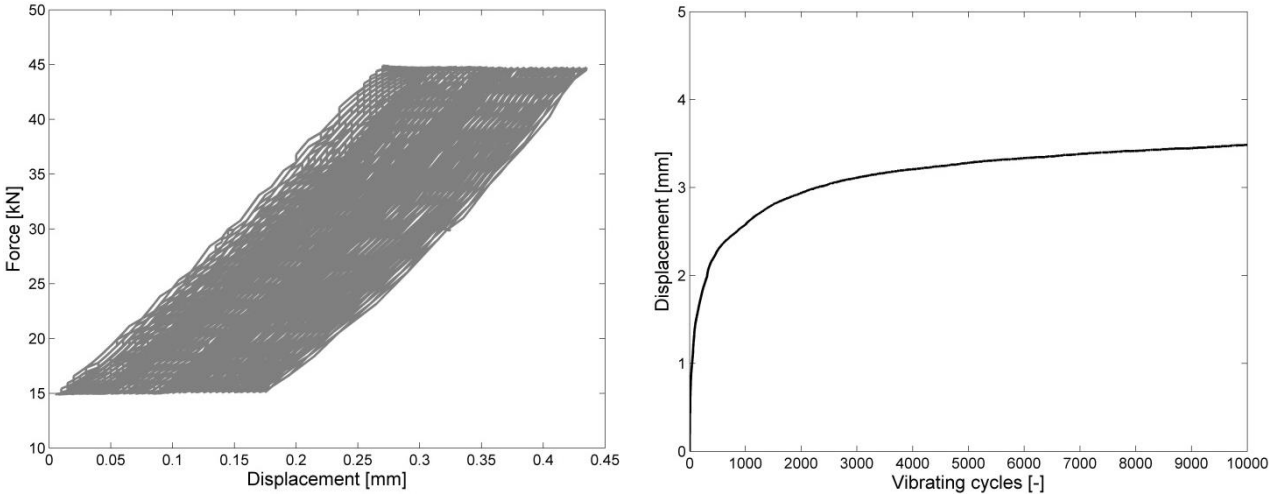

a: the dynamic loading b: settlement of the test sample

Fig. 4-2. The dynamic loading and accumulated settlement of the test sample in the box test

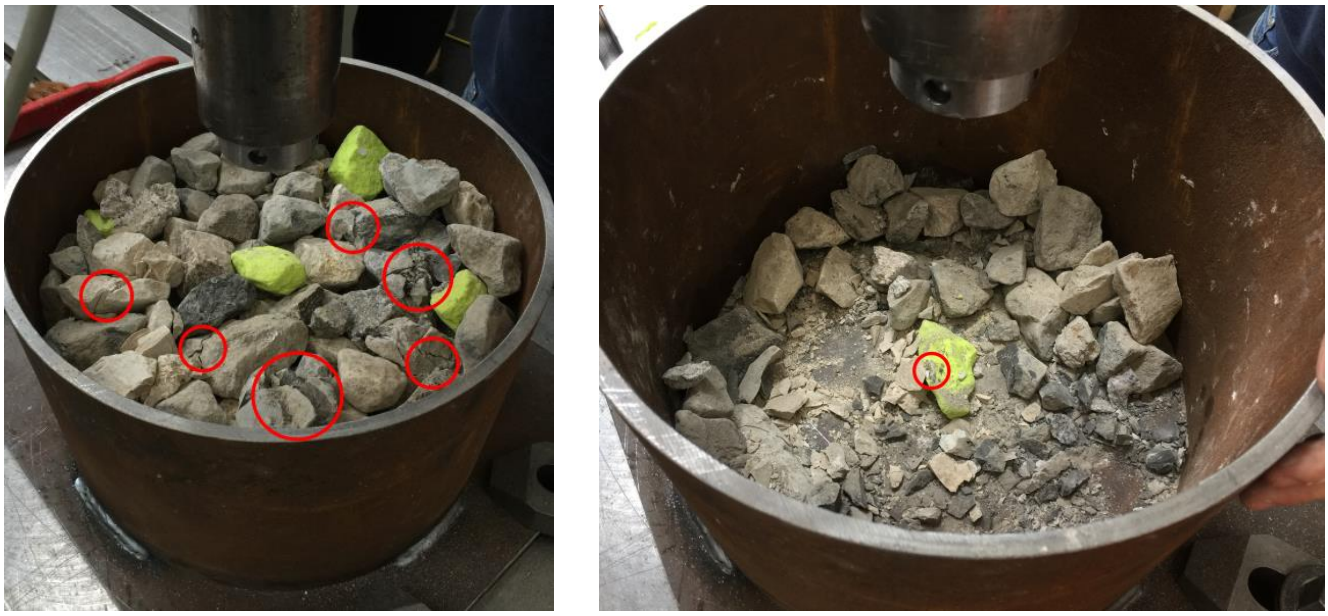

a: breakage on the surface b: ballast fragments settled down to the bottom

Fig. 4-3. Ballast aggregate with breakage after loading

Fig. 4-3 shows the ballast stones after the loading process. The red circles in the left figure mark the breakages caused by the loading. The number of breakage is comparably small to the total ballast number. However, as shown in the figure on the right

side, the fragments and dusts produced by the loading are notable. These remains are not only a result of the breakage but also the abrasion, as the marked area on the colored stone.

4.2 The modeling process of the DEM calibration model

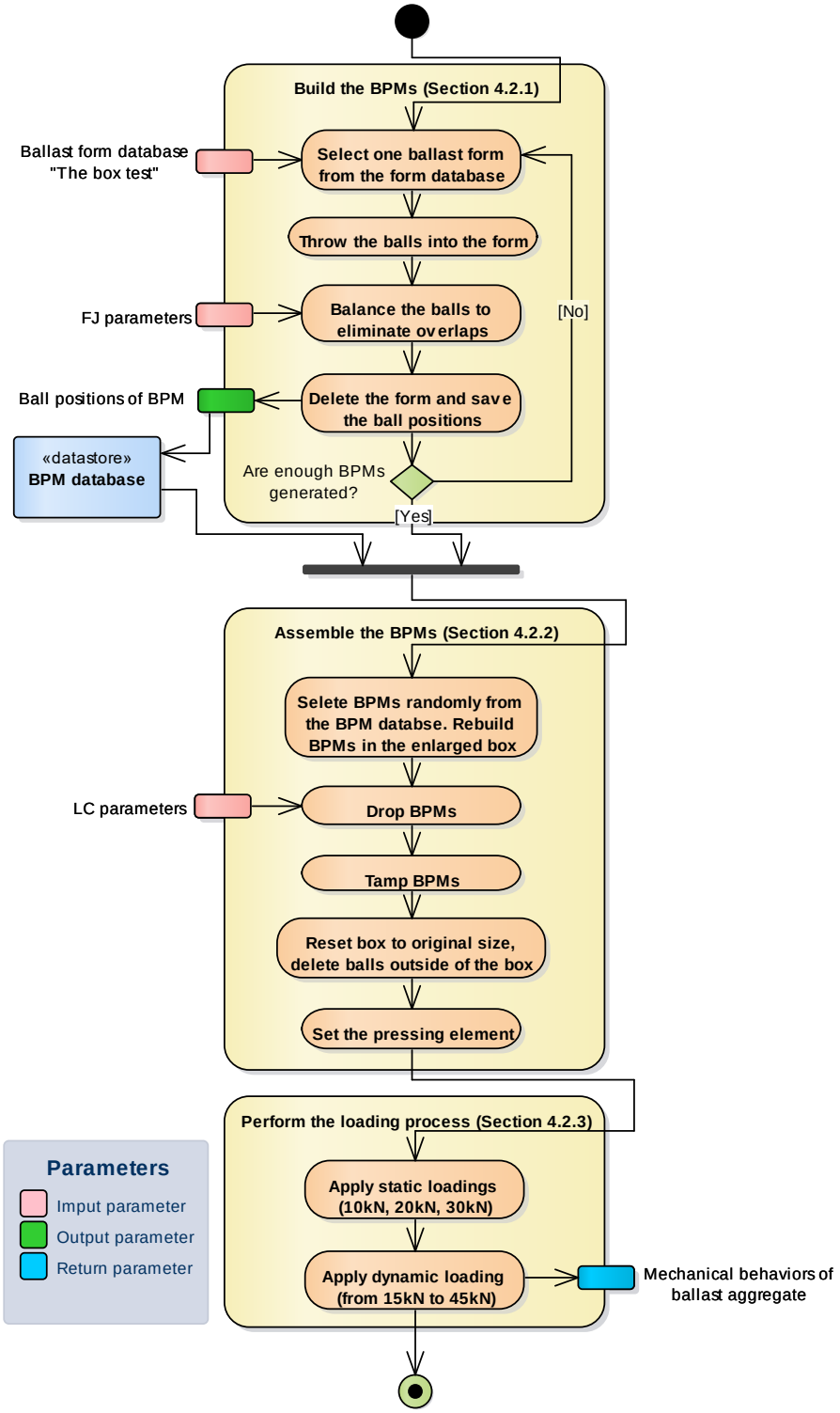

Fig. 4-4. The modeling process of the DEM calibration model

In this study, the DEM calibration model is established by using the software PFC. The model is a duplicate of the box test described in the section above, where the ballast stones are simulated by BPMs. The modeling process can be roughly divided into three steps: first, building of the BPMs; second, assembling of the BPMs; third, loading process (see Fig. 4-4). Important to note is that the model is established in 2D. The reason to do so is expatiated in section 4.3.

4.2.1 Building of the Bonded Particle Models (BPMs)

To simulate the box test, the ballast stones have to be firstly created in the simulation. In this study, the ballast stones are simulated by using the BPMs, where the bonds between the balls are described by the FJ model. A ballast form database, i.e., the form database “the box test”, is created using the geometrical parameters of the ballast aggregate of the box test listed in Table 4.1 by the form generator expatiated in chapter 3. Ballast stone representatives are created and used in further modeling steps.

The simulated ballast stones are created by means of the material-modeling support. However, currently the material-modeling support can only generate test specimens with regular shapes (e.g. rectangle and circle in FISHTank version 20). Specimens with irregular shapes such as ballast stones cannot be created and investigated. Nonetheless, it is crucial to mimic the shape of individual ballast stone in the simulation, since its irregularity ensures the interlocking and stabilization of the ballast aggregate, guaranteeing a much more realistic force-displacement response [33].

In this study, the material-modeling support is improved so that the BPMs, with user-defined specimen-liked angular shapes (polygons), can be generated and tested. This goal is achieved by editing the FISH functions in the version of FISHTank (FISHTank 20, fistPkg20) to expend the user-defined shape functionalities. With the purpose of using this improvement for subsequent versions of the FISHTank, the damage of the original structure of the FISHTank is avoided. For each function that needs to be improved, the original function is taken as the basis and a new function is created outside the FISHTank. These newly designed functions will be called only when a BPM with a user-defined shape is to be created.

Comparing to regular shaped BPM, the major difference of using a polygon shaped BPM is the calculation of its area and cross-sectional length, which are essential for

calculating some key parameters such as the BPM stress and strain and the masses of the particles. For the calculation of the area, the polygon is divided into n triangles (see Fig. 4-5). The area is the sum of area of each triangle:

$$A_{sum} = \sum_{i=1}^{n} \left| \overrightarrow{v_1^a} \times \overrightarrow{v_2^a} \right| / 2 \tag{4.1}$$

where $\overrightarrow{v_1^a}$ and $\overrightarrow{v_2^a}$ are respectively vectors from the two vertexes of a sharing edge on both the triangle and the original polygon to the third point. The third point has to be inside of the polygon to assure a right calculation. The area of a concave polygon cannot be calculated by this method. However, it is reasonable to exclude this case since the chance of a concave ballast stone is very low.

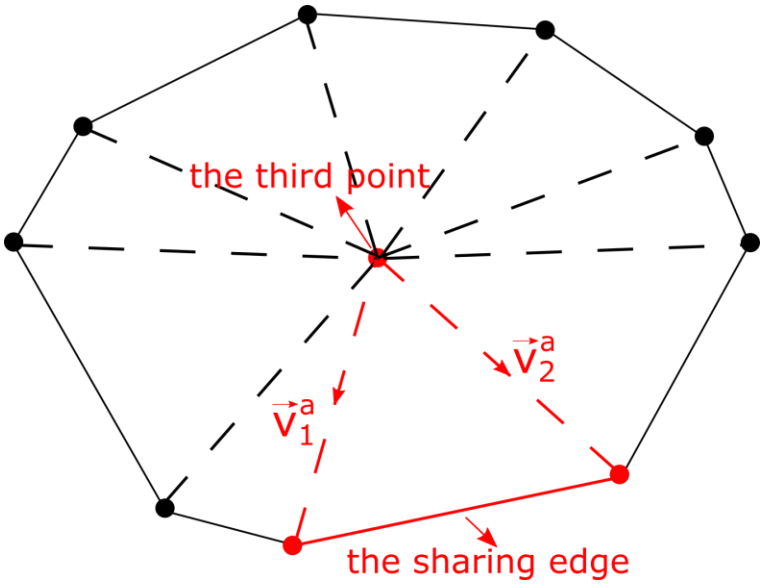

Fig. 4-5. Calculation of the area of a polygon (a ballast form)

To calculate the cross-sectional length, every edge of the polygon is firstly projected to the cross section. The cross-sectional length is then the sum of the projected lengths divided by two.

$$L_{sum} = \sum_{i=1}^{n} \left| cos\theta * L_{edge} \right| / 2 \tag{4.2}$$

where θ is the intersection angle of the edge and the cross section to be projected, L_{edge} is the length of the edge.

The building of the BPMs can be divided into four sub-steps. They are illustrated in Fig. 4-7 and explained in detail in the following paragraph.

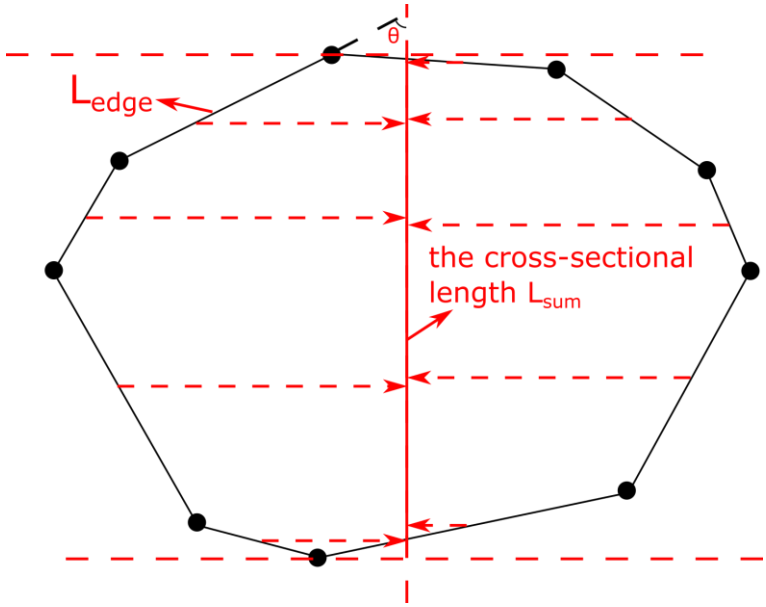

Fig. 4-6. Calculation of the cross-sectional length

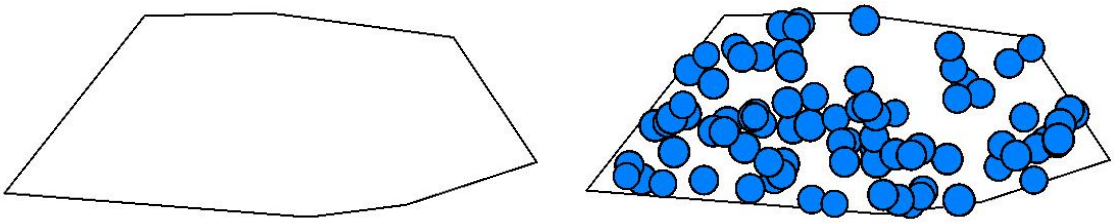

a: subsequent selection of one ballast form from the form database

b: throw the balls into the form

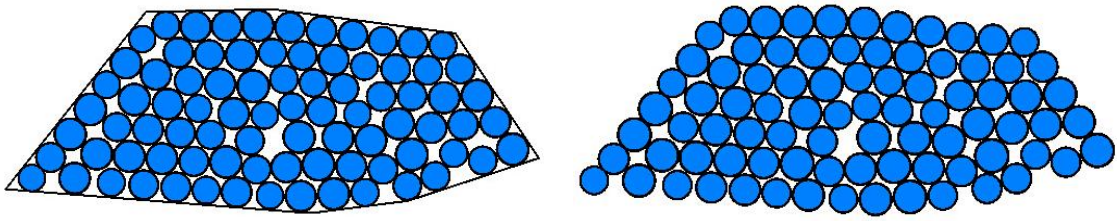

c: automatic balancing process

d: save the positions of the balls

Fig. 4-7. Sub-steps of building the BPMs

a. Select one ballast form from the form database. Transform this geometrical form into the FPC element “wall”
b. Throwing the balls into the generated walls. The balls are not yet bonded by the FJ model and they can have huge overlap between each other. The interaction between the balls in current state is described by the Linear Contact (LC) model in PFC
c. Using the LC model, the more overlap between two balls, the higher contact force (pressure) there will be. The balls with overlaps will be then automatically pushing

each other, until the overlap is eliminated. Here, a citation is set to stop the balancing. If the average force ratio, which is defined as the ratio of the average value of the unbalanced force over all bodies to the average value of the sum of the magnitudes of the contact forces, body forces and applied forces over all bodies, is smaller than 8e-3 (default value from the material-modeling support), the balancing will be stopped

d. The walls, which were used as a confiner of the balls, are deleted. The FJ model is installed between balls. The BPM is further relaxed for 1,000 calculation cycles, meaning the balls are further pushing each other without confining, and the overlaps are further reduced. The positions of the balls are saved for the later usage in the modeling process

The sub-steps a to d are the generation of a single ballast representation. These sub-steps are repeated for each ballast form in the form database. The positions of the balls using every form in the database are saved as a BPM database, which is a precondition of the further modeling steps.

4.2.2 Assembling of the BPMs

Having all the positions of the balls of each BPMs, which are representations of a ballast aggregate fitting a certain shape and size distribution, these BPMs need to be re-read into the simulation and assembled to reproduce the box test. The assembling of the BPMs can be divided into four sub-steps. They are illustrated in Fig. 4-8 and explained in detail in the following paragraph.

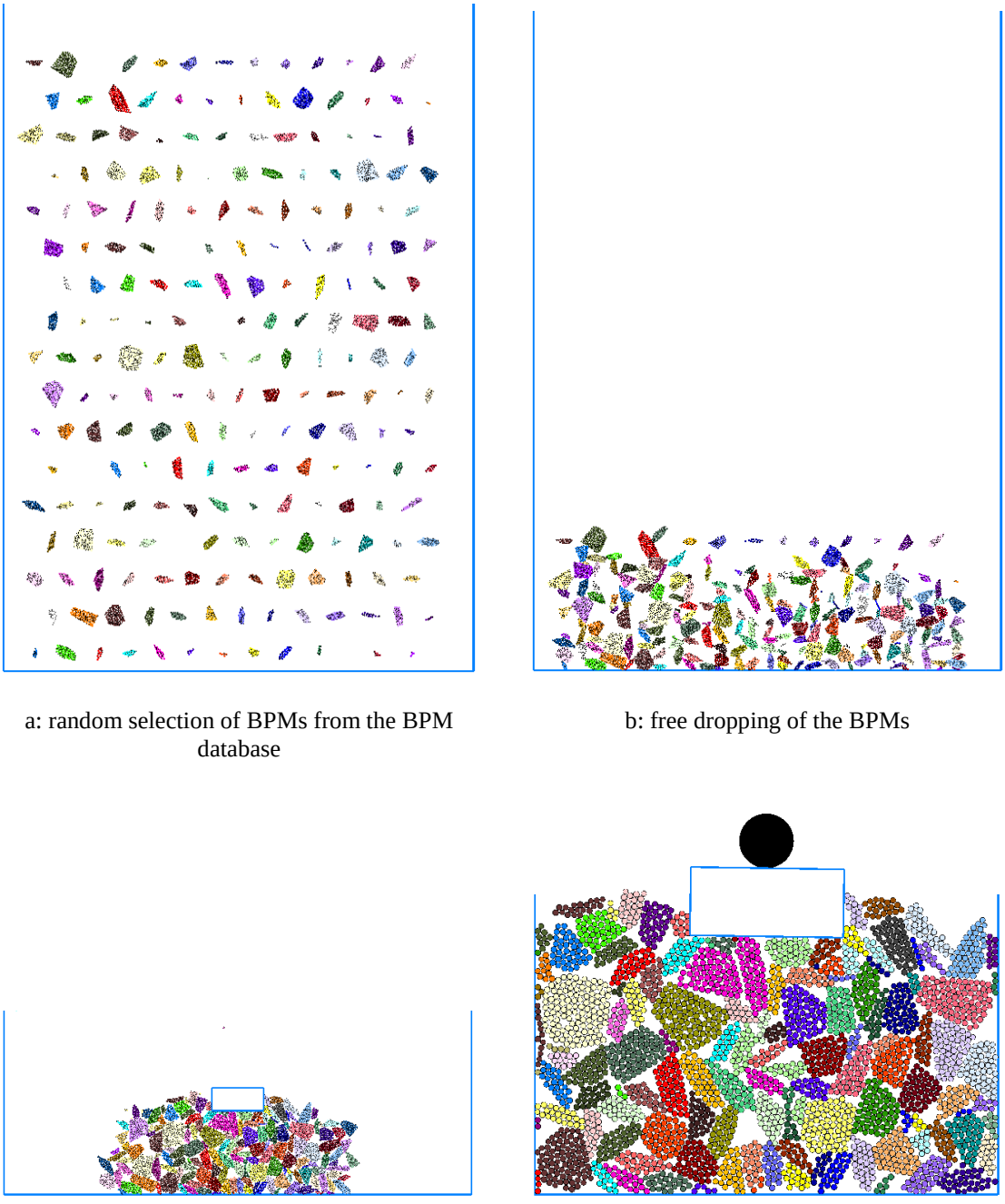

a: random selection of BPMs from the BPM database

b: free dropping of the BPMs

c: tamping of the BPMs

d: container reset and pressing element setups

Fig. 4-8. Sub-steps of assembling the BPMs

a. Random selection of BPMs from the BPM database. Rebuild the BPMs at appropriate positions, which follow the criterion that the interspace should neither be too big, which causes a higher computational time; nor be too small, which arouses an interpenetration of the BPMs
b. The BPMs drop freely under gravity. To accelerate the progress, the acceleration of gravity is increased to 1,000 m/s^2. In this case, to avoid breakage caused by

the drastic dropping, the tensile strength and cohesion of the FJ bonds are correspondingly increased. The dropping process is stopped by a FISH callback function, which monitors the changing of speed direction in vertical direction of the BPM with the highest position. The changing of speed direction indicates that all the BPMs have started to bounce up, and they are already vertically settled

c. After vertically settling, the BPMs should be horizontally settled. A tamping-like process is performed. First, all the balls with the vertical positions higher than 18cm is deleted (the depth of the ballast aggregate in the box test is 18cm). Second, a clump, which is implemented to simulate the pressing plate in the box test, is created at the corresponding position according to the test. The clump is fixed by a FISH callback function, which reset its speed to zero at every calculation cycle, so that the BPMs in the tamping process will not push the clump upwards. The reason to use a clump rather than a wall is that the clump can be freely rotating during the loading process, which is exactly the case of reality. It is essential in the simulation to reproduce this phenomenon so that the stress between the clump and the BPMs can be well distributed and no unrealistic breakage is aroused. Third, the BPMs are given centripetal speeds so that they can assemble at the axis of symmetry and form a compacted aggregate. With the fixed pressing plate, the BPMs will rush against to the plate, consequently eliminate the incomplete contact between the pressing plate and the ballast stones, which will cause an instable settlement of the pressing plate in the simulation later on
d. The container was set to be much bigger to give enough space of the process of BPM dropping and tamping. In this sub-step, the container is reset to the original dimension in the test. First, the balls, which fall out of the original dimension of the container, are deleted. Second, the container is reset to the original dimension, where the bottom of the container is segmented into 20 walls, which is beneficial for the research on the force propagation angle later on. Third, the pressing element is simulated by a ball and is placed on the top of the clump. The purpose of using a ball for loading is that the force addressed on the ball can be easily monitored during the loading process. Fourth, the model is relaxed by running 10,000 calculation cycles without external loads, so that the internal stress can be eased

4.2.3 Loading process

As performed in the box test, the loading process in the simulation can be divided into the static loading process and dynamic loading process. The loading ball, which is the representation of the loading element in the test, is monitored in aspect of its addressed force and its vertical displacement.

In the static loading process, the BPMs are loaded sequentially to $10\ kN$, $20\ kN$ and $30\ kN$ like how it is in the test. To each individual load target value, at every 10,000 calculation cycles, the mean value of the sum of the forces addressed on the pressing ball in the previous 10,000 calculation cycles will be calculated. If the relative error of the mean value to the target value is higher than 2.5%, the static loading will continue to the next 10,000 calculation cycles and the relative error will be checked again; otherwise, it is considered that the BPMs are stably pre-pressed, and the static loading process will move on to the next target loading, or will be stopped if it is already the final loading target (i.e., 30kN, see Fig. 4-9).

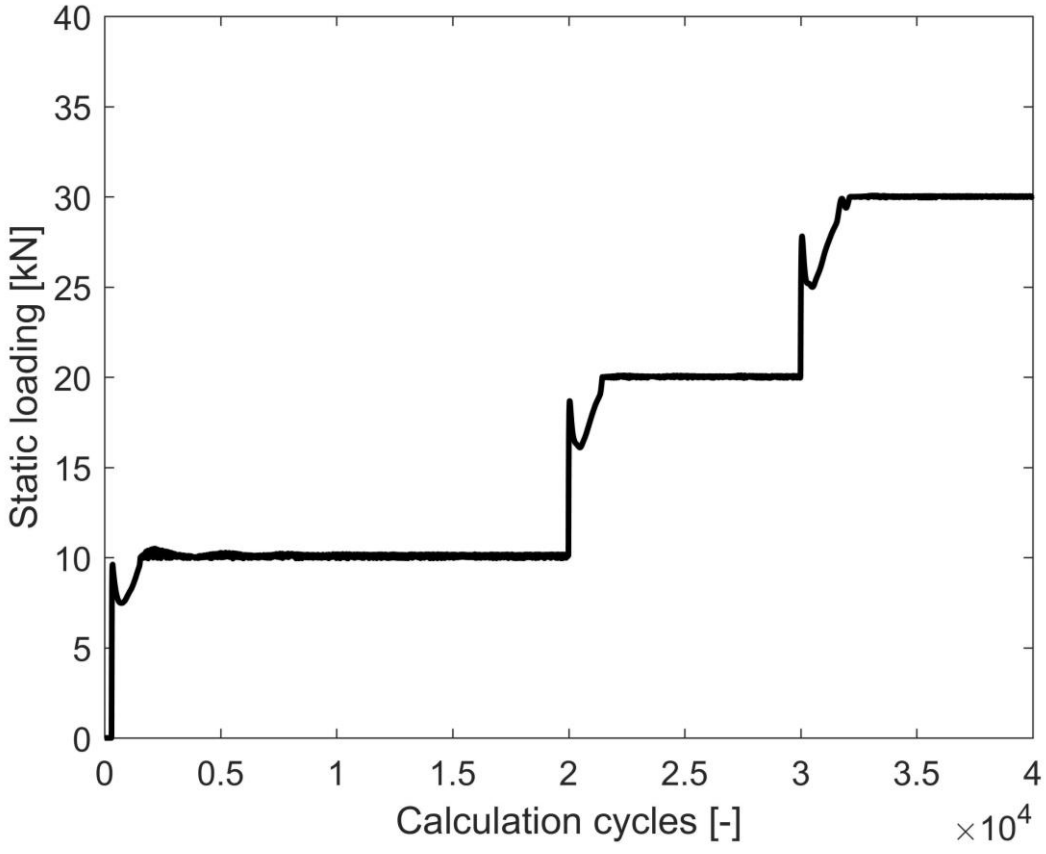

Fig. 4-9. The static loading process

In the dynamic loading process, the BPMs are loaded under a cyclic dynamic force with a maximal value of $45\ kN$ and a minimal value of $15\ kN$. A FISH callback func-

tion is set up for monitoring the force acted upon the loading ball. If the force exceeds either of the boundary forces, the speed direction of the loading ball is changed. The speed of the ball is set to be decreasingly changed under two considerations: first, when the force of the ball exceeds either one of the two boundary limits and the speed direction is just changed, a higher speed of the ball is needed to accelerate the loading or unloading process in order to increase the computational efficiency; second, when the force of the ball is about to reach either one of the two boundary limits, the speed of the ball needs to slow down to prevent a strike to the BPMs. Considering the computational intensity of the simulation, only 1,000 loading steps are performed in the simulation instead of 10,000 loading steps in the test (see Fig. 4-10. Note that only part of the dynamic loading is presented. Otherwise the loading curve would be too crowded to be seen clearly).

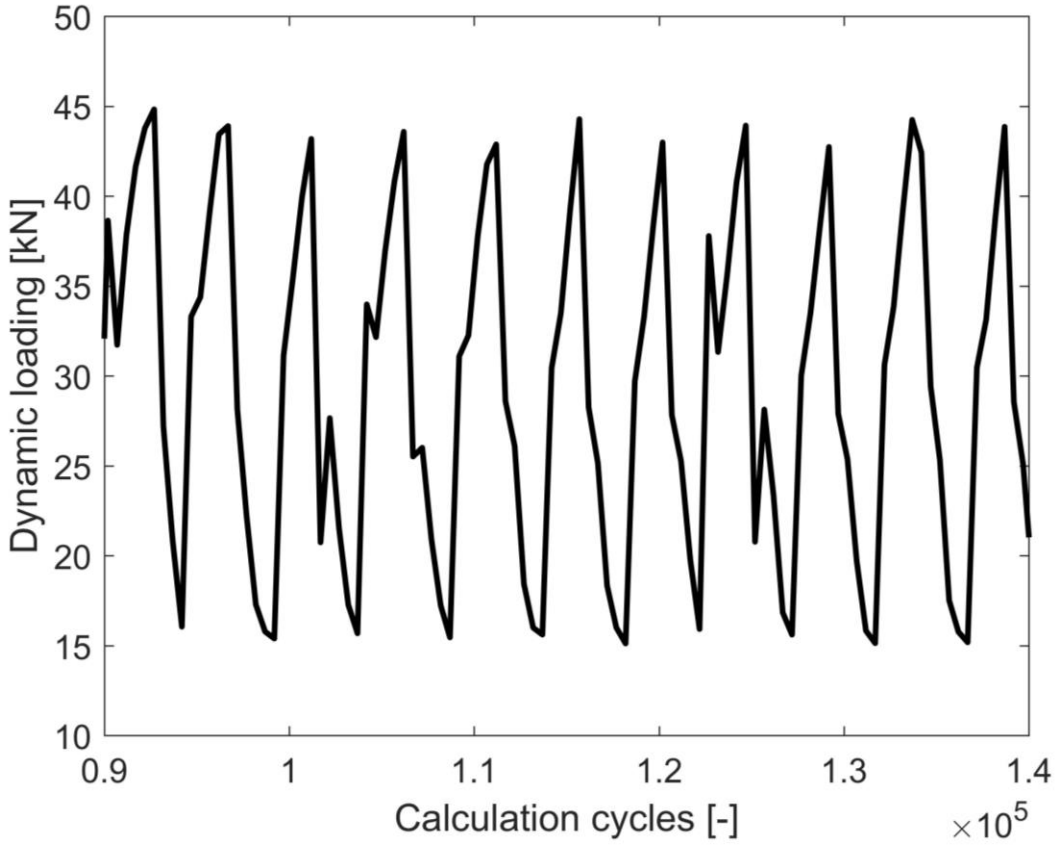

Fig. 4-10. The dynamic loading process (partially demonstrated)

FISH functions are defined to calculate the mechanical behavior of the simulated ballast aggregates. During the dynamic loading process, these functions are called at the end of every loading cycle, so that the changing of the mechanical behavior can

be monitored. Detailed description for calculating the mechanical behavior please see section 4.5.1.

4.3 Model calibration

With the generated ballast form databases, the simulative ballast stones can be created. In this study, the ballast stones are simulated by the BPMs, where the bonds between balls in each BPM are defined by the FJ model (see section 2.2.2.3 for detailed justifications). Except for the simulation of one single breakable ballast stone, the simulation of interaction between ballast stones is also crucial. The LC model, which provides linear and dashpot components to simulate the linear elastic (no-tension) frictional behavior and viscous behavior between the modeling components (i.e., ballast stones, the pressing plate, the pressing element and the container), is employed [13]. Using the form database “the box test”, which is with the same geometrical properties and hard-soft rock ratio of the testing sample, the calibration of the model parameters is performed by matching the settlement of the aggregates from the test and simulation. The calibrated parameters are listed in Table 4.2. Considering the computational intensity of the simulation, only 1,000 loading steps are performed in the simulation instead of 10,000 loading steps in the test.

In this study, the material-modeling support is used for setting the relevant properties of the FJ and LC model. Relevant properties such as k_n and k_s are set by effective modulus E^* and normal to shear stiffness ratio κ^* for FJ model, and E_n^* and κ_n^* for LC model (see Table 4.2):

$$k_n := E^*/L, \;\; k_s := k_n/\kappa^*, \;\; with\; L = \begin{cases} R^{(1)} + R^{(2)}, & ball - ball \\ R^{(1)}, & ball - facet \end{cases} \tag{4.3}$$

Table 4.2. The calibrated modeling parameters

	Parameter	Description	Value (hard rock / soft rock)
FJ model	MP	mass proportion	0.7 (-) / 0.3 (-)
	ρ	density	2950 (kg/m^3) / 2800 (kg/m^3)
	g_i	installation gap	$(D_l^{(j)}/2) * 0.4$ (m)
	$(\phi)^+_{\{B,G\}}$	bonded and gapped fraction	{1.0, 0.0} (-)
	g_0	initial surface gap	0.0 (-)
	N_r	number of FJ elements	1 (-)
	C_λ	radius multiplier code	0 (-)
	λ_v	radius multiplier value	1 (-)
	E^*	effective modulus	2.5e9 (Pa) / 4.0e9 (Pa)
	κ^*	normal to shear stiffness ratio	2.5 (-) / 2.0 (-)
	μ	friction coefficient	0.5 (-)
	F_{str-co}	strength and cohesion scaling factor	3.5 (-) / 3.5 (-)
	σ_c	tensile strength	F_{str-co} * 5.4e5 (Pa) / 3.0e5 (Pa)
	c	cohesion	F_{str-co} * 60.0e5 (Pa) / 9.0e5 (Pa)
	ϕ	friction angle	0.0 (°)
LC model:	E_n^*	effective modulus	5.0e9 (Pa)
	κ_n^*	stiffness ratio	2.5 (-)
	μ_n	friction coefficient	0.7 (-)

In Table 4.2, g_i is the installation gap. If current gap between particles is less than g_i, the FJ contact model will be installed. The value of the installation gap is chosen to be in relationship with the particle radius, where $D_l^{(j)}$ is the diameter of the smaller ball of the two contact balls. ϕ_B^+ and ϕ_G^+ are the fractions of initially bonded or gapped FJ contacts to the total FJ contacts (with $\phi_S^+ = 1 - \phi_B^+ - \phi_G^+$ is the fraction of slit FJ contact). ϕ_B^+, ϕ_G^+ and ϕ_S^+ are defined by:

$$\phi_B^+ = n_B/n_{FJ}, \quad \phi_G^+ = n_G/n_{FJ}, \quad \phi_S^+ = n_S/n_{FJ} \tag{4.4}$$

where n_B, n_G and n_S are the number of bonded, gapped and slit FJ contacts and $n_{FJ} = n_B + n_G + n_S$ is the total number of FJ contacts. g_0 is the initial surface gap and it determines whether the initial FJ contact is bonded, gapped or slit ($g_0 = 0$, bonded or slit; $g_0 > 0$, gapped). By choosing the reasonable value of g_0 and the fractions, the initial internal cracks of rocks can be well represented. Since the selected ballast stones are with low porosity, $g_0 = 0$ is used in order to exclude the initial gapped contacts while $\phi_S^+ = 0$ is used to exclude the initial slit contacts. These two aspects assure that, all the FJ contacts are bonded and no initial cracks are inside of the BPM. N_r is the number of interface elements of the FJ bond, whose minimum value is used to reduce the calculation time. When $C_\lambda = 0$, the radius-multiplier value λ_v need to be set to a specified value. $C_\lambda = 0$ and $\lambda_v = 1$ are chosen to simplify the BPM. σ_c is the tensile strength of the FJ bond. If the normal stress σ exceeds the tensile strength, the FJ bond breaks in tension. c is the cohesion, which is used for calculating the shear strength:

$$\tau_c = c - \sigma tan\phi \tag{4.5}$$

where ϕ is the friction angle, which is the ratio of shear stress τ and normal stress σ. If the shear stress τ exceeds the shear strength τ_c, the FJ bond breaks in shear.

For the BPM, the micro-properties such as effective modulus E^*, normal to shear stiffness ratio κ^* and friction coefficient μ_n (both in FJ and LC model) as well as tensile-strength σ_c, cohesion c and friction angle ϕ cannot be directly derived from laboratorial data. They are usually set by a calibration process, in which the macro-behavior of the BPM aggregate, which is influenced by the above-mentioned micro-properties, will be matched to the macro-behavior of the ballast aggregate in standardized test (e.g., the box test). With a comprehensive test data, the correlation between the macro-behavior of the BPM aggregate and the micro-properties used in the simulation model can be investigated.

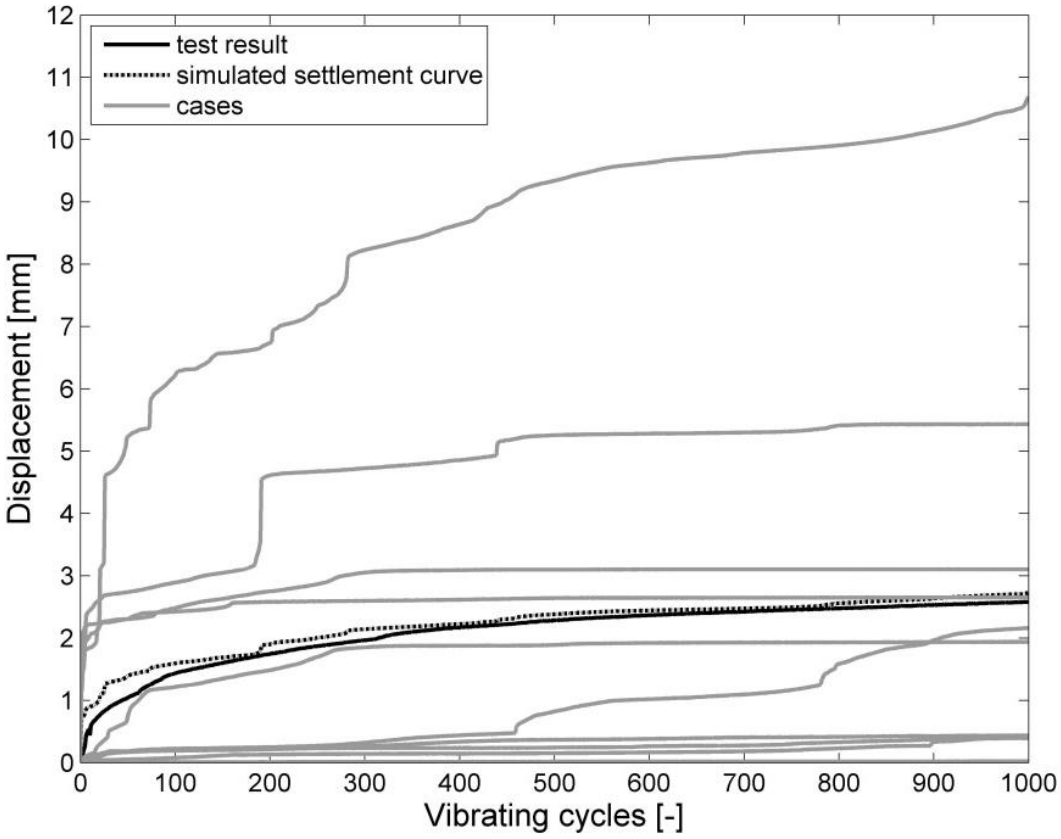

Fig. 4-11. Ballast settlements of simulation cases, their mean value and the test result

The matched settlement curves are illustrated in Fig. 4-11. It is shown in Fig. 4-11 that the simulated settlement curve (the dashed curve) matches with the one from the test (the solid black curve). However, it is important to point out that the simulated settlement curve is the average value of 10 simulation cases[1] (the gray curves), where the modeling parameters are exactly the same, while the results vary greatly. The reason for this difference is that the ballast forms, which are from the same form database, are randomly picked and vary from time to time. Besides, even though the material distribution of the database is fixed, the one of the selected ballast stones for simulations can change (see Fig. 4-12). In this case, the modeling parameters can be considered as calibrated only if enough cases (10 cases in this study) are performed and their mean value of results matches the test result. Only in this way can the randomness be statistically reduced.

[1] Simulation cases: simulation models with the same modeling parameters and the same used form database, but vary due to the random pick of the forms, the materials from the database and the random assembly of the aggregate

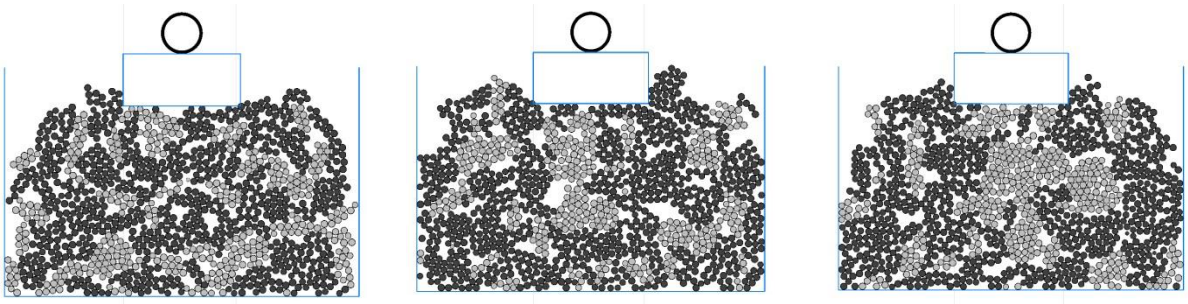

simulation case 1 simulation case 2 simulation case 3

Fig. 4-12. Three simulation cases with different selected ballast forms and materials (black: hard rock, gray: soft rock) from the same ballast form database

Furthermore, even though a tamping-like process is performed (see Fig. 4-8, c) to form a compacted aggregate and eliminate the incomplete contact between the pressing plate and the ballast stones, some void will still show up from time to time, which will cause an excessive settlement of the pressing plate (see Fig. 4-13). Unlike in the test, where the ballast stones are manually placed and the ones under the pressing plate can be manually rearranged to find a balanced and firm contact to the pressing plate, in the simulation, the void is hard to be avoided and adjusted. It is another reason for running multiple cases and getting the mean value as the final result, so that this randomness can be reduced as much as possible.

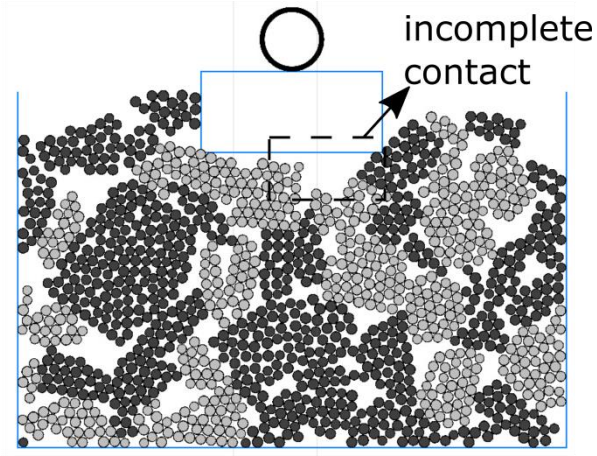

Fig. 4-13. The incomplete contact (the void) between the pressing plate and the ballast stones

In this study, 2D models are used instead of 3D models. Since the ballast breakage behavior is one of the mechanical behaviors to be investigated in this study, the BPM has to be implemented. However, BPM is a very computational intensive model. In every calculation cycle, the status of every bond inside a BPM has to be updated, all the belonging parameters have to be calculated. In 3D models, the simulation pieces and the bonds are geometrically increased comparing to ones in 2D, which results a

much longer computational time for each simulation case. Nevertheless, it might be acceptable if only few 3D cases need to be performed. However, as discussed earlier, multiple cases (10 cases) are required to reduce the randomness of the simulation results caused by random selecting and placing of ballast stones. Besides, there are multiple scenarios (15 form databases) need to be tested so that the optimized scenario can be found. In the end, 150 cases need to be performed. An example case in 3D with breakable ballast models is performed and it takes over five days to finish (see Appendix II). To accomplish all the cases, it would take 750 days, which is unacceptable. If the possibility of investigating breakage behavior is abandoned, namely, if unbreakable ballast models are used, simulation for one case will take two days to finish (see Appendix III). On the contrary, a 2D simulation case needs only 3 hours, which means that only 18 days are needed for the whole simulation work. From the perspective of computing time, 2D model is more preferable.

2D simulation not only saves time, but also provides eligible results. On one hand, 2D simulation result with calibrated DEM parameters fits decently to the test result in this section, and the mechanical behavior of the simulated ballast stones in chapter 5 demonstrates great coherence in trend to the reality. On the other hand, 3D model can also fit the test in a certain extent, but the matching degree is not better than 2D while taking so much higher computing time (see Appendix III). An obvious advantage of 3D simulation is not found in this study. In the end, the key point of this study is to discover the difference of specific mechanical behavior caused by different form distributions of ballast stones, and thus find out the changing trend of the mechanical behavior, so that the optimized ballast aggregate regarding to its form distribution can be found. In this case, since finding the trend is the key point, 2D simulation is already enough.

4.4 Parametric study

The settlement of a ballast aggregate under loading is a result of iterative ballast degradation and position rearrangement. In the simulation, the degradation is governed by the tensile strength and the cohesion of the FJ bonds of the BPMs, while the position rearrangement is controlled by the friction coefficient between the simulated ballast stones. In this section, a parametric study of these modeling parameters is performed to investigate their influence on the settlement of ballast aggregate. 10 simu-

lation cases of each simulation scenario[2] with the same parameter set are performed and their mean value of result is considered as the final result of the scenario so that the randomness discussed in section 4.3 can be reduced.

Since there are two types of materials (soft and hard rock) and two strength related parameters (tensile strength and cohesion) in the simulation, a strength and cohesion scaling factor F_{str-co} is proposed to simplify the parametric study. By multiplying the factor to each tensile strength and cohesion, the simulated ballast stones are proportionally strengthened or softened (see Table 4.2). Simulation scenarios with five values of the factor are performed and the result is illustrated in Fig. 4-14. It is shown in the figure that the accumulated settlement of ballast aggregate increases with the decreasing value of F_{str-co}. It fits the common sense that softer stones will break easier and thus yield higher settlement.

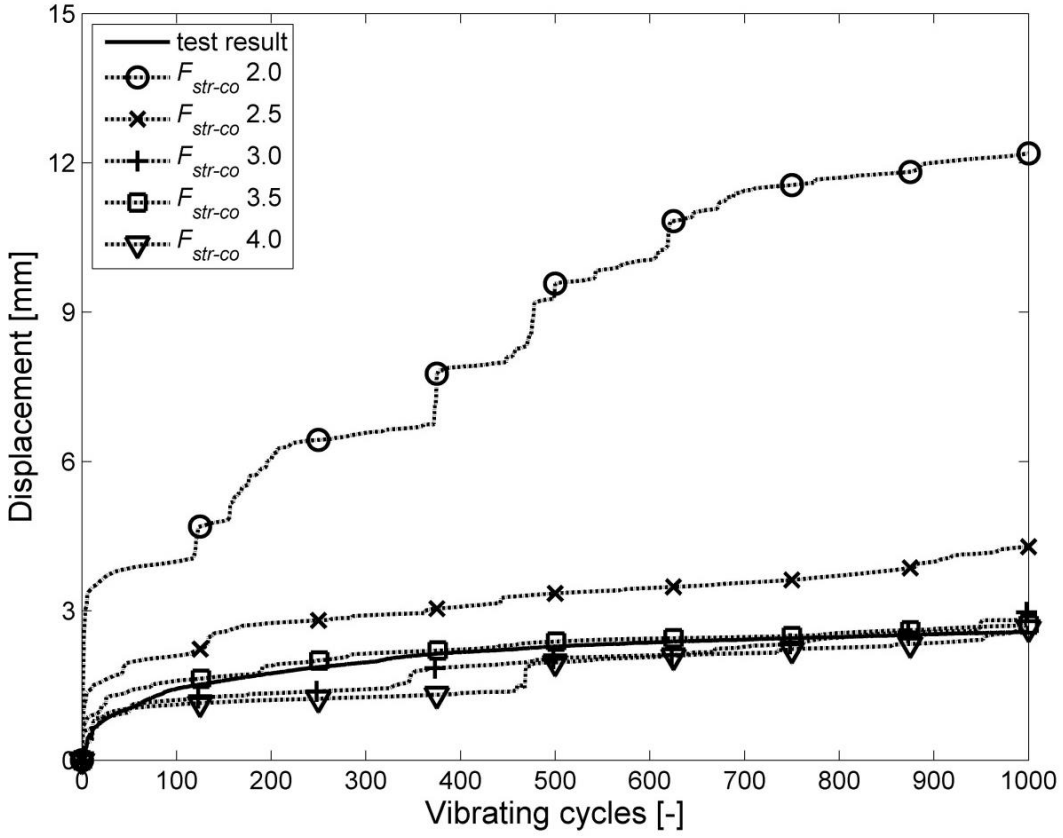

Fig. 4-14. Result of simulation scenarios with changing strength and cohesion scaling factor F_{str-co}

[2] Simulation scenarios: simulation models with different parameter sets or different used form databases.

On the other hand, four simulation scenarios with the changing friction coefficients μ are performed. The higher the friction coefficient is, the higher resistant shear force will be produced, which reduces the lateral relative motion between two simulated ballast stones. The simulation result shown in Fig. 4-15 proves this standpoint, where the model with lower friction coefficient yields higher settlement and vice versa. It is proven by the parametric study that the strength and cohesion scaling factor F_{str-co} and the friction coefficients μ have great influence on the settlement of a ballast aggregate. They should be selected carefully in such type of research.

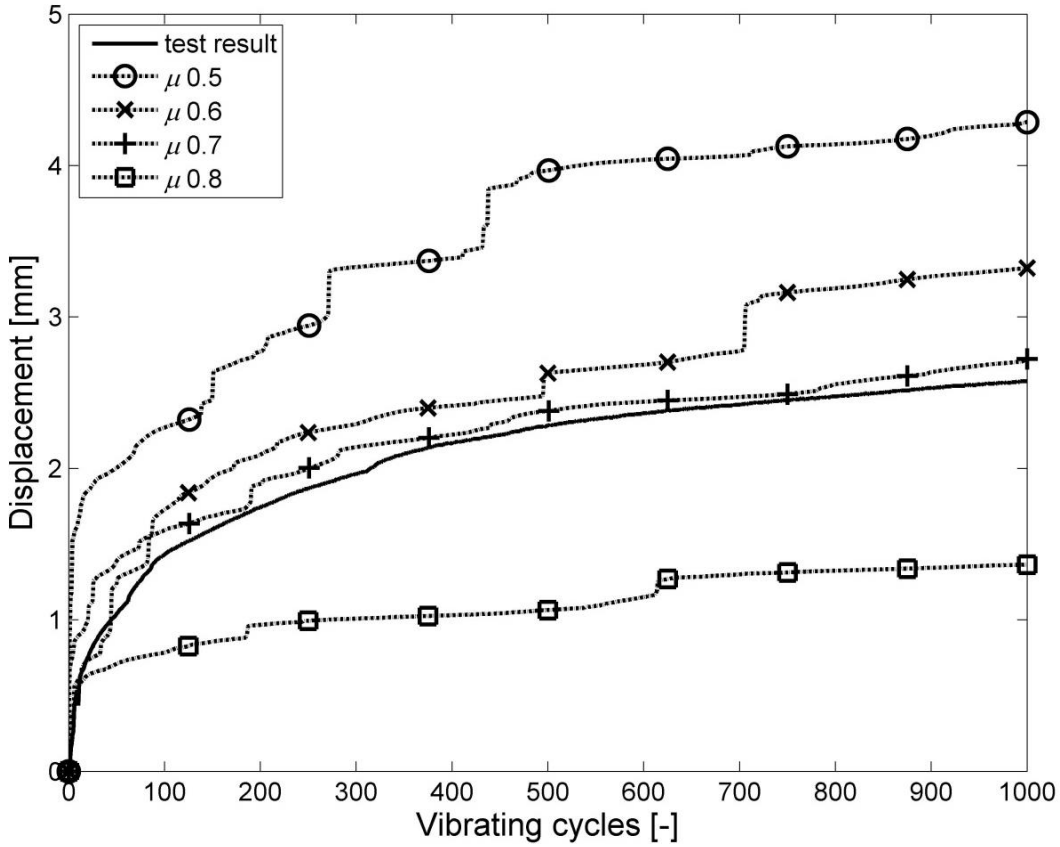

Fig. 4-15. Result of simulation scenarios with changing friction coefficient μ

4.5 Simulative quantification methods of the mechanical behavior

The mechanical behavior of ballast aggregate discussed in this study includes settlement, breakage rate, force propagation angle, void ratio and particle coordination number. Unlike tests, in which the mechanical behavior is time and cost consuming to be evaluated, in DEM simulations, the mechanical behavior can be easily quantified and demonstrated. In this section, according to the definitions of these mechanical behaviors expatiated in section 2.4, their corresponding quantification methods in

the simulation will be firstly introduced. Later on, two typical simulation cases are selected the simulative results of the mechanical behavior.

4.5.1 Simulative quantification methods of the mechanical behavior

The settlement of ballast aggregate in the test is determined by the vertical displacement of the loading element (see section 4.1). In the simulation, as discussed in section 4.2.3, it corresponds to the vertical displacement of the pressing ball (see Fig. 4-8).

The breakage rate is currently not defined in reality. Its definition should be able to show the level of breakage of a ballast aggregate under loading. In the simulation, it is defined as the ratio of broken FJ bonds to the FJ bonds in total (FJ_{Total}). Since the FJ bonds can be disabled in tension (FJ_T) and in shear (FJ_S), the breakage rate is also divided into breakage rate in tension BR_T and breakage rate in shear BR_S:

$$BR_T = FJ_T / FJ_{Total} \tag{4.6}$$

$$BR_S = FJ_S / FJ_{Total} \tag{4.7}$$

The total breakage rate BR is then:

$$BR = BR_T + BR_S \tag{4.8}$$

The force propagation angle was defined as the 90% of the total force measured by the pressure platform in [47]. In the simulation, the bottom of the container is simulated by 20 equidistant segmented walls, which enable the measurement of forces address on the bottom. The force propagation angles on the left and right side of the model FA_{left} and FA_{right} are individually determined also by the 90% of the total force on each side (see Fig. 4-16). The force propagation angle of each simulation case is then the averaged force propagation angles on the left and right side:

$$FA_{averaged} = (FA_{right} + FA_{left})/2 \tag{4.9}$$

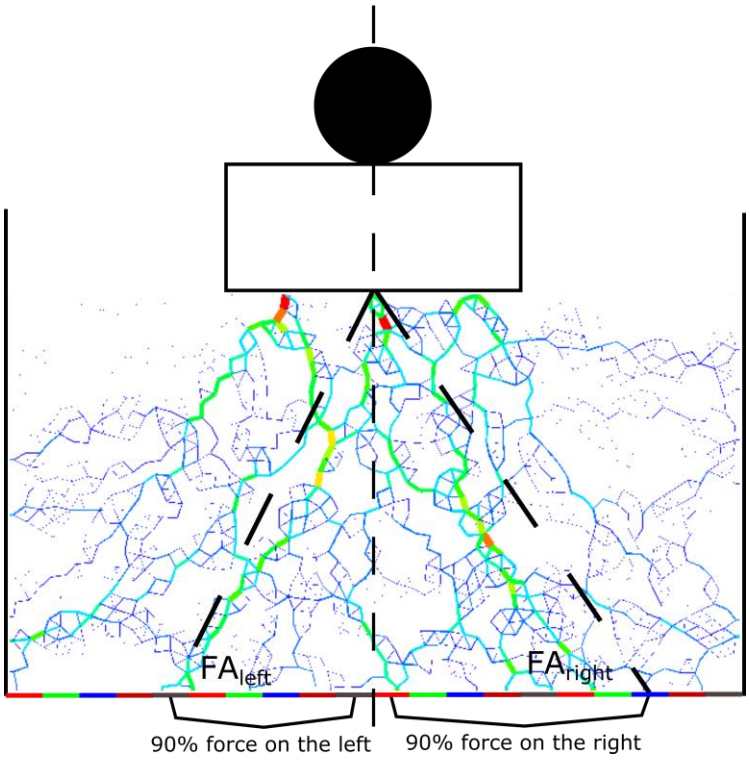

Fig. 4-16. The force propagation angle in the simulation

It is important to point out that the force propagation angle is normally calculated based on the left and right bottom corner of the pressing plate (or the sleeper in reality), but not its bottom middle point. However, due to the dimensional limitation of the model such as its low depth and width, using the normal definition of the force propagation angle could result an angle larger than 90 degree. It is the reason why an adjusted definition is applied. Since all the simulations adopt the same definition, it is still reasonable to comparing the different force propagation angles in simulated ballast aggregates with different form distributions.

The voids created by discrete ballast stones provide hydraulic conductivity of a ballast aggregate. On the premise of maintaining the load carrying ability and structural performance of the ballast layer, the voids should be as large as possible to provide adequate drainage. In DEM simulations, the degree of voids can be expressed as the void ratio VR, which is defined as the ratio of the voids area A_{void} and the total area A_{total}:

$$VR = A_{void}/A_{total} \tag{4.10}$$

The particle coordination number is defined as the number of contacted neighbor particles of a certain particle. The higher particle coordination numbers of ballast stones indicate a better contacted and structuralized aggregate. The particle coordi-

nation number can be also used to identify the “ghost particles”, which are the particles that do not take a significant structural load (see Fig. 4-17).

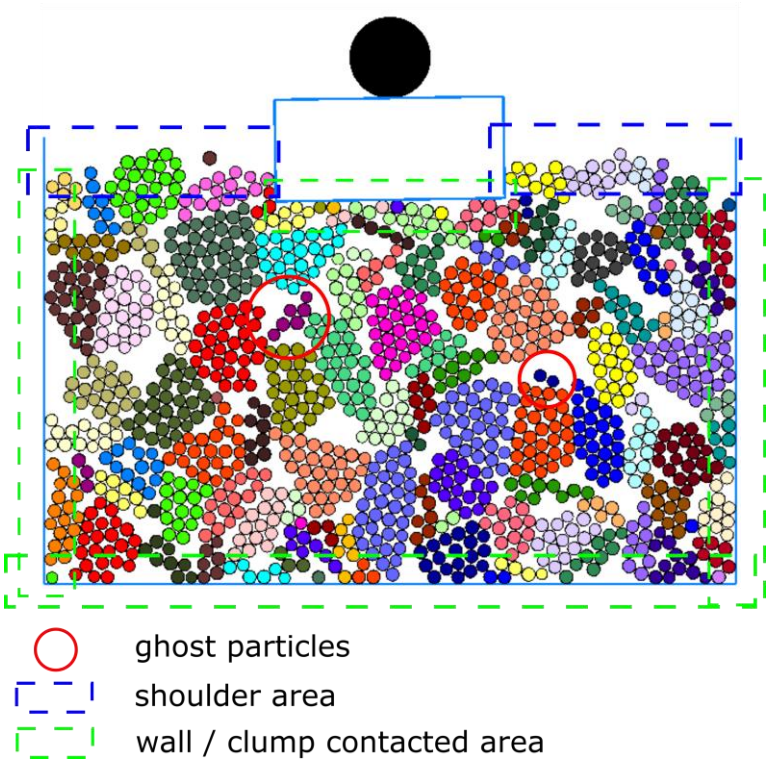

Fig. 4-17. The particle coordination number and the ghost particle

In the simulation, the particle coordination number for each simulated ballast stone is calculated by a FISH function, which determines the number of contacts from other particles around the center particle. The ghost particles are defined in the simulations as the particles, which have less than or equal to 2 contacts from other particles. It is to be noted that the particles, which are in contact with the container, are excluded in the process of finding the ghost particle even though they fit the above-mentioned criterion due to the reason that these particles usually do take a significant loading. Besides, the particles at the shoulder area of the aggregate are also excluded, because they will not take loads in any cases (see Fig. 4-17).

4.5.2 Two simulation cases for demonstrating the mechanical behavior

In this section, two simulation cases are performed. In the first simulation case, the form distribution of the ballast stones in the box test, which yields relatively large particles, is used. On the contrary, the second simulation case uses an artificial form

distribution, which is created by the ballast random form generator and has relatively small particles.

Simulation case 1 – with large particles

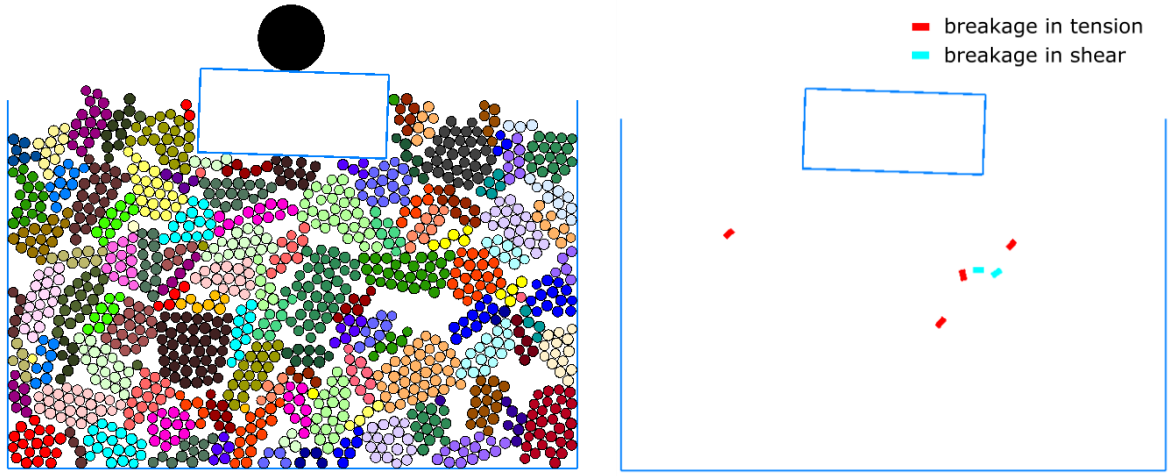

a: the simulation case 1 b: the breakages after loading

Fig. 4-18. The simulation case 1 and its breakages after loading

Fig. 4-18 demonstrates the simulation case 1 and its breakages after loading. Only 6 breakages appear in this case, in which 4 of them are breakages in tension and the other 2 are breakage in shear. Furthermore, the positions of the breakages are somewhat near the simulated pressing plated (i.e., the clump), which fits the reality that the breakages of ballast stones under realistic traffic loading happen direct under the sleeper in the most cases.

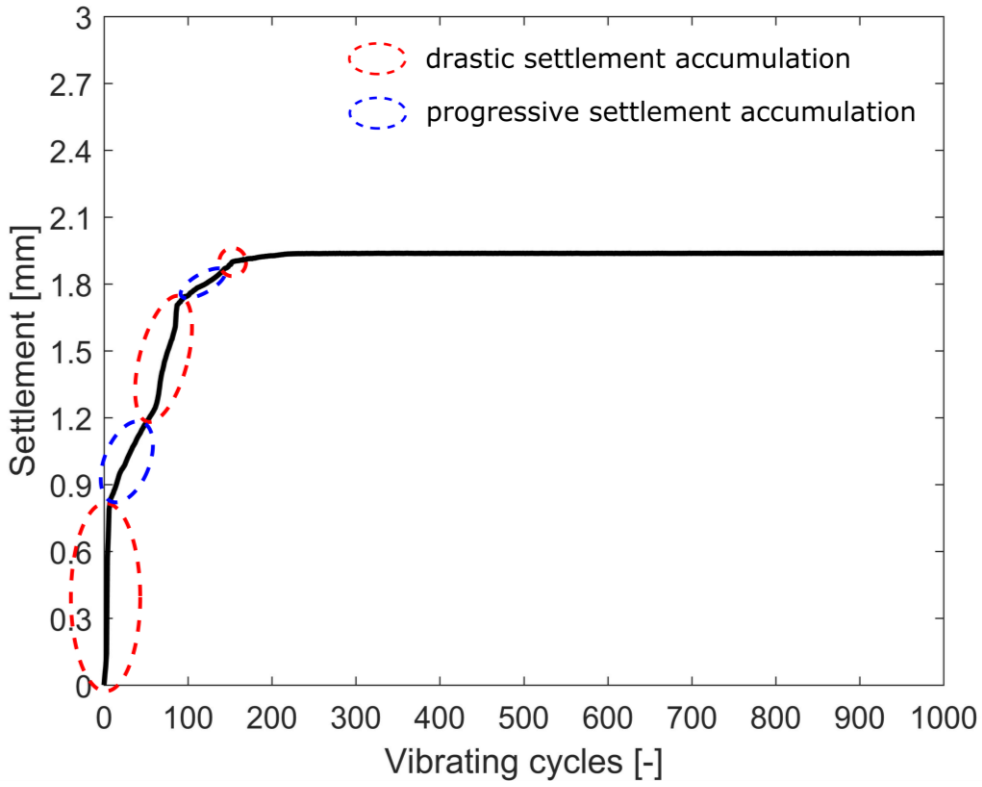

a: the settlement

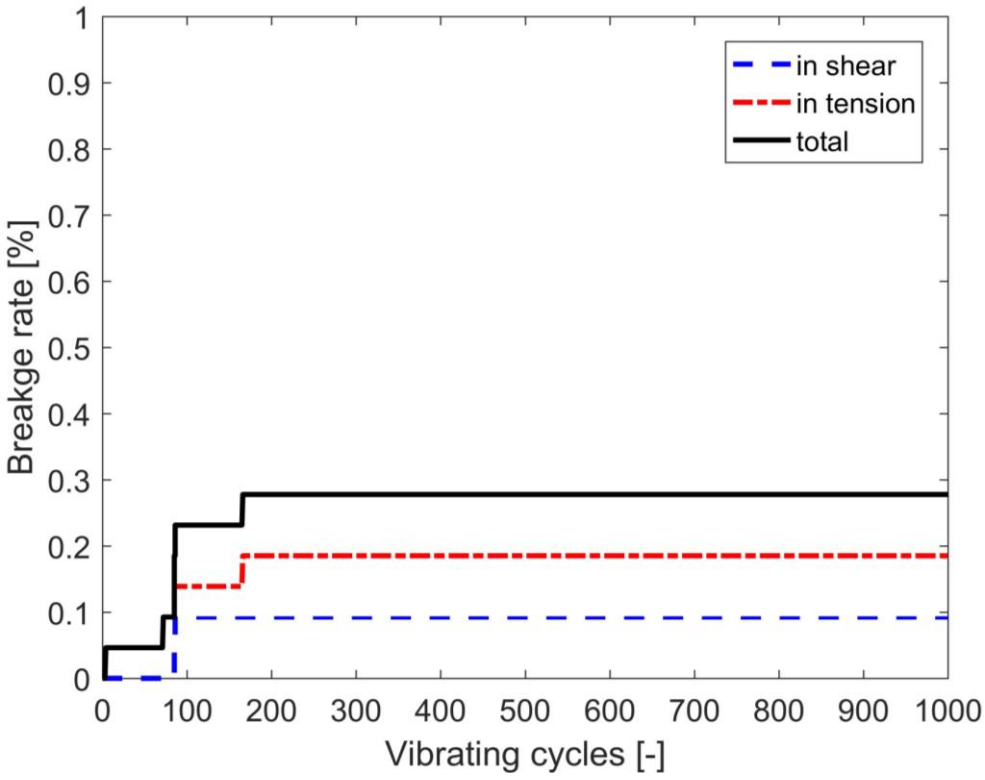

b: the breakage rate

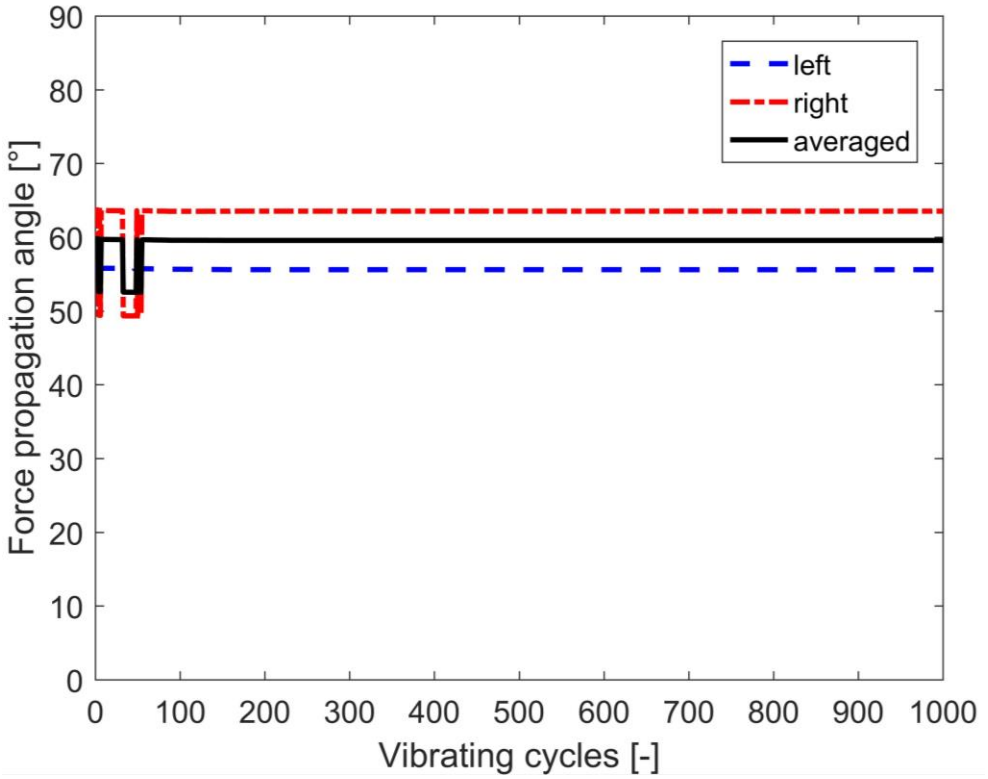

c: the force propagation angle

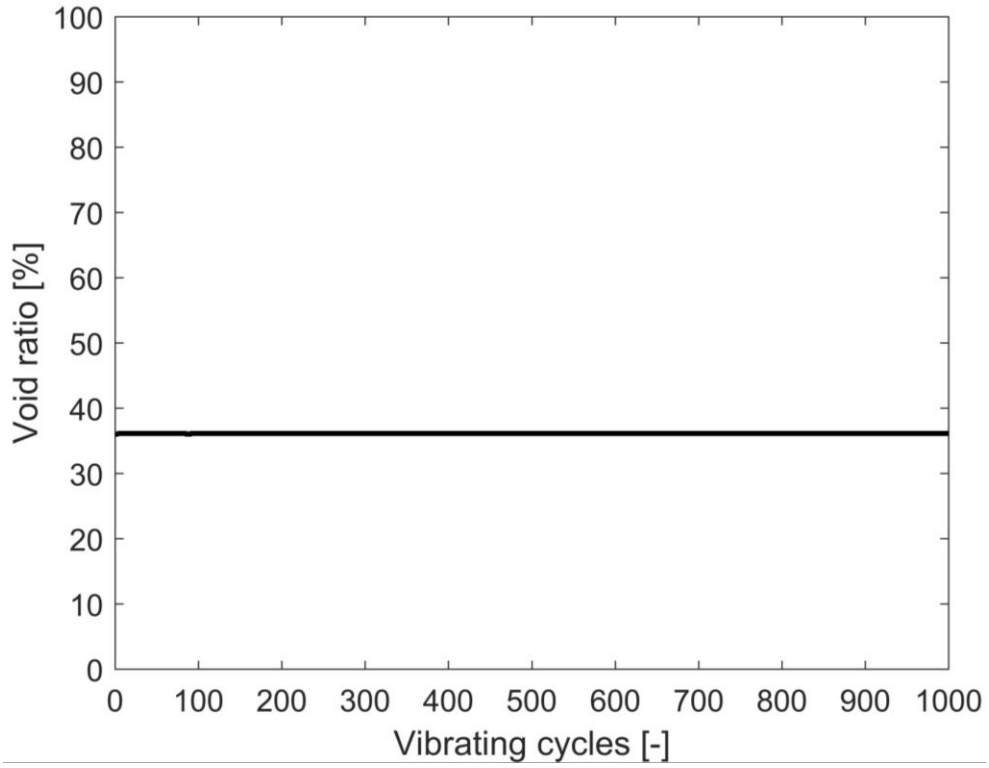

d: the void ratio

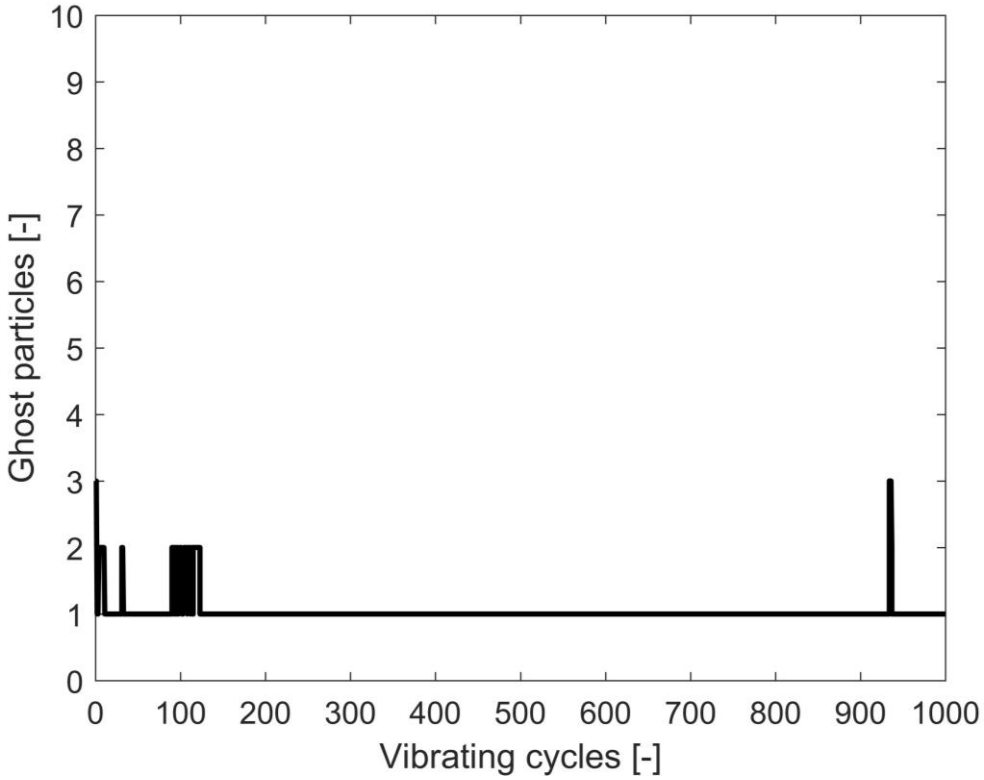

e: the ghost particles

Fig. 4-19. The mechanical behavior of the simulation case 1

Fig. 4-19 shows the mechanical behavior of the simulated ballast stones in the simulation case 1 under dynamic loading. In Fig. 4-19, a, it can be seen that the settlement of the ballast aggregate can be characterized into drastic and progressive settlement accumulations, where drastic means the accumulation of settlement is rapid and the settlement curve is steep, while progressive means the opposite. From Fig. 4-19, b, it can be speculated that the drastic settlement accumulations are caused by the breakages, since every time breakages occur (i.e., at the beginning, around 100 and 170 vibrating cycle), drastic settlement accumulations appear. On the other side, the progressive settlement accumulations are caused by the rearrangement of the ballast aggregate after breakages. It should be related to the interlocking effect of the ballast aggregate, where the friction coefficient between the simulated stones and their forms play an important role. After all the breakages appear (i.e., after 200 vibrating cycles), the settlement stabilizes. It indicates that the form distribution of the simulation case yields low progressive settlement without breakage. A different form distribution with smaller stones is to be investigated in the following section.

Fig. 4-19, c demonstrates the force propagation angle of the simulated ballast aggregate under dynamic loading. Similar to the settlement, the force propagation angle changes more drastic when breakage occurs, whereas it is basically constant if there is no breakage. A similar situation appears by the curve of the ghost particles (see Fig. 4-19, e). However, as shown in Fig. 4-19, d, there is only a small change around 100 vibrating cycle, which is small enough to be neglected. The reason for such a stable void ratio is that the vibration cycles in the simulation are not enough to create more breakages to make a significant change. In fact, it is reasonable to assume that aggregates with different form distributions will yield much more difference of the void ratios that their changes during dynamic loadings.

Simulation case 2 – with small particles

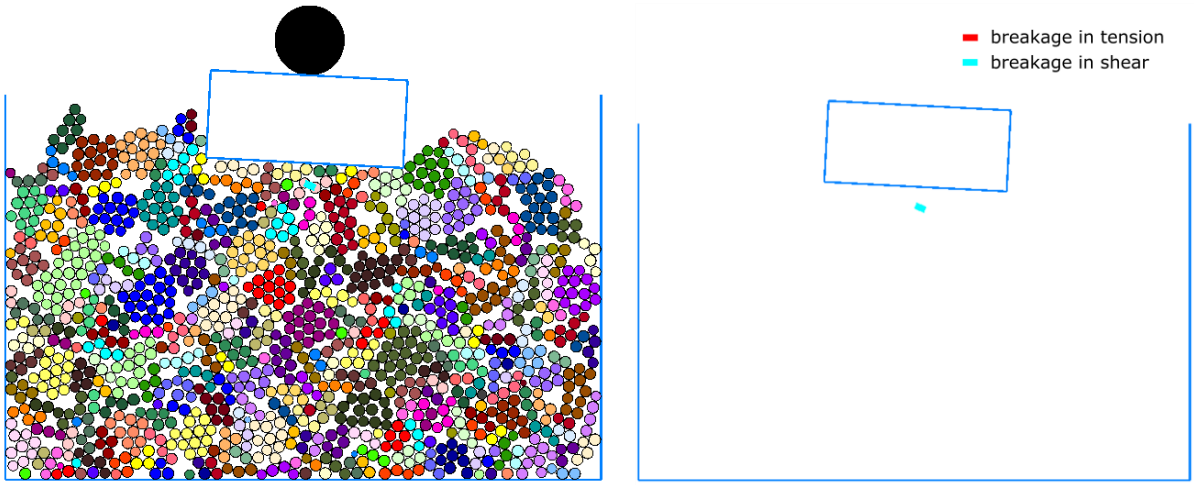

a: the simulation case 2 b: the breakages after loading

Fig. 4-20. The simulation case 2 and its breakages after loading

Fig. 4-20 demonstrates the simulation case 2 and its breakages after loading. It can be seen in Fig. 4-20, a, that the sizes of simulated ballast stones are comparatively smaller than the ones in the simulation case 1. In the case, only 1 breakage, i.e., a breakage in shear, occurs during the dynamic loading process. Similar to the simulation case 1, the breakage happens direct under the simulated pressing plate.

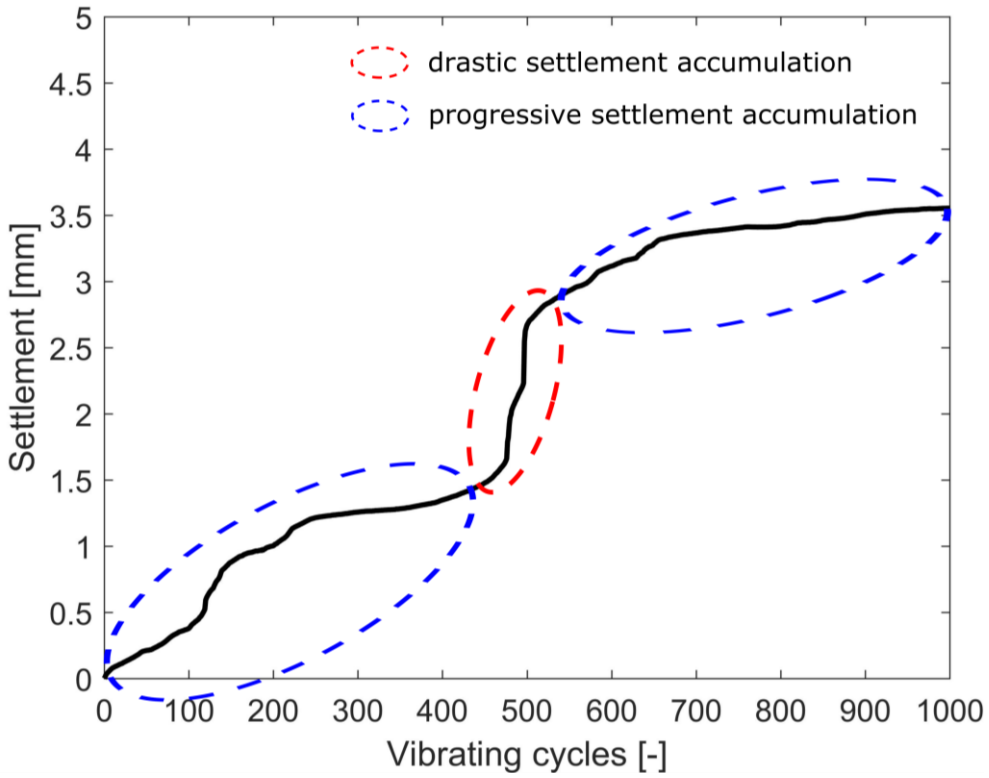

a: the settlement

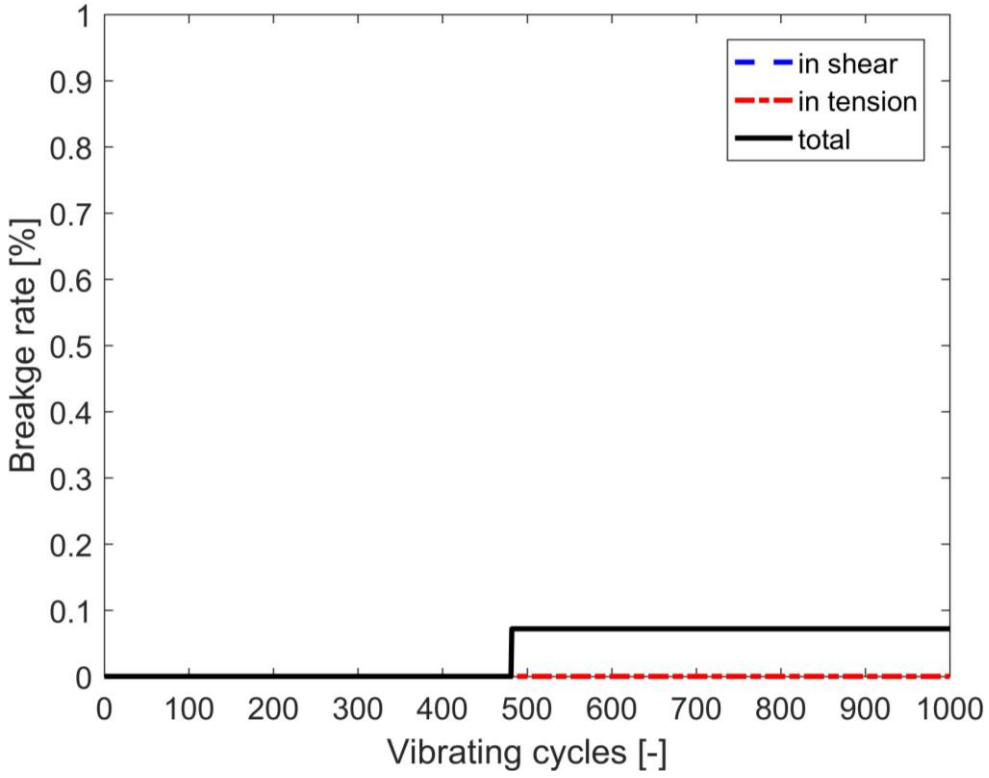

b: the breakage rate

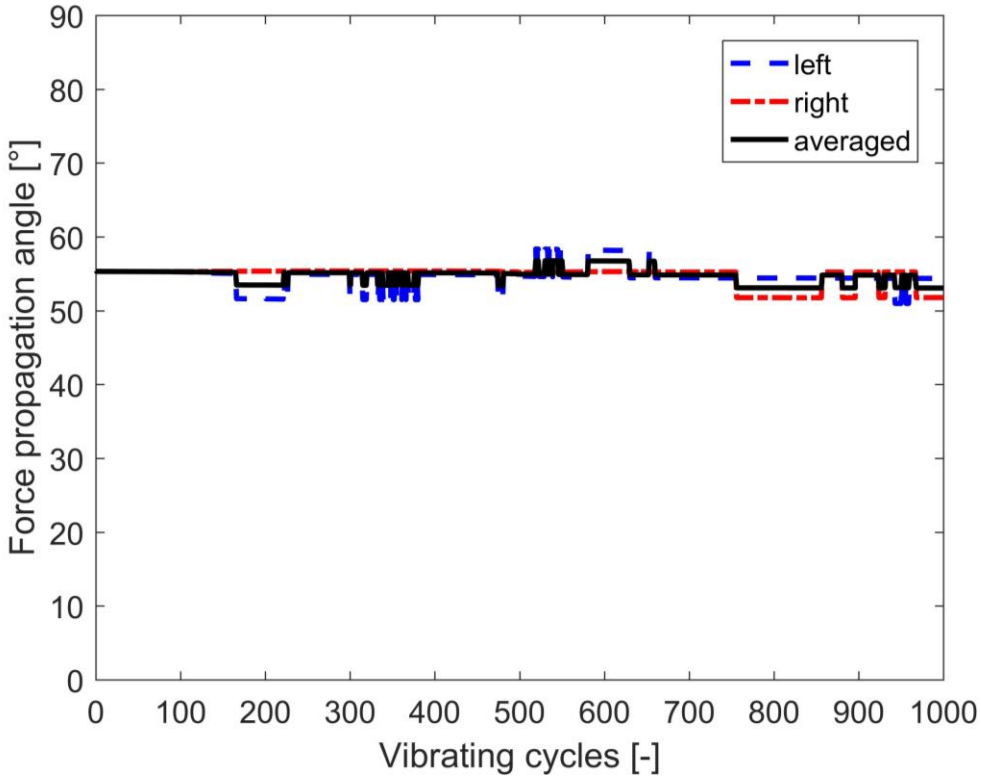

c: the force propagation angle

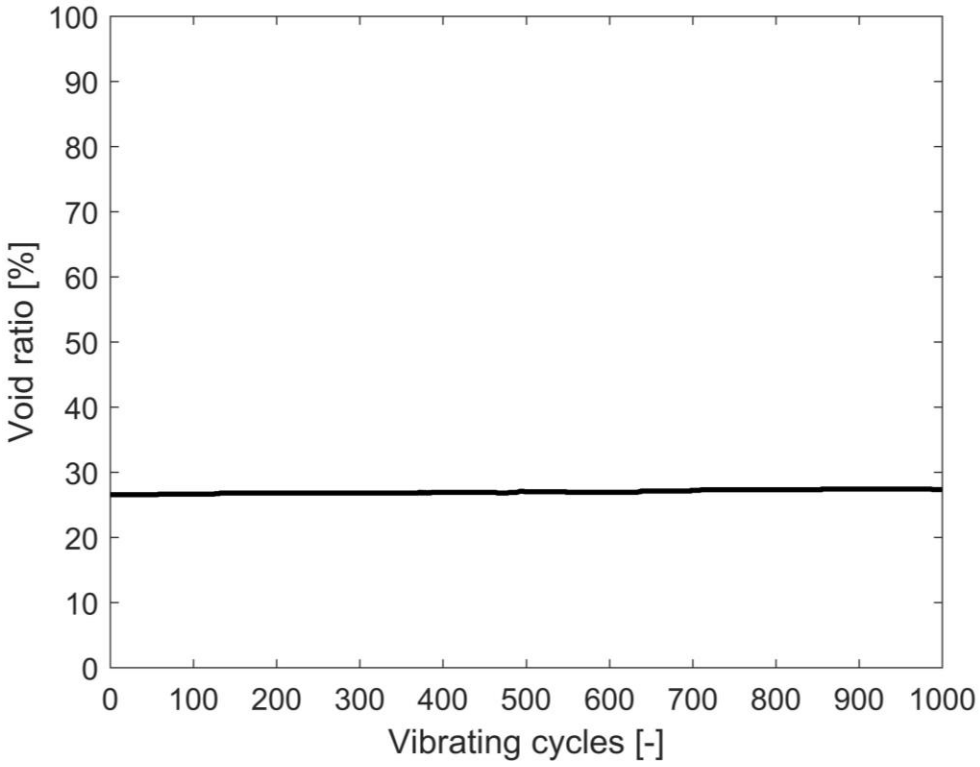

d: the void ratio

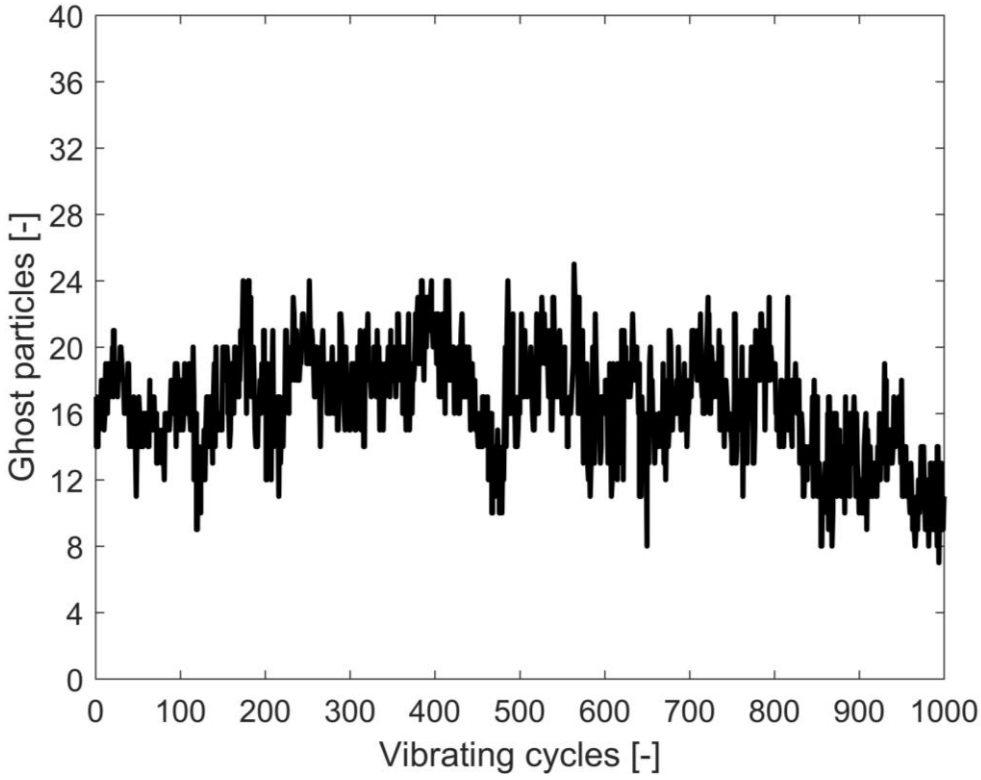

e: the ghost particles

Fig. 4-21. The mechanical behavior of the simulation case 2

Fig. 4-21 illustrates the mechanical behavior of the simulated ballast stones in the simulation case 2 under dynamic loading. Similar to case 1, drastic settlement accumulation happens when the breakage occurs (around 500 vibrating cycle) in this case. However, the differences between the two cases are: first, there is much more progressive settlement in case 2; second, the curve of the progressive settlement in case 2 is more smoothly changed. This phenomenon indicates a weaker interlocking effect of this ballast aggregate. Since the friction coefficient between the simulated ballast stones remains unchanged in case 2, the reason of the weak interlocking effect can be attributed to the changed form distribution, more specifically, the decreasing sizes of simulated ballast stones. Smaller ballast stones would obviously weaken the stability of the ballast aggregate.

The force propagation angle and the number of ghost particles change more drastic comparing to case 1. They change during the whole dynamic loading process, regardless when the breakage happens, indicating that they are mainly associated with the settlement of the aggregate under loading, rather than its breakage. Since aggregates with smaller particles generally yield more settlement, the changes of the force

propagation angle and the number of ghost particles are more severe. Besides, the two mechanical behaviors decrease slightly along the loading process. The decrease of the number of ghost particles is apparent, because the aggregate is increasingly better compacted. On the other side, if the aggregate is more compacted, it behaves more like a continuous medium rather than a discrete medium. It is reasonable to claim that the force propagation angle in a continuous medium is smaller than the one in a discrete medium.

5 Influence of ballast form distribution on ballast performance

5.1 Introduction

Ballast form distribution, including its size and shape distribution, has a great influence on the mechanical behavior of ballast aggregates. In this chapter, the previously generated 15 form databases (i.e., 5 databases with changing mean sizes as group 1, 5 databases with changing size distributions as database group 2 and 5 databases with changing shape distributions as database group 3) are used to create the ballast aggregates used in DEM simulations. Their mechanical behavior such as the ballast settlement, the breakage rate, the ghost particle number, the force propagation angle and the void ratio during dynamic loading are investigated and compared. For ballast aggregate based on each form database, 10 simulation cases are performed and the mean value of the above mentioned mechanical behavior is calculated and used as the final result of the database, so that the randomness caused by random selecting and packing of the ballast stones can be reduced.

5.2 Influence on the ballast settlement

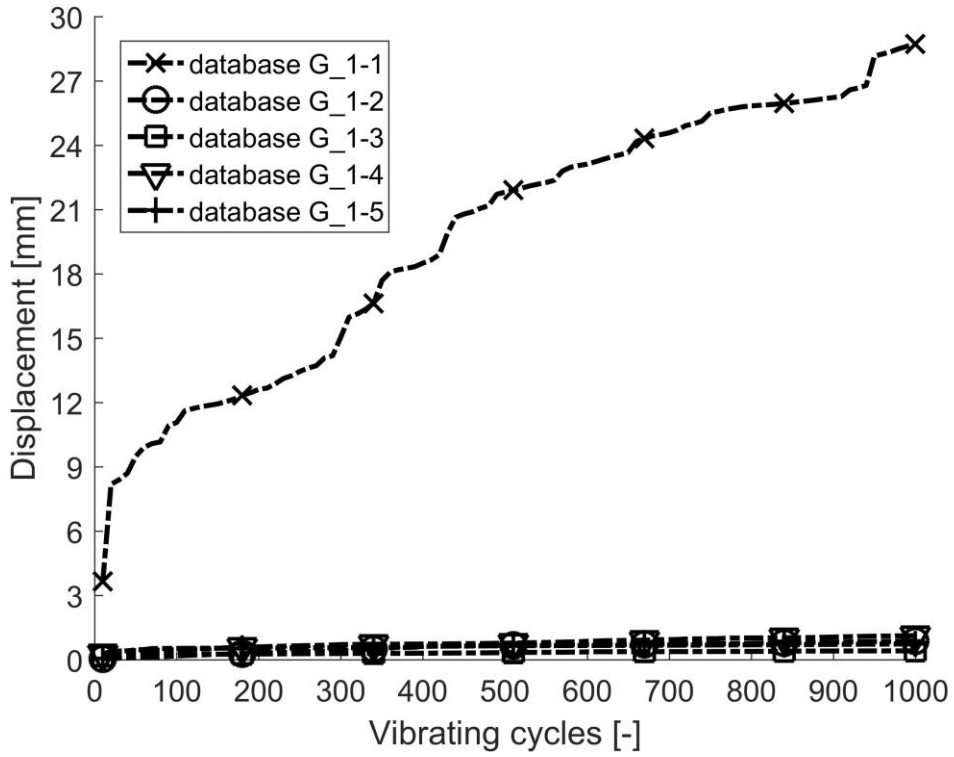

database group 1: changing mean sizes

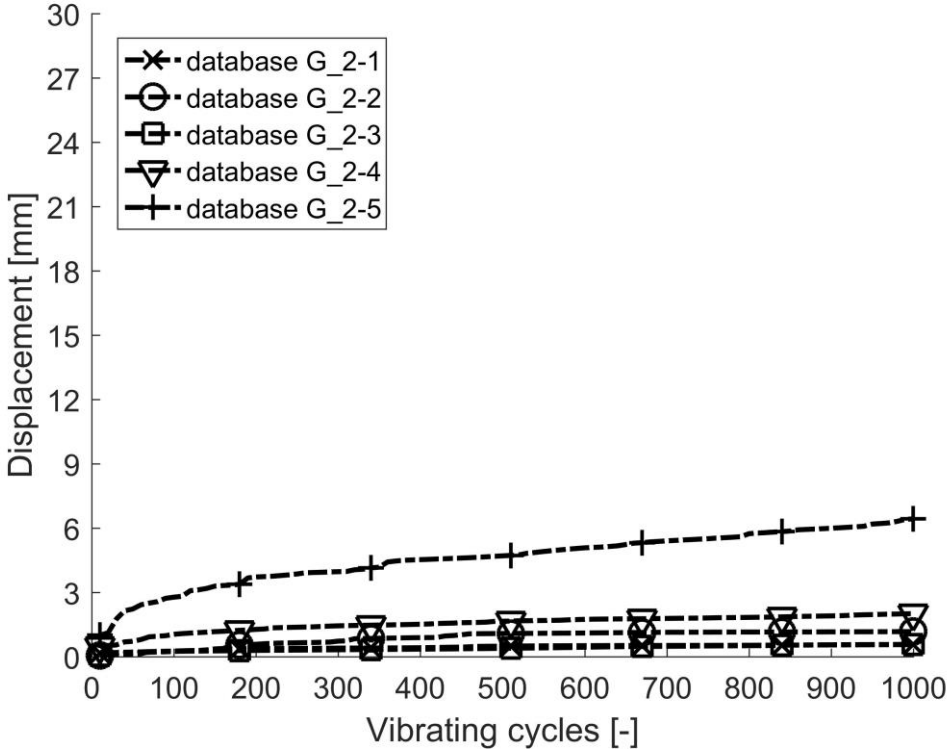

database group 2: changing size distributions

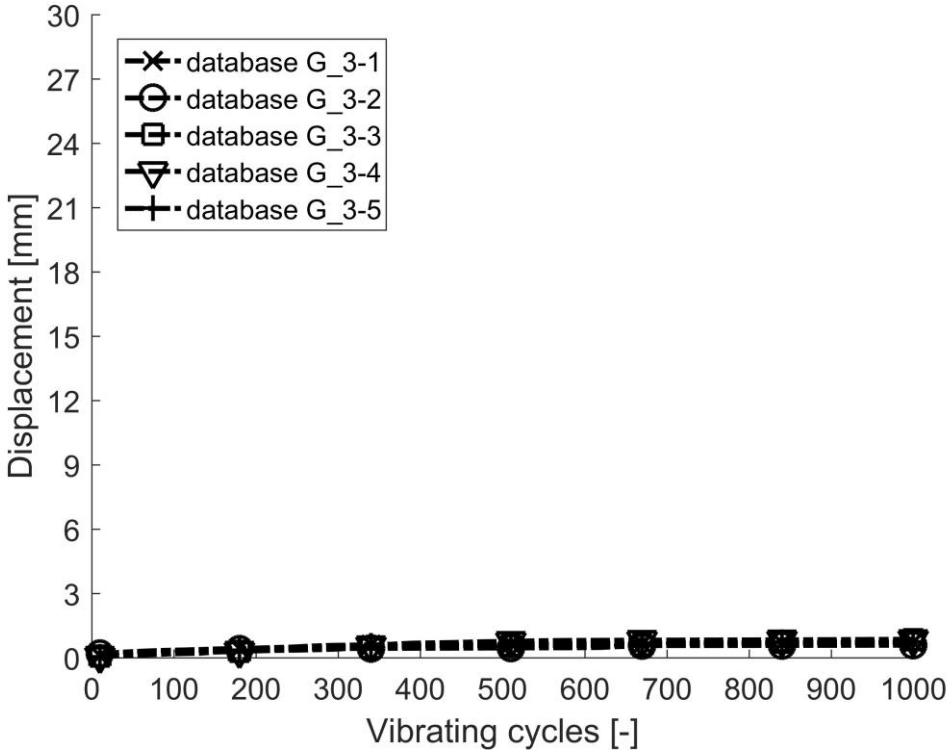

database group 3: changing shape distributions

Fig. 5-1. Influence of ballast form distribution on the ballast settlement

Fig. 5-1 demonstrates the settlements of ballast aggregates based on the 15 form databases. For database group 1 with changing mean sizes of the simulated ballast stones, it is expected that the settlement would be stably decreasing with the increase of the ballast mean size (from database G_1-1 to G_1-5, see also Fig. 3-6). However, the simulation result indicates that the settlements of ballast aggregates with databases G_1-2 to G_1-5 are basically the same and they are dramatically decreased comparing to the first database. On one hand, for database G_1-1, the settlement curve matches the expectation that extremely small particles (e.g., sand) may create a structural instable aggregate due to the loss of the interlocking effect. On the other hand, for databases G_1-2 to G_1-5, the dramatically decrease of settlements indicates that the interlocking effect of ballast stones is not proportionally increased with the mean sizes of ballasts. It is more like a yes-or-no occurrence, which means that from a certain value of the ballast mean size, it will appear and exert complete influence. To this end, if the consideration of other mechanical behavior is dismissed and only the settlement is concerned, a wide range of optimal ballast mean size can be used as long as the interlocking comes into effect.

The settlement of ballast aggregates with database group 2 shows a reasonable tendency. With the increase of mass proportion (or particle number) of small-sized ballast stones (from database G_2-1 to G_2-5, see also Fig. 3-7), the settlement of the aggregate increases. Similar to the database group 1, in group 2, there are also four databases (i.e., G_2-1 to G_2-4) demonstrating the similar settlement behavior, while the other one (i.e., G_2-5) results in a relatively higher settlement. However, comparing to database group 1, the settlement curves based on the four databases in group 2 are not that overlapped, while the ending value of the other settlement curve is not that high (6mm comparing to 30mm). For database group 3, the settlement curves are overlapped just like the four databases (G_1-2 to G_1-5) in group 1.

The key reason for different settlement behaviors of ballast aggregates based on different form databases is mass proportion of small-sized ballast stones. Table 5-1 shows the percentages passing by mass for ballast stones with sizes smaller than 22.4mm of each form database. In database group 1, the percentages decrease from G_1-1 to G_1-5, where G_1-1 is with an extremely high percentage, which correspondingly results a very high settlement of the ballast aggregate. Furthermore, in database group 2, the percentages increase from G_2-1 to G_2-5, which causes an

increasing settlement of ballast aggregates correspondingly. At last, the percentages in database group 3 are the same, which is the reason why the settlements stay also the same.

Table 5-1: Percentage passing by mass for small ballast stones

percentage passing by mass for ballast stones with sizes smaller than 22.4mm (%)					
database group 1	G_1-1	G_1-2	G_1-3	G_1-4	G_1-5
	78	16	9.5	6.5	3.5
database group 2	G_2-1	G_2-2	G_2-3	G_2-4	G_2-5
	1.5	5.5	9.5	13.5	17.5
database group 3	G_3-1	G_3-2	G_3-3	G_3-4	G_3-5
	9.5	9.5	9.5	9.5	9.5

Important to notice is that for the ballast aggregates with low settlements (i.e., database group 1: G_1-2 to G_1-5, database group 2: G_2-1 to G_2-4, database group 1: G_3-1 to G_3-5), the percentages are always smaller than 16% (G_1-2). If the percentage is increased to 17.5% (G_2-5), the settlement would be considerably higher. This indicates that above a certain value from 16% to 17.5% of the mass proportion of ballast stones smaller than 22.4mm, the ballast aggregate will become instable, and the interlocking effect is lost. It implies that, to control the ballast settlement, it is important to reduce the mass proportion of small ballast stones.

5.3 Influence on the breakage rate

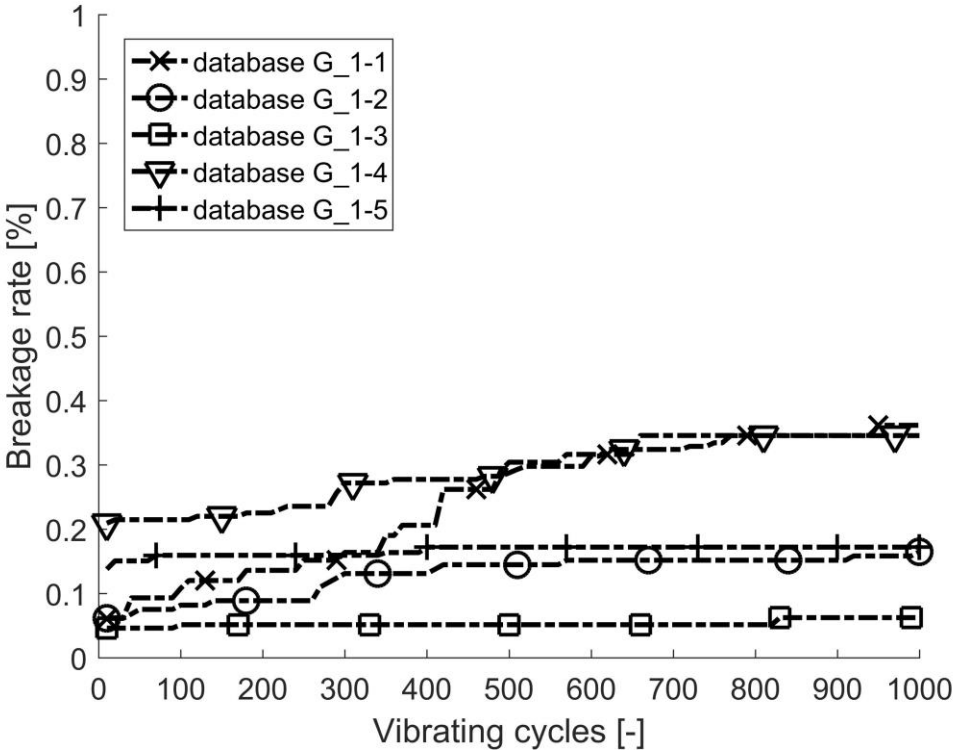

database group 1: changing mean sizes

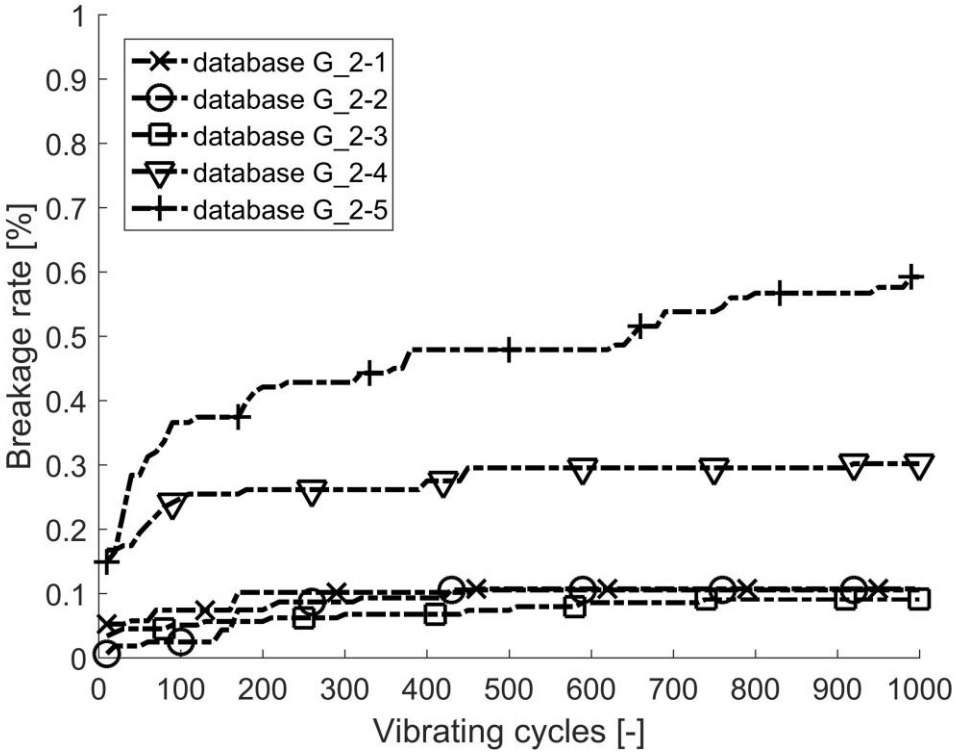

database group 2: changing size distributions

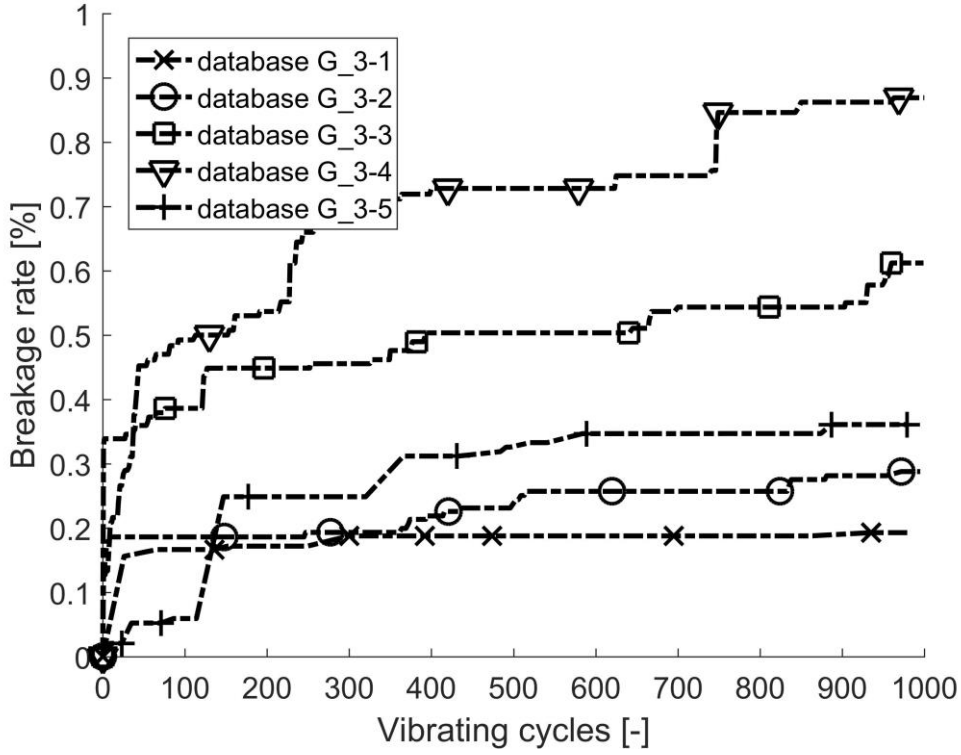

database group 3: changing shape distributions

Fig. 5-2. Influence of ballast form distribution on the breakage rate

Fig. 5-2 demonstrates the breakage rates of ballast aggregates based on the 15 form databases. It was expected that some trends could be shown in the figure, such as the ballast aggregate with larger ballast stones (e.g., G_1-5) might have higher breakage rate comparing to the one with smaller ballast stones (e.g., G_1-1), due to its higher internal force caused by the better interlocking effect; or the ballast aggregate with more flat ballast stones (e.g., G_3-5) might yields more breakages than the one with more normal ballast stones (e.g., G_3-1), since a flat ballast stone is much easier to break under loading due to its reduced cross-sectional area. However, the results shown in Fig. 5-2 are mainly irregular. None of trends are clearly demonstrated. The key reason could be that the 1000 loading cycles are not enough for generating enough breakages. It is noticed in Fig. 5-2 that the breakage rates in all the 15 form databases are very low (smaller than 1%). To further confirm the insufficient of breakages, the number of breakages of the 15 form databases after dynamic loading is illustrated in Fig. 5-3.

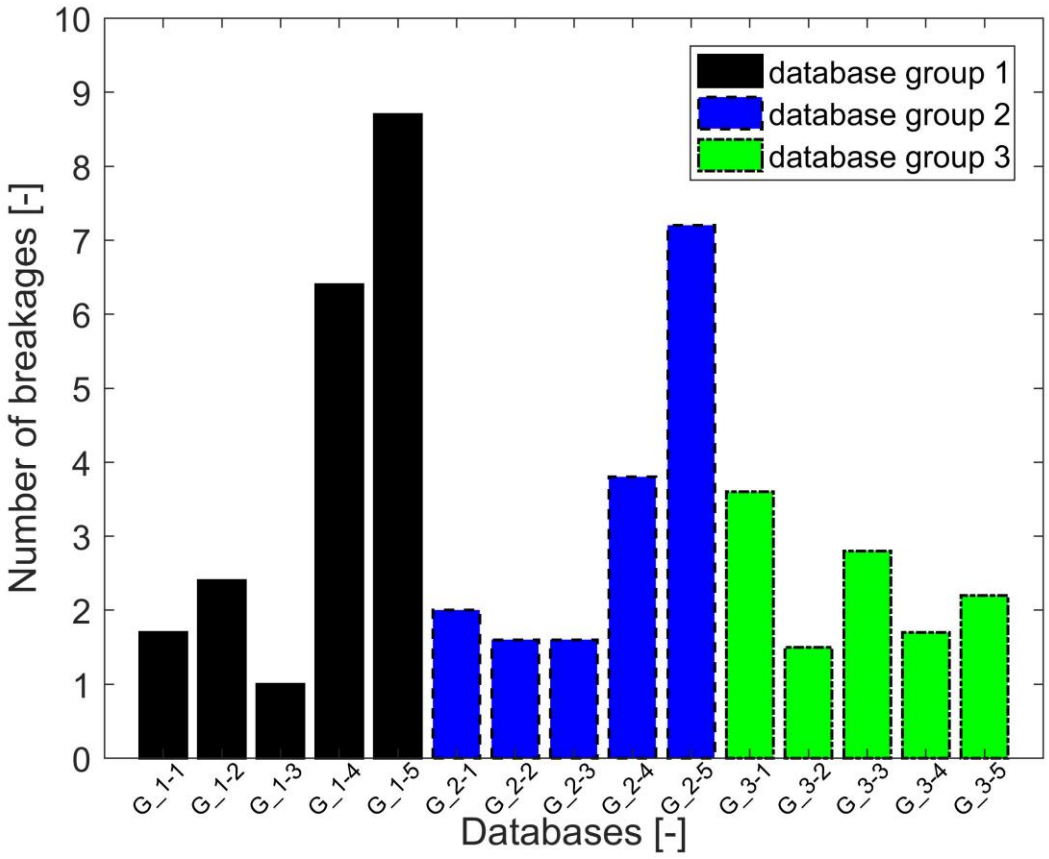

Fig. 5-3. Number of breakages after the dynamic loading process

In Fig. 5-3, the numbers of breakages of the 15 form databases are illustrated. For each form database, the demonstrated value of breakage number is the mean value of 10 simulation cases. It is clear to see that numbers of breakages are generally very low, in which the highest value is just above 8. This is clearly not statistically enough to form any convincing trend. The ballast breakage is a long-term behavior of ballast aggregate. Considering the typical maintenance cycle of a conventional ballast track, there should be millions of loading cycles before notable breakages occur. However, due to the computational intensity of the BPM, it is unpractical to simulate such a long-term behavior. A more efficient breakable model for ballast stones should be proposed in the future.

5.4 Influence on the ghost particles

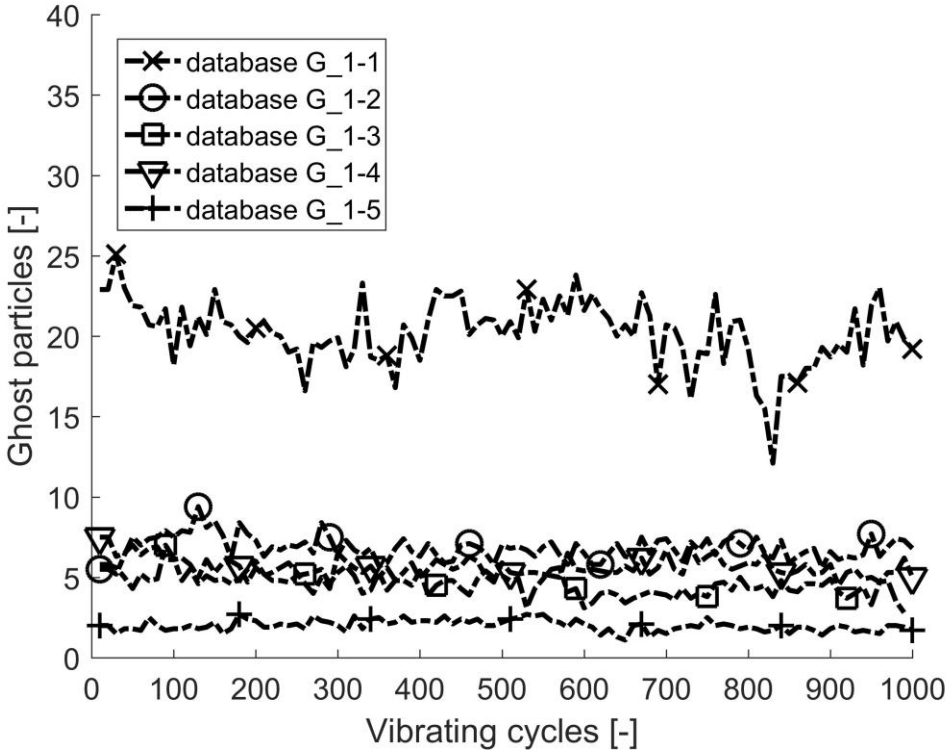

database group 1: changing mean sizes

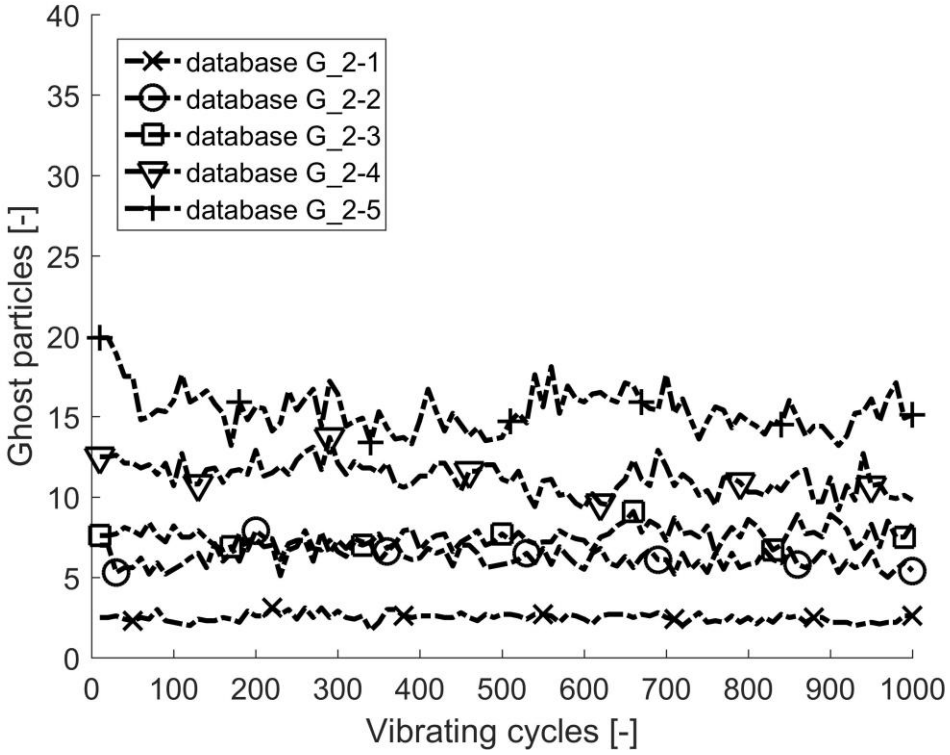

database group 2: changing size distributions

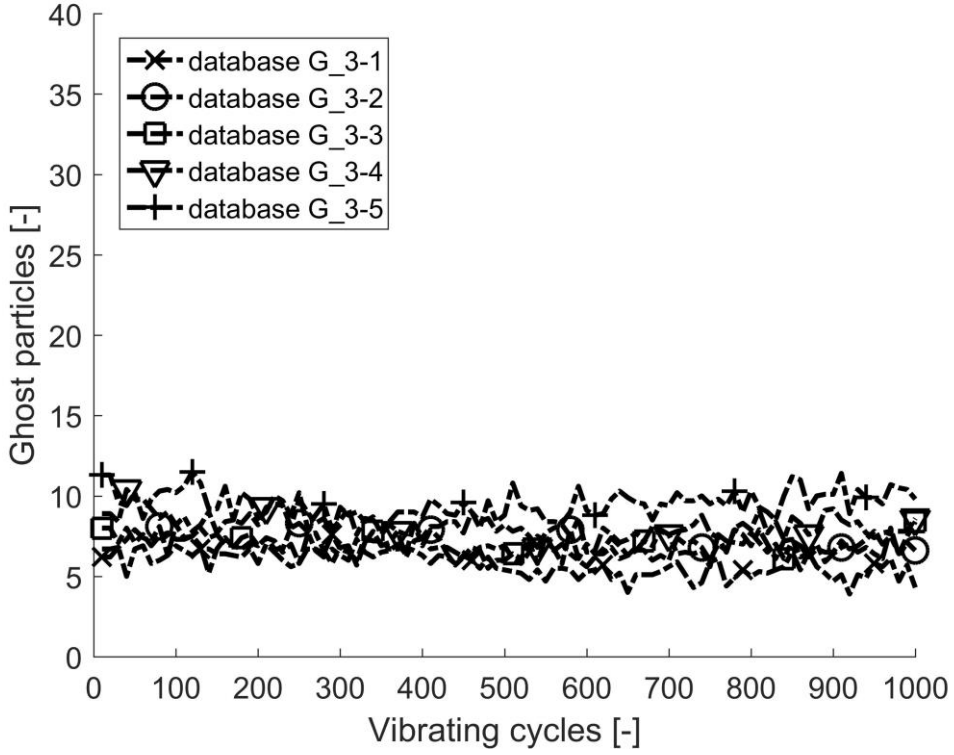

database group 3: changing shape distributions

Fig. 5-4. Influence of ballast form distribution on the ghost particles

Fig. 5-4 demonstrates the ghost particles of ballast aggregates based on the 15 form databases. Clear trends of the three database groups are shown as expected. For group 1, the number of ghost particles decreases with the increase of the mean ballast stone size (from database G_1-1 to G_1-5), where the database G_1-1 has a great number of ghost particles, while the difference of other four databases is not that notable. For group 2, the number of ghost particles reduces with the decrease of the mass proportion of small-sized ballast stones in the aggregate (from G_2-1 to G_2-5). For group 3, the number of ghost particle increases with the proportion of flat ballast stones in the aggregates (from G_3-1 to G_3-5). However, the curves are more or less overlapped comparing to database group 2, the difference is relatively smaller.

It is noticed that the number of ghost particles is strongly corresponded to the settlement of the ballast aggregate. For database group 1, the both parameters bases on G_1-1 are distinctly different comparing to the other four form databases, which yield roughly the same result. For database group 2, the curves of the both parameters are more scattered, while for database group 3, they are more overlapped. The reasons

are, on one hand, the ghost particles are the ballast stones, which are not taking any loads during the loading process in an aggregate. The more ghost particles there are, the less structural stability there should be. This results in a high settlement of the ballast aggregate. On the other hand, as discussed in section 5.2, the settlement is related to the number of particles with sizes smaller than 22.4mm. These particles are highly possible to become ghost particles if they settled inappropriately.

Furthermore, it is expected to see the reduction of the ghost particles as the dynamic loading proceeds, due to the assumption that the loading process may create more densified ballast aggregate, and thus force some of the ghost particles to get contact to other particles and to take structural load. The expectation is fulfilled at database G_1-1, G_2-4 and G_2-5, which are the databases with higher original number of ghost particles. The reduction is inconspicuous but still can be seen. For other databases, there is no clear trend for decreasing of the ghost particles. The reason for the stable number of ghost particles could be, first, the original number of ghost particles is already low. Second, these form databases create structurally stable ballast aggregates. The loading cycles are not enough to create enough breakages, which destroys the stable structures and arouses the position rearrangements of ballast stones. Without this positional rearrangement, the original ghost particles will basically stay where they are, and thus cannot be eliminated.

5.5 Influence on the force propagation angle

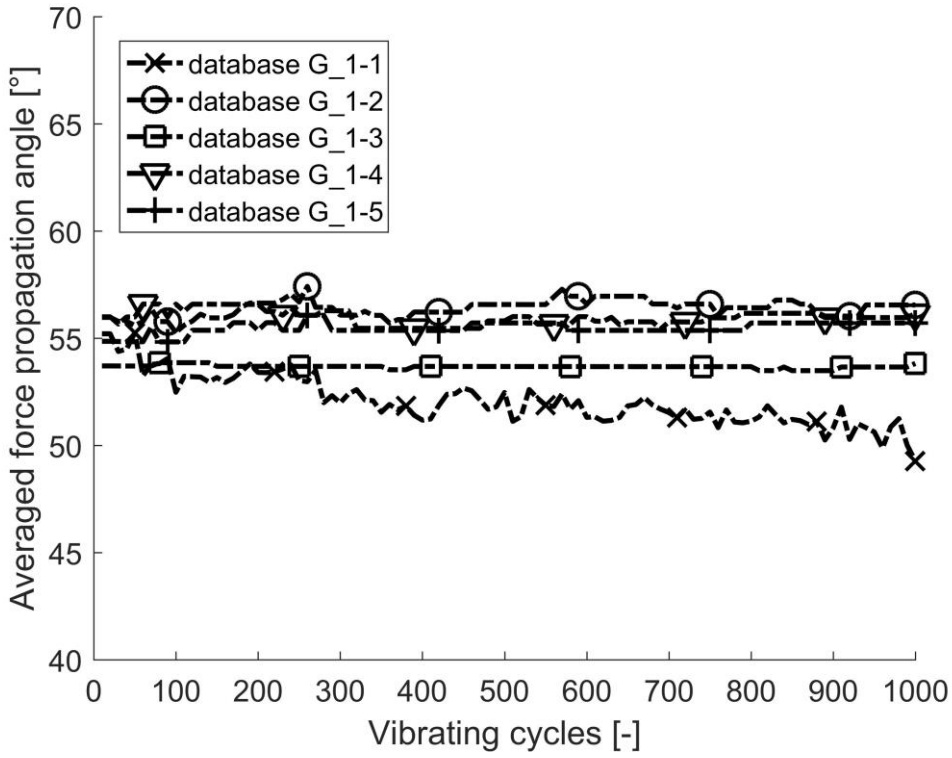

database group 1: changing mean sizes

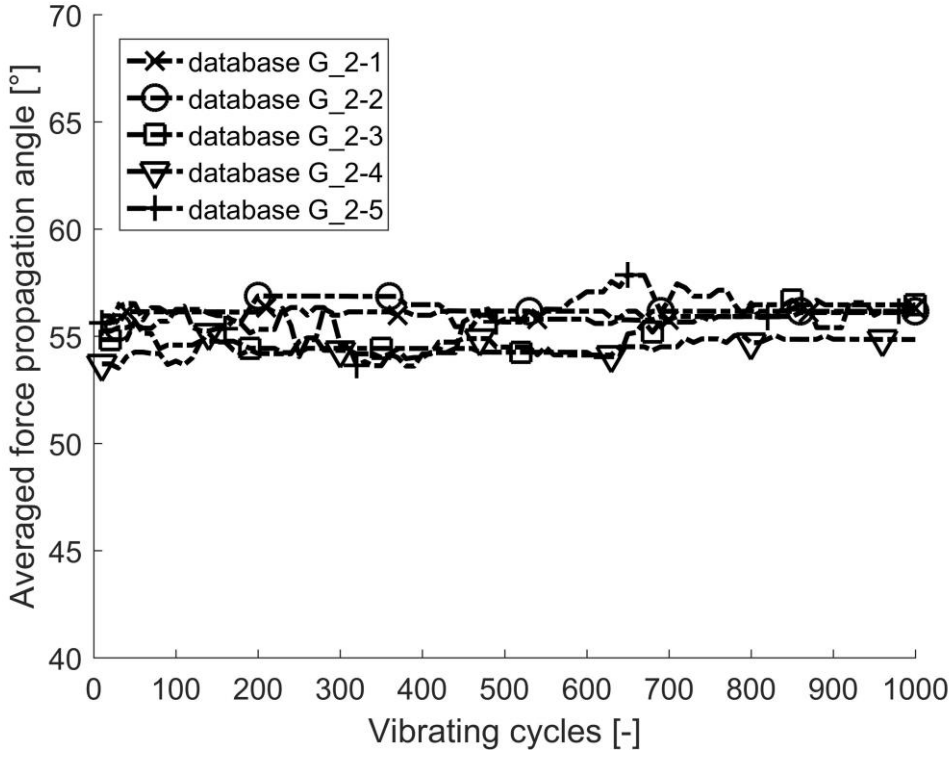

database group 2: changing size distributions

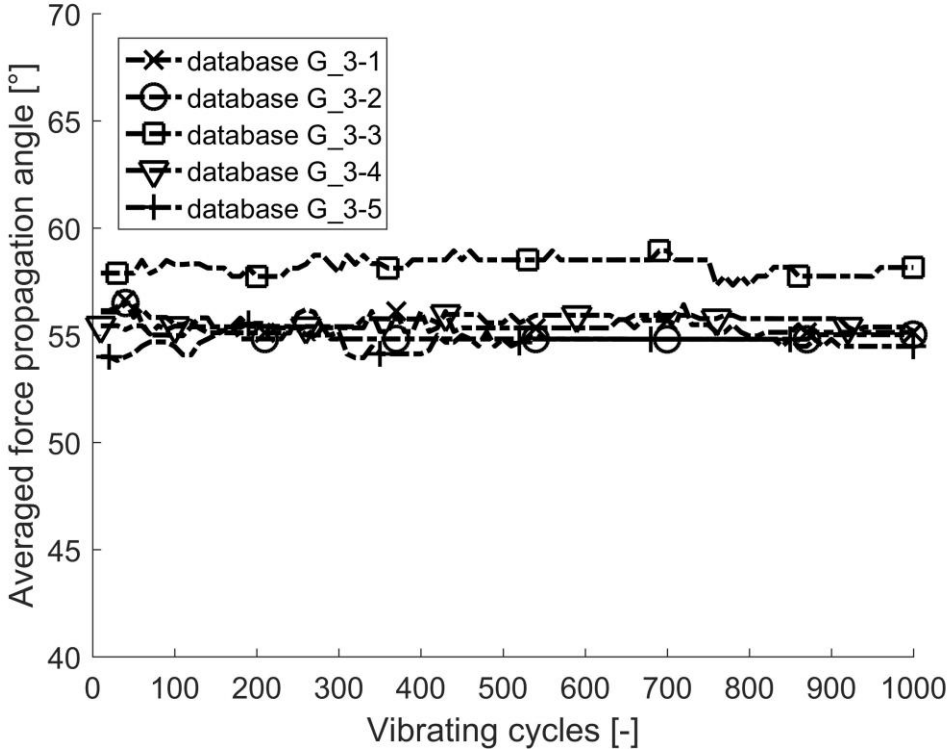

database group 3: changing shape distributions

Fig. 5-5. Influence of ballast form distribution on the force propagation angle

Fig. 5-5 demonstrates the force propagation angles of ballast aggregates based on the 15 form databases. Most of the force propagation angles stay the same (about 55°) along the loading cycles except for G_1-1 and G_2-5, which are dramatically changing during the dynamic loading process. The both databases include considerable small sized particles. Apparently, these small particles could jeopardize the stability of the ballast aggregates and enlarge their settlements, which consequently rearranges the position of ballast stones and changes the contacts between them. As a result, the loading patterns are constantly changing during the dynamic loading process. On the contrary, larger ballast stones will create stable ballast aggregate, in which the loading pattern stays mainly unchanged, and thus results an unchanged curve of force propagation angle.

5.6 Influence on the void ratio

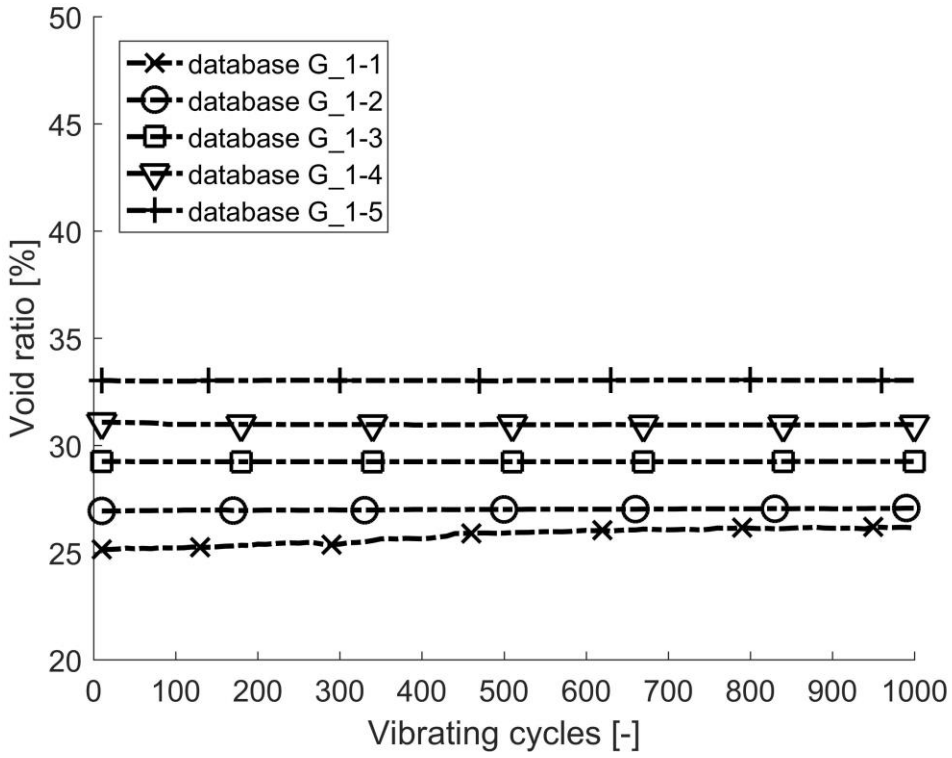

database group 1: changing mean sizes

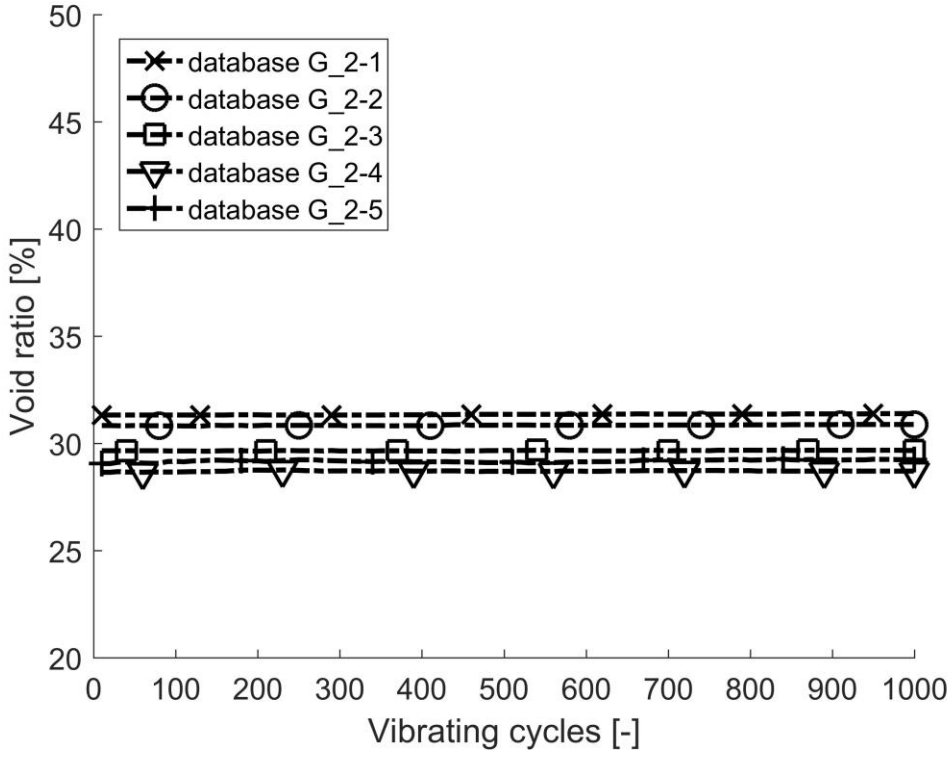

database group 2: changing size distributions

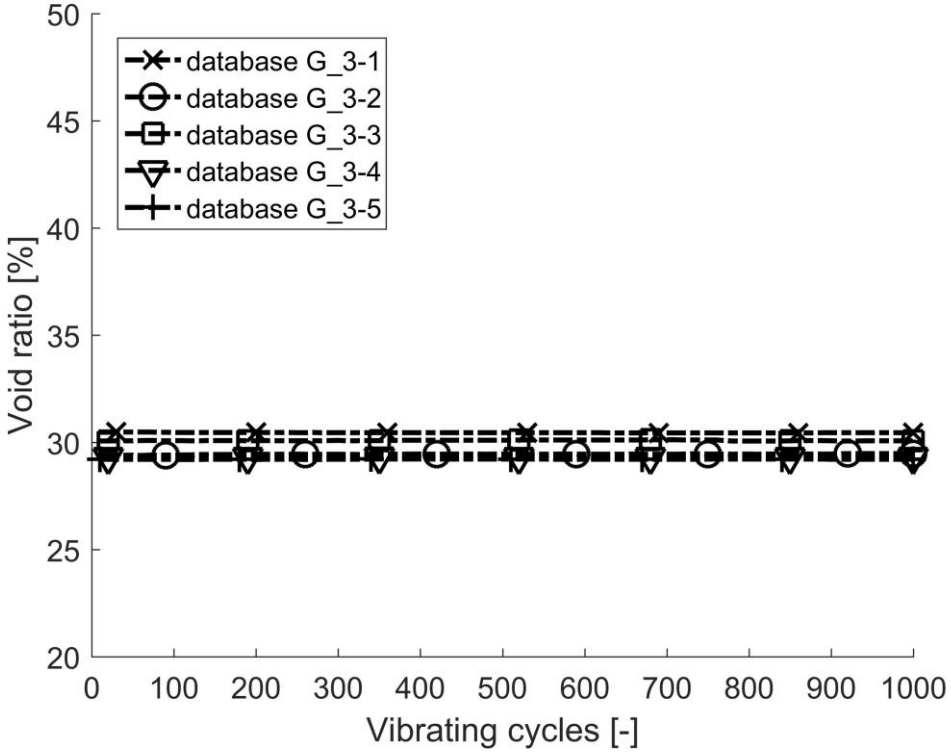

database group 3: changing shape distributions

Fig. 5-6. Influence of ballast form distribution on the void ratio

Fig. 5-6 demonstrates the void ratio of ballast aggregates based on the 15 form databases. The five form databases in database group 1 demonstrate an expected trend: the ballast aggregate with big mean size of ballast stones (G_1-5) will create more voids comparing to the one with small mean size (G_1-1). For database group 2, it is demonstrated that the ballast aggregate with less small particles (G_2-1) will yield more voids. It is easy to understand since there are not so many small ballast stones to fill the voids created by the big stones. For database group 3, it is shown that the changing shape distribution does not influence the void ratio greatly. Comparatively, the mean size of ballast stones is the most influential parameter for the void ratio.

For each form database, the void ratio stays almost unchanged during the dynamic loading process. It does not match the common sense that the ballast aggregate will be densified by loading. The reason is, first, the ballast aggregates are already pre-densified during the tamping process to a very high level, which is not the case of a conventional newly-built ballast track; second, the loading cycles are not enough to create enough breakages, and thus the voids between large particles cannot be filled

by the broken pieces. Besides, it is noticed that the void ratio of database G_1-1 is slightly increased instead of decreased along the loading cycles. The reason is that the starting void ratio of this database is already small (25%), which means that this ballast aggregate is already well compacted at the beginning. During the dynamic loading process, the ballast aggregate cannot be further compacted. On the contrary, it is loosened by the vibration of the particles caused by the loading, and thus more voids between the particles are created.

5.7 Relationship between mechanical behaviors of ballast aggregate

In this study, the investigated mechanical behavior of ballast aggregate during dynamic loading are: the ballast settlement, the breakage rate, the ghost particle number, the force propagation angle and the void ratio. In this section, the interrelationship between the mechanical behaviors is discussed in detail. To ensure an easier discussion, as listed in Table 5-2, the interrelationship between each two mechanical behaviors A and B is symbolized as Interrelationship Index IRI_A-B.

Table 5-2: Interrelationship Index (IRI) of the investigated mechanical behavior of ballast aggregates

	Ballast Settlement (BS)	Breakage Rate (BR)	Ghost Particle (GP)	Force Propagation Angle (FPA)	Void Ratio (VR)
Ballast Settlement (BS)	not applicable	IRI_BS-BR	IRI_BS-GP	IRI_BS-FPA	IRI_BS-VR
Breakage Rate (BR)	-	not applicable	IRI_BR-GP	IRI_BR-FPA	IRI_BR-VR
Ghost Particle (GP)	-	-	not applicable	IRI_GP-FPA	IRI_GP-VR
Force Propagation Angle (FPA)	-	-	-	not applicable	IRI_FPA-VR
Void Ratio (VR)	-	-	-	-	not applicable

IRI_BS-BR: It is expected that a higher breakage rate would cause a higher settlement. However, the phenomenon is not shown in the simulation. The reason is that the breakages in the simulation are very rare, which are not enough to form a statistic stability. To investigate the relationship, a dynamic loading process with more loading cycles should be implemented.

IRI_BS-GP: The ballast settlement and the ghost particle number are clearly positively related. The more ghost particles there are, the higher settlement there is after the loading. The both mechanical behaviors are related to the mass proportion of small particles with sizes smaller than 22.4 mm in the aggregate. The small particles will in all probability become ghost particles in a ballast aggregate. These ghost particles do not take any structural forces, and thus can jeopardize the stability of the aggregate and cause a high settlement.

IRI_BS-FPA: A high settlement can dramatically change the loading pattern of a ballast aggregate, and thus arouses a radically changing force propagation angle. The reason is that the settlement causes the position changes of ballast stones, which reconstructs the contacts between them. On the contrary, a low settlement indicates a stable, well interlocked ballast aggregate. As a result, the force propagation angle will be relatively more stable.

IRI_BS-VR: The ballast settlement and the void ratio are negatively related. A high settlement indicates a low void ratio. Although the low void ratio is not the direct reason that a high ballast settlement occurs, the both mechanical behaviors have a same origin: the mass proportion of small ballast stones in the aggregate.

IRI_BR-GP: No relationship is found between the breakage rate and the number of ghost particles, because the breakages are not enough to form a statistically stable trend.

IRI_BR-FPA: No relationship is found between the breakage rate and the force propagation angle, because the breakages are not enough to form a statistically stable trend.

IRI_BR-VR: No relationship is found between the breakage rate and the void ratio, because the breakages are not enough to form a statistically stable trend.

IRI_GP-FPA: A drastically changing number of ghost particles is accompanied by a drastically changing force propagation angle. The both mechanical

behaviors are indicators for a changing loading pattern during the loading phase, which will very likely happen if the mass proportion of small ballast stones is low.

IRI_GP-VR: If the number of ghost particles is high, the void ratio will be low. The ghost particles will take the void spaces between large ballast stones, and thus reduce the hydraulic conductivity of a ballast aggregate.

IRI_FPA-VR: No direct relationship is found between the force propagation angle and the void ratio. However, a low void ratio usually indicates a large number of ghost particles, which is responsible for the changing pattern of loading and force propagation angle.

5.8 The optimized ballast aggregate

Taking all the 5 investigated mechanical behaviors into consideration, the optimized ballast aggregate should have particular properties such as low ballast settlement, low breakage rate, low and stable number of ghost particles, high and stable force propagation angle and high and stable void ratio.

The low settlement of ballast aggregate is the most important characteristic of the optimized ballast aggregate. The low settlement ensures the smoothness of the rail, and thus reduces the dynamic impact on the rail and prolongs the maintenance cycle. It should be considered in first priority when optimizing the conventional ballast track. The low breakage rate and the high and stable force propagation angle indicate a good force distribution inside of the optimized ballast aggregate under loading. As result, the aggregate is structurally stable and there is no excessive position change of ballast stones. The low number of ghost particles and the high void ratio guaranties a decent hydraulic conductivity of the optimized ballast aggregate, which is important for preventing railway defects such as mud pumping.

Regarding to the form distribution, the optimized ballast aggregate should be: first, has small mass proportion (at most 16%) of small ballast stones (smaller than 22.4mm) to avoid excessive number of ghost particles, which jeopardizes the structural stability and hydraulic conductivity of the aggregate. Second, the mean size of the ballast stone should be reasonably enlarged, so that a better interlocking effect and a high force propagation angle can be guaranteed. Third, there should not be a

large proportion of flat ballast stones in the aggregate. It is still believed that flat ballast stones could be easier broken under loading, even though a clear relationship is not shown in the simulation due to the lack of simulated loading cycles.

Under the conditions stated above, the form distributions of optimized ballast aggregates (from the 15 generated form databases) can be: G_1-5, G_2-1 and G_3-1. The three form databases have large mean size of forms, low mass proportion of small ballast stone and flat ballast stones. The simulated ballast aggregates using the databases yield low settlement, low breakage rate, stable and high force propagation angle, low and stable number of ghost particles and decent void ratio.

6 Conclusions and future works

6.1 Conclusions

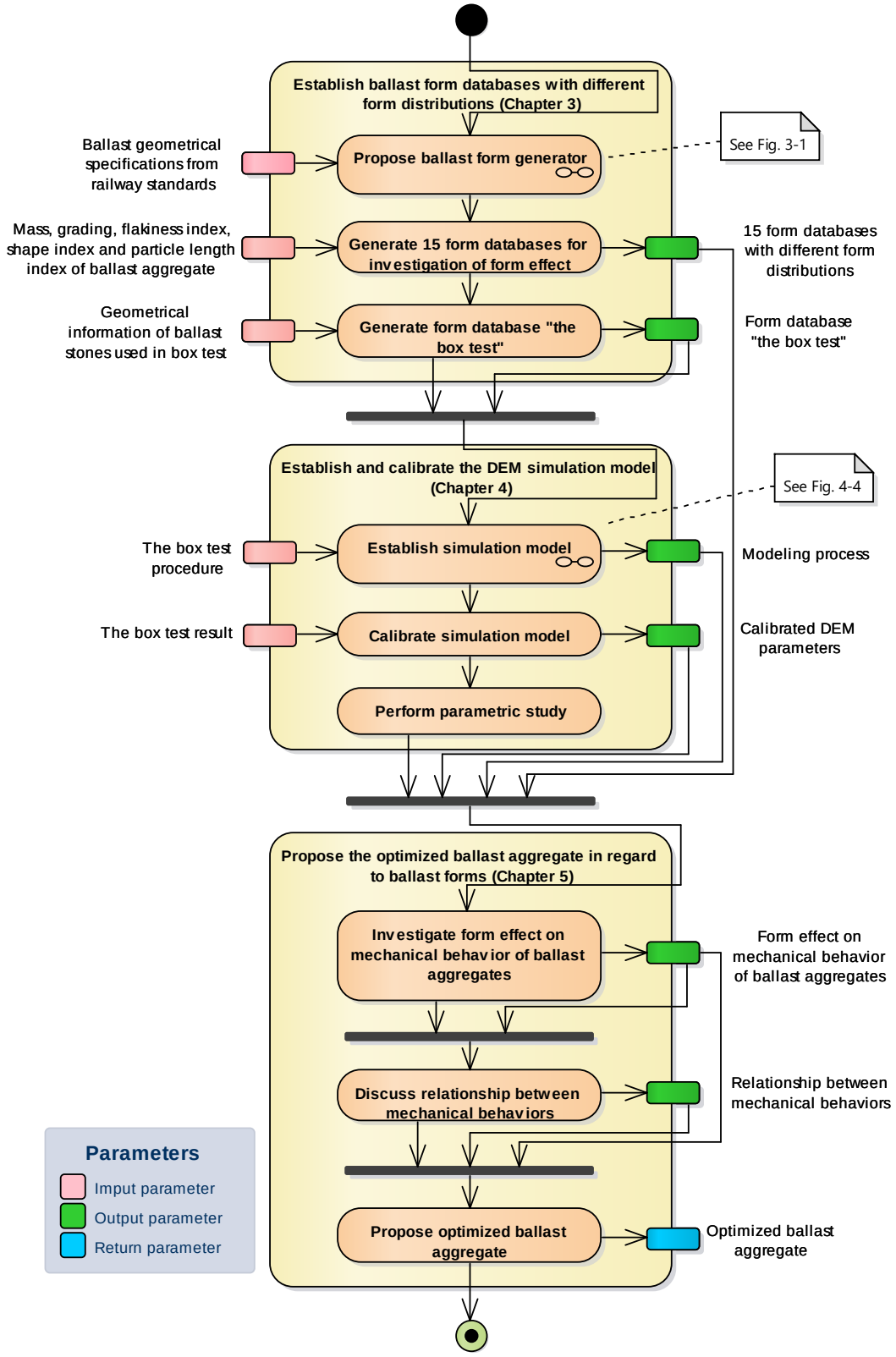

Fig. 6-1. The complete workflow of this dissertation

In this dissertation, in order to support the optimization of ballast stones regarding to their geometrical properties, Discrete Element Method (DEM) based simulations are performed to investigate the form effects of ballast stones on mechanical behavior of ballast aggregates. An optimized ballast aggregate should have low ballast settlement, low breakage rate, low and stable number of ghost particles, high and stable force propagation angle and high and stable void ratio. As a preparation of the DEM simulation, a ballast random form generator is proposed in Chapter 3, which is designed to capture the form distribution of given ballast aggregate, or to establish non-exist ballast form databases for the latter study on the form effect. The establishment, calibration of the DEM and a parametric study of the calibrated DEM parameters are performed in Chapter 4, simulative quantification methods of the mechanical behavior are also explicated. In Chapter 5, based on the generated 15 form databases, the influence of ballast form distribution on ballast performance is investigated. Characteristics of optimized ballast aggregate are summarized. The complete workflow of this study, including activities and their input/output parameters in each chapter, is demonstrated in Fig. 6-1.

The main achievements of this dissertation are summarized as follows:

a. An algorithm-based random form generator for ballast stones is introduced. The generator uses geometrical specifications of ballast stones according to the European standards of ballast aggregates to quantify the form of a single ballast stone, as well as to generate ballast aggregate with the given form parameters. 15 aggregates are created to examine the reliability of the generator. The result shows good performance of the generator, especially when a larger aggregate is to be created. The generator can be used for creating ballast aggregates with different form parameters, so that their impact on the mechanical behavior of ballasted tracks can be studied further in DEM simulations
b. An approach for simulating one ballast stone by using Bonded Particle Model (BPM), as well as a simulative method for assembling the simulated ballast stones, are proposed. The material modeling support of DEM software Particle Flow Code (PFC) is improved so that the ballast stones can be simulated by irregular-shaped polyhedrons. The proposed establishment process of the DEM model, i.e., the simulation of one ballast stone, ballasts assembling and the load-

ing process can be used universally for all ballast aggregate including ballast layer of a conventional ballast track

c. A box test is performed. The test procedure is expatiated. the test result is used for the calibration of the DEM model
d. A parametric study of two DEM parameter, i.e., the strength and cohesion scaling factor F_{str-co} and the friction coefficients μ, is performed. It is shown that the accumulated settlement of ballast aggregate increases with the decreasing value of F_{str-co}, while a higher value of friction coefficient μ will cause a higher resistant shear force, which ease the relative motion of two particles and increase the settlement of ballast aggregate under loading
e. Simulative quantification methods of mechanical behavior are elaborated. Two simulation cases are presented to testify the methods. It is found that there are two types of settlements: progressive settlement and drastic settlement. The reason for progressive settlement is the rearrangement of ballast stone positions under loading. It happens more often if the sizes of ballast stones are generally smaller. The drastic settlement is caused by breakages of ballast stones, which happens more if the ballast stones are generally bigger
f. Influence of ballast form distribution on ballast mechanical behavior is investigated. Ballast DEM aggregates are generated based on 15 form databases, which vary in different mean sizes, size and shape distributions of ballast stones. For each form database, the final result is determined by the mean value of 10 simulation cases, so that the randomness caused by random picking of the form from the database can be reduced. Main conclusions are listed as follows:
    - Small ballast stones will cause a loss of interlocking, which results a high settlement and instability of the aggregate
    - The interlocking effect is a yes-or-no incident, i.e., it will appear and exert complete influence from a certain value of the ballast mean size
    - Above a certain value from 16% to 17.5% of the mass proportion of ballast stones smaller than 22.4mm, the ballast aggregate will become instable
    - No clear trend is shown regarding to the breakage rate. The number of breakages is quantitatively low (smaller than 1% of the total bonds). The reason is that the simulative loading steps are not enough. A longer loading process should be performed to investigate the breakage behavior

- The number of ghost particles is strongly corresponded to the settlement of the ballast aggregate. Since the ghost particles are the ones which do not take any structural loads, the more ghost particles there are, the less structural stability there should be. Besides, the small sized ballast stones, which causes high settlement, would be highly possible to become ghost particles if they settled inappropriately
- The force propagation angle is related to the stability of the ballast aggregate. A unstable aggregate will arouse constant change of force propagation angle
- The void ratio basically stays unchanged during the loading process. To acquire a higher void ratio, the mean size of the ballast stones should be high and the proportion of small ballast stones should be low

g. Interrelationship between mechanical behaviors is discussed. A high settlement of ballast aggregate will be usually accompanied by high number of ghost particles, low void ratio and drastically changing force propagation angle. These properties of ballast aggregates will cause multiple defects, and they are all related to the mass proportion of small ballast stones. To this end, an optimized ballast aggregate should have small mass proportion of small ballast stones and enlarged mean size. Meanwhile, even though the correlation between proportion of flat ballast stones and breakage rate is not clearly shown, it is still believed that the flat ballast stones would break easier due to their reduced cross section area. therefore, a large number of flat ballast stones should be avoided in an optimized ballast aggregate

Based on the main achievements of this dissertation, several suggestions can be provided to improve the mechanical behavior of ballast track in real world. First, mass proportion of small ballast stones (sizes smaller than 22.4mm) should be lower than 16%, so that the number of ghost particles, which jeopardizes the stability and the hydraulic conductivity of the ballast bed, can be minimized. Second, bigger ballast stones should be used, because they forms a more stabilized ballast aggregate with better interlocking effect. Third, ballast stones with cubical forms should be more used, since breakage behavior of such stones is better than the flat ones.

6.2 Future works

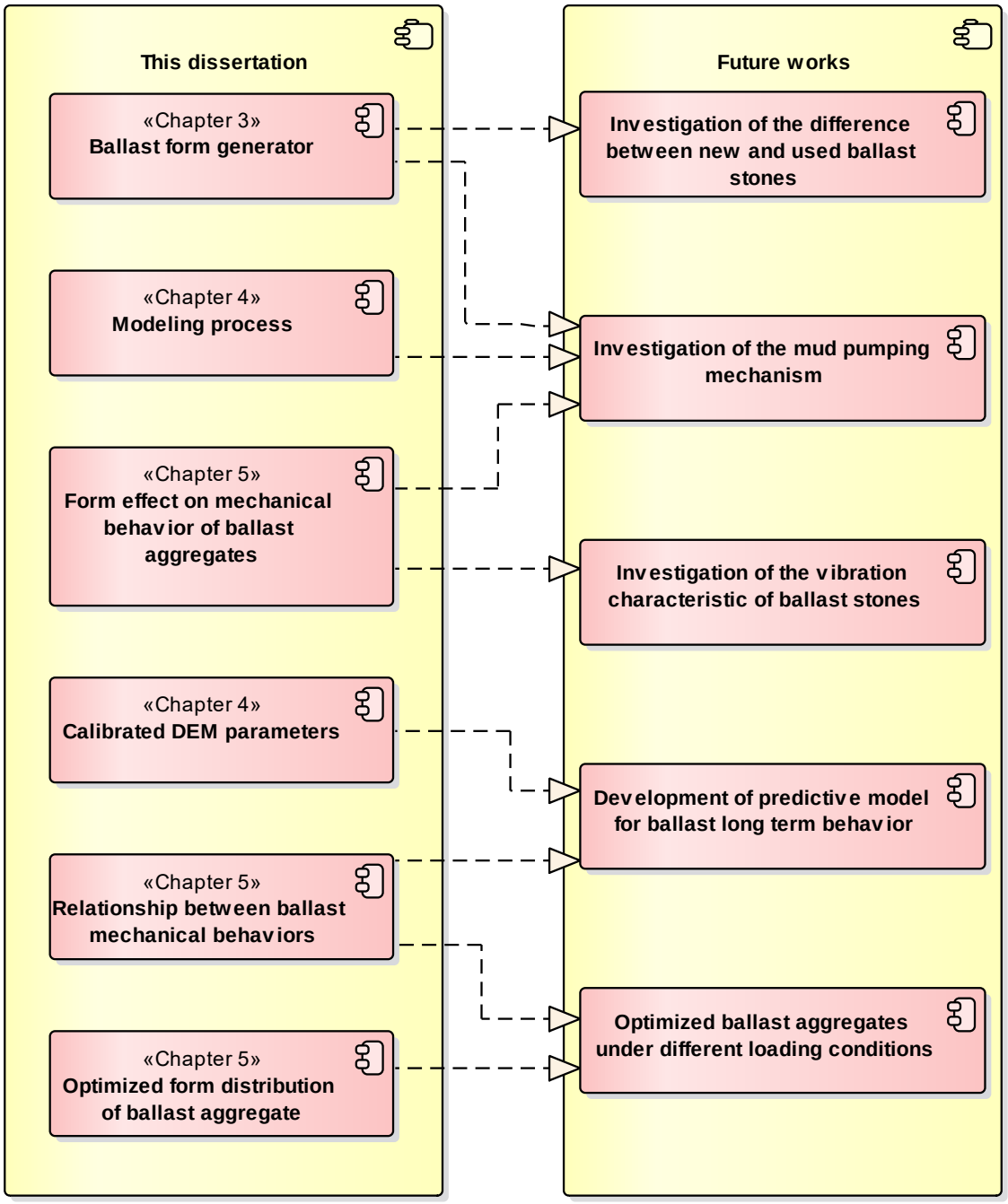

Fig. 6-2. Future works

In this study, using discrete element modeling, the form effect on ballast mechanical behavior is investigated. Based on the achievements of this dissertation, suggestions for future research are made, demonstrated (see Fig. 6-2), and expatiated in the following list:

a. Under repetitive train load, ballast stones degrade from sharp-edged new stones to sphere-shaped used stones due to abrasion. If ballast stones are represented

by polyhedrons, it is clear that a used ballast stone has more vertexes. Using the ballast random form generator, used ballast stone can be created by adjusting the number of vertexes. It is interesting to find out the relationship between degree of usage (employed years, total amount of loading or number of trains) and degree of roundness (number of vertexes) of ballast stones. Afterwards, the form generator can generate ballast aggregate with given degree of usage, and thus its mechanical behavior can be studied in further DEM simulations (a loss of interlocking is expected within the used ballast aggregate)

b. Mud pumping is a typical defect of conventional ballast track. It decreases the elasticity of the track bed, causes a loss of hydraulic conductivity, and even worse, it leads to unsupported sleepers. On the basis of the modeling technic proposed in this dissertation, the subgrade of ballast track, which is usually made up of fine particles, can be simulated by a cluster of small balls. The moisture of the mud, which reduces the interacting frictional forces between ballasts, can be reproduced by reducing the DEM parameter friction coefficient. The formation of mud pumping, which is that the subgrade particles go up to the ballast layer under loading, can be simulated. Its mechanism can be then studied, so that preventive methods can be proposed
c. Long term behavior of ballast stone should be investigated. The currently used BPM model is too computational intensive for long term behavior. Therefore, a simplified DEM model, which requires less computing power and at the same time maintains the ability of capturing the breakage and abrasion behavior of ballast stones, should be firstly proposed. Afterwards, a predictive failure model of ballasts track based on the evaluation of track condition according to its mechanical behavior can be proposed. In this way, track failures can be foreseen and appropriate remedy work can be performed beforehand
d. DEM simulation enables investigation of vibration characteristics of ballast stones. Based on the proposed ballast aggregate model, the position change of ballast stones can be extracted in every calculation cycle. The acceleration of ballast stones in the time domain can be derived, and thus be transferred into the frequency domain by using Fast Fourier Transform. It is reasonable to assume that vibration in high frequency could possibly cause more abrasions of ballast stones, which makes them less angular and causes a loss of interlocking effect; while vi-

bration in low frequency would create higher local stress, which could yield more breakages. Besides, the result of vibration analysis of ballast aggregate should be used for its optimization in the aspect of energy dissipation, which is crucial for preventing the vibration from propagating to sensible objects such as hospitals, schools or precision instrument factories

e. Optimized ballast aggregates of conventional ballast track under different loading conditions should be proposed. The gained result of this dissertation forms a good foundation for the whole-track study in the sense of the modeling technic, the proposed relationship between ballast mechanical behaviors and the optimized ballast aggregate based on the box test. There should be a step forward to the real ballast track and the optimized ballast track can be customized for operation programs with various traffic loads such as high speed passenger train, freight train and metro

Abbreviations

BPM	Bonded Particle Model
BR	Breakage Rate
BS	Ballast Settlement
CB	linear Contact Bond model
DEM	Discrete Element Method
FJ	Flat Joint model
FPA	Force Propagation Angle
GP	Ghost Particle
IEV	Institute of Railway and Transportation Engineering (in German: Institut für Eisenbahn- und Verkehrswesen)
IRI_A-B	Interrelationship Index of mechanical behaviors A and B
LC	Linear Contact model
MD	Molecular Dynamics
MPA	Material Testing Institute (Materialprüfungsanstalt in German)
PB	linear Parallel Bond model
PFC	Particle Flow Code
SD	Size Diversity
VR	Void Ratio

Notations

Parameters in railway standards

D	The maximal size of the particles (in mm) in the ballasts testing sample
d_i/D_i	Particle (ballast stone) group, where d_i and D_i are respectively the smaller and bigger meshing size of two sieves, between which the particle group stays after shaking
E	The particle thickness
FI_i	The flakiness index of the group d_i/D_i
FI	The flakiness index of the whole ballast sample
$FI_{RB}X$	The flakiness index category X
$G_{CRB}X$	The grading category X
L	The particle length
$L_{RB}X$	The particle length category X
M	The minimal mass of the ballast testing sample
M_1	The mass of the ballast testing sample after drying
m_i	The mass of the particles (flat ballast stones), which go through the corresponding grid sieve of particle group d_i/D_i
M_2	The summed mass of particles, which go through the grid sieves
$\sum M_{1i}$	The sum of mass of all the particle groups
$\sum M_{2i}$	The sum of mass of the non-cubic particles in each particle group
P	The mass of the ballast stones which go through all the sieves
PM_i	The percentage passing by mass of the ith ballast group
R_i	The mass of ballast group on the ith sieve of the sieve tower after

	shaking
SI	The shape index of the whole ballast sample
$SI_{RB}X$	The shape index category X

DEM modeling parameters

A_{sum}	Area of a polygon (a ballast form)
$D_l^{(j)}$	The diameter of the smaller ball of the two contact balls
E^*, E_n^*	Effective modulus of the FJ and LC model
F_c	Total contact force of two contacted balls
$F_{n,s}^{(e)}$	The resolved tension and shear force of the element contact force
F_{str-co}	Strength and cohesion scaling factor
$F^{(e)}$	The element force at the center of the interface of FJ contact
g_i	The installation gap for FJ model installation
g_0	The initial surface gap
$k_{n,s}$	The normal and shear stiffness of the FJ model
L_{sum}	The cross-sectional length of a polygon (a ballast form)
L_{edge}	The length of a edge of a polygon
M_c	Total moment of two contacted balls
$M^{(e)}$	The element moment at the center of the interface of FJ contact
$M_{t,b}^{(e)}$	The resolved twisting and bending moment of the element moment
$\hat{n}_c$	The normal direction of the FJ element plane
$n_{B,G,S}$	The number of bonded, gapped and slit FJ contacts
n_{FJ}	The total number of FJ contacts
N_r	The number of interface elements of the FJ bond

$N_{r,a}$	The number of FJ elements in radial and circumferential direction
u_n	The overlap of contacted particles in DEM
$\overrightarrow{v_{1,2}^a}$	Vectors from one vertex of the triangle to the other two
x_c	The center of the interface of two contacted balls
$\phi_{B,G,S}^+$	The fractions of initially bonded, gapped and slit FJ contact
C_λ	The radius multiplier code
λ_v	The radius multiplier value
σ_c	Tensile strength of the FJ bond
τ_c	Shear strength of the FJ bond
c	Cohesion
ϕ	The friction angle. Ratio of shear stress τ and normal stress σ
μ	Friction coefficient
κ^*, κ_n^*	The normal to shear stiffness ratio of the FJ and LC model

Parameters of the random form generator for ballast stones

a, b, c	The three orthogonal dimensions of one generated ballast form
V_{sum}	The volume of a polyhedron (a ballast form)
$\overrightarrow{v_{1,2,3}^v}$	Vectors from the three vertexes of a sharing facet on both the ith tetrahedron and the original polyhedron to the fourth point, which is inside of the polyhedron

Parameters of mechanical behavior of ballast aggregates

A_{void}	The voids area
A_{total}	The total area
BR	Total breakage rate
$BR_{T,S}$	Breakage rate in tension and shear

$FA_{averaged}$	Averaged force propagation angles on the left and right side
FA_{left}	The force propagation angles on the left side
FA_{right}	The force propagation angles on the right side
VR	The void ratio

Glossary

Ballast form	Geometrical property of a ballast stone including its size and shape
Ballast form distribution	The gradation of a ballast aggregate
Breakage rate	The ratio between the broken FJ bonds and the FJ bonds in total, which shows the level of breakage of a ballast aggregate under loading
Calculation cycle / cycle sequence	An ordered set of operations within one timestep in DEM simulation. Each operation has a floating point number assigned to it, termed a cycle point
FISH callback function	An additional operation, which can be added to the cycle sequence at various places by assigning its cycle point
Force propagation angle	The angle of railway loading propagation in a ballast aggregate
Ghost particle	A particle, whose particle coordination number is less than or equal to 2
Material-modeling support	A consistent set of FISH functions, which supports material genesis and testing of PFC materials with microstructural monitoring
Particle coordination number	The number of contacted neighbor particles of a certain particle
Settlement of ballast aggregate	The vertical displacement of the loading element in the box test simulation
Simulation scenarios	Simulation models with different parameter sets or different used form databases.
Simulation cases	Simulation models with the same modeling parameters and the same used form database, but vary due to the random

	pick of the forms and the materials from the database
Void Ratio	The degree of voids of a ballast aggregate

Appendix I: Research framework at Institute of Railway and Transportation Engineering (IEV) on railway constructive direction

Research framework on railway constructive direction at IEV is shown in Appendix Fig. 1. This dissertation is part of research from direction 2. All the three directions interact with each other in aspects of data exchange and method validation. Under such structure, one research focus could benefit from others, and a comprehensive understanding about railway infrastructure could be gained [48,49,51].

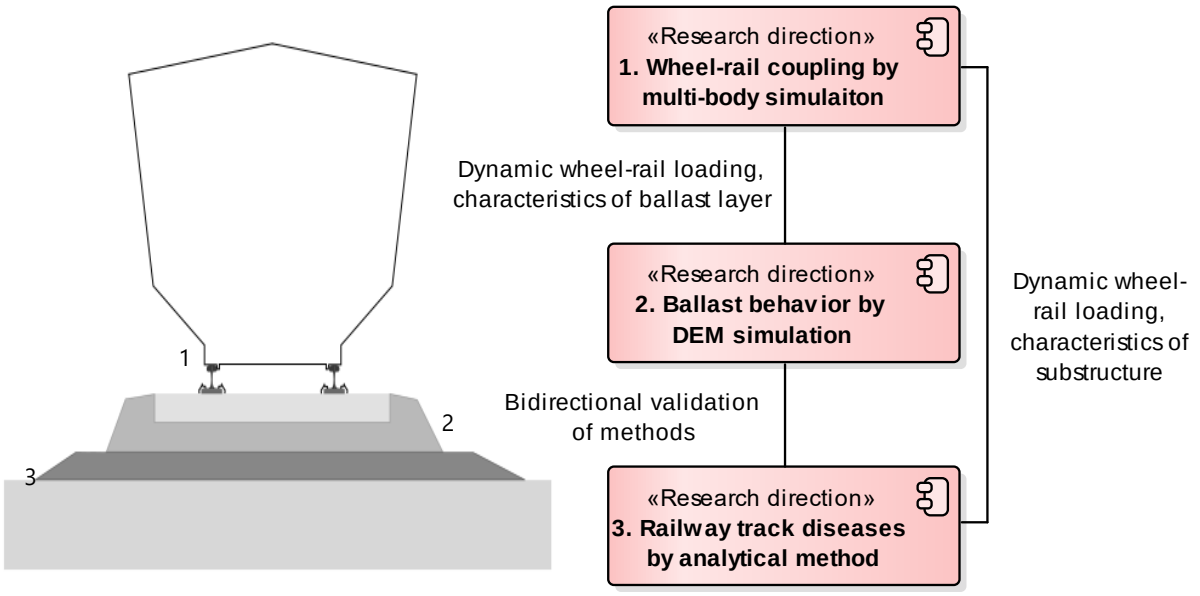

Appendix Fig. 1. Research framework at IEV

Appendix II: A 3D simulation case with a breakable ballast model

To support the argument that it is appropriate to use 2D simulation instead of 3D simulation in this study, a 3D simulation case of the box test with a breakable ballast model is performed. The modeling process is briefly introduced. The simulation result is presented. The hardware of the computer used for the 3D simulation case is listed in Appendix Table 1.

Appendix Table 1: Computer configuration

Processor	Intel Xeon E5-2620 v4 ,8x 2.1GHz
RAM	32GB DDR4-2400 Corsair Vengeance LPX | 4x 8GB
Graphics card	NVIDIA Quadro K620 2GB DDR3
Motherboard	ASUS X99-E WS/USB 3.1
Hard drive	Samsung SSD 850 Pro 256GB + WD Caviar Red 1TB
CPU cooler	Shadow Rock Slim 135mm PWM-Cooler
Computer case	AeroCool Aero 1000
Power supply	6000W Straight Power E10 CM
Operating system	Windows 10 Enterprise, 64-bit

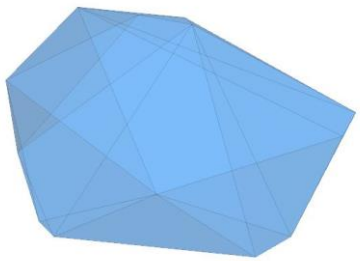

a: subsequent selection of one ballast form from the form database

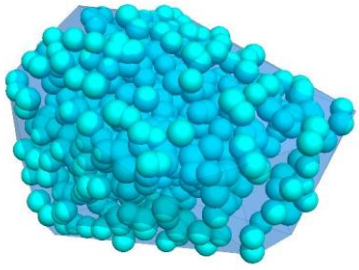

b: throw the balls into the form

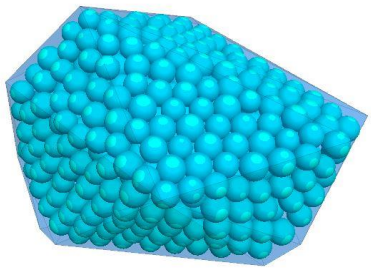

c: automatic balancing process

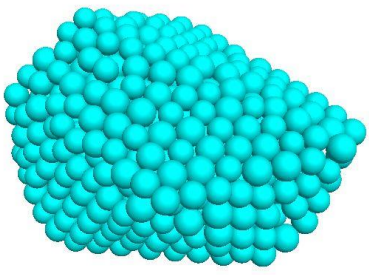

d: save the positions of the balls

Appendix Fig. 2. Sub-steps of building a BPM in 3D

The modeling process of a 3D simulation case is similar to a 2D one, which is explained in section 4.2. The process is divided into two steps: Building of the Bonded Particle Models (BPMs, see Appendix Fig. 2) and assembling of the BPMs (see Appendix Fig. 3). For detailed explanation of the sub-steps please refer to section 4.2.

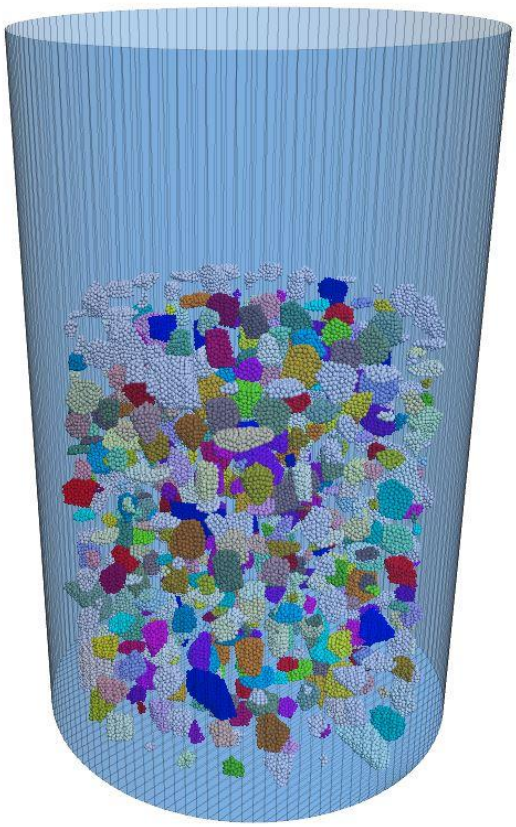

a: random selection of BPMs from the BPM database

b: free dropping of the BPMs

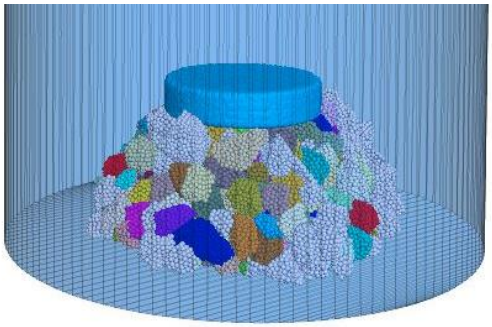

c: tamping of the BPMs

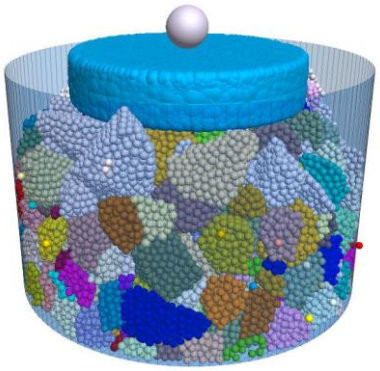

d: container reset and pressing element setups

Appendix Fig. 3. Sub-steps of assembling the BPMs in 3D

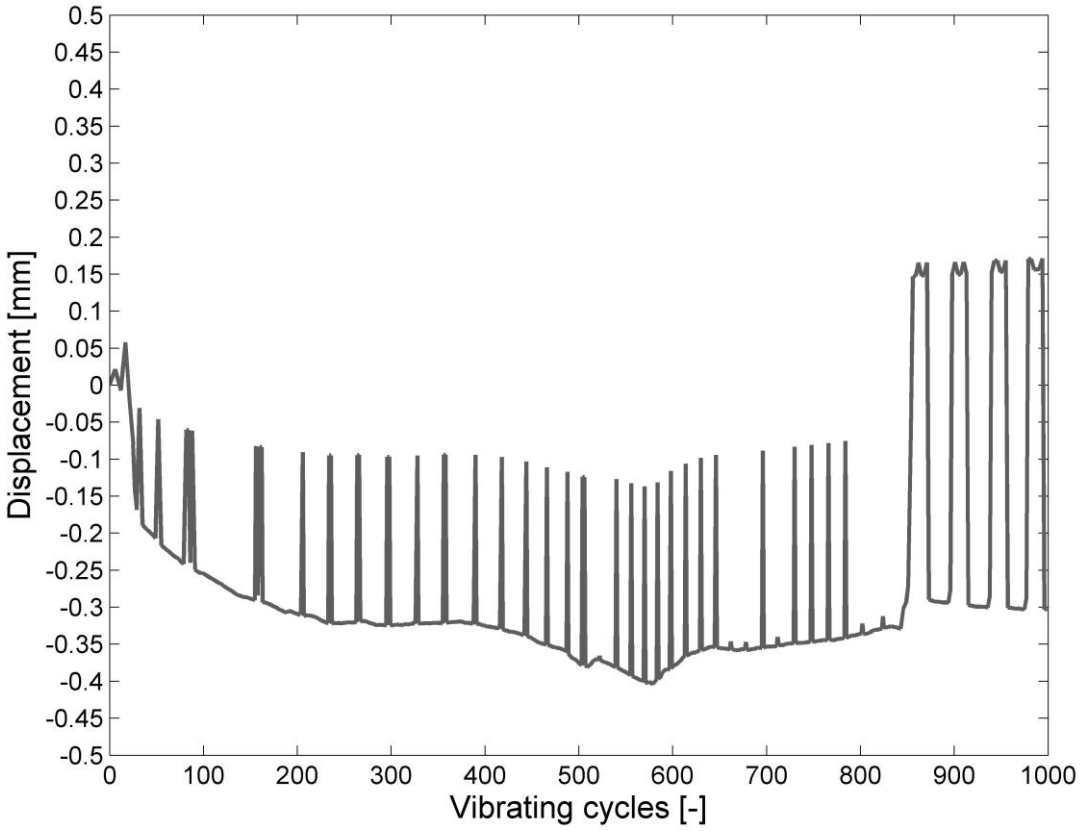

Appendix Fig. 4. Ballast settlement of the 3D simulation case

The 3D simulation case takes over five days to finish. However, as shown in Appendix Fig. 4, the simulation result is not satisfactory. A desired gradual accumulation of settlement is not shown. Instead, the settlement curve is zigzag, which indicates the ballast aggregate is really hard and rigid. On one hand, it means that a loading cycle can be done in a relatively short time, which means to get a desired settlement curve, it takes even more time than five days; on the other hand, it proves the point that 3D simulation is not an option for this study, since a calibrated model cannot be built just once and calibration is way too expensive regarding to time.

The calibration of the 3D model includes the calibration of modeling parameters and the calibration of the modeling procedure. After calibration, convincing 3D simulation result can be obtained and be comparing to 2D model.

Appendix III: A 3D simulation case with an unbreakable ballast model

To compare results from the 2D model and the 3D model, parameters in the 3D model must be calibrated. While it is too difficult to calibrate the breakable ballast 3D model (see Appendix II) because of the computing time, in this section, a simulation case with unbreakable ballast model is proposed. The unbreakable ballast model, i.e., the “clump” in PFC, is consisted of pebbles. A pebble is in great extent similar to a ball. However, unlike a collection of balls, there is no interaction between pebbles inside of a clump, meaning relative motions and forces between pebbles do not exist in the simulation. As a result, using clump to simulate ballast stone can save great computing time.

The modeling process of a 3D simulation case with unbreakable ballast model is divided into two steps: Building of the clumps (see Appendix Fig. 5) and assembling of the clumps (see Appendix Fig. 6). The assembling process is similar to the one with breakable ballast model, which is shown in Appendix II. However, the clump building process is totally different comparing to the BPM building process. Here, an algorithm called “Bubble Pack” is used for generating the clumps (i.e., the ballast stones).

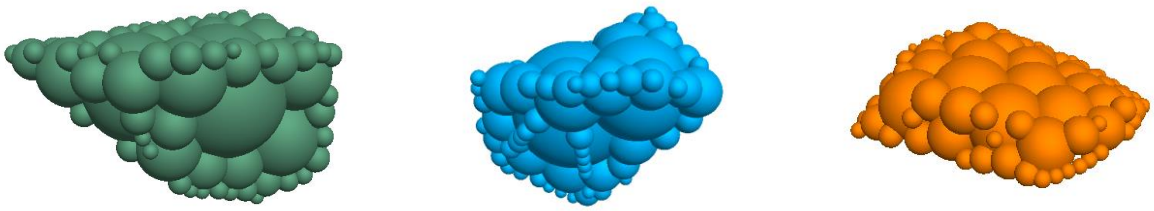

a: clump 1 b: clump 2 c: clump 3

Appendix Fig. 5. Three created clumps representing ballast stones with different forms

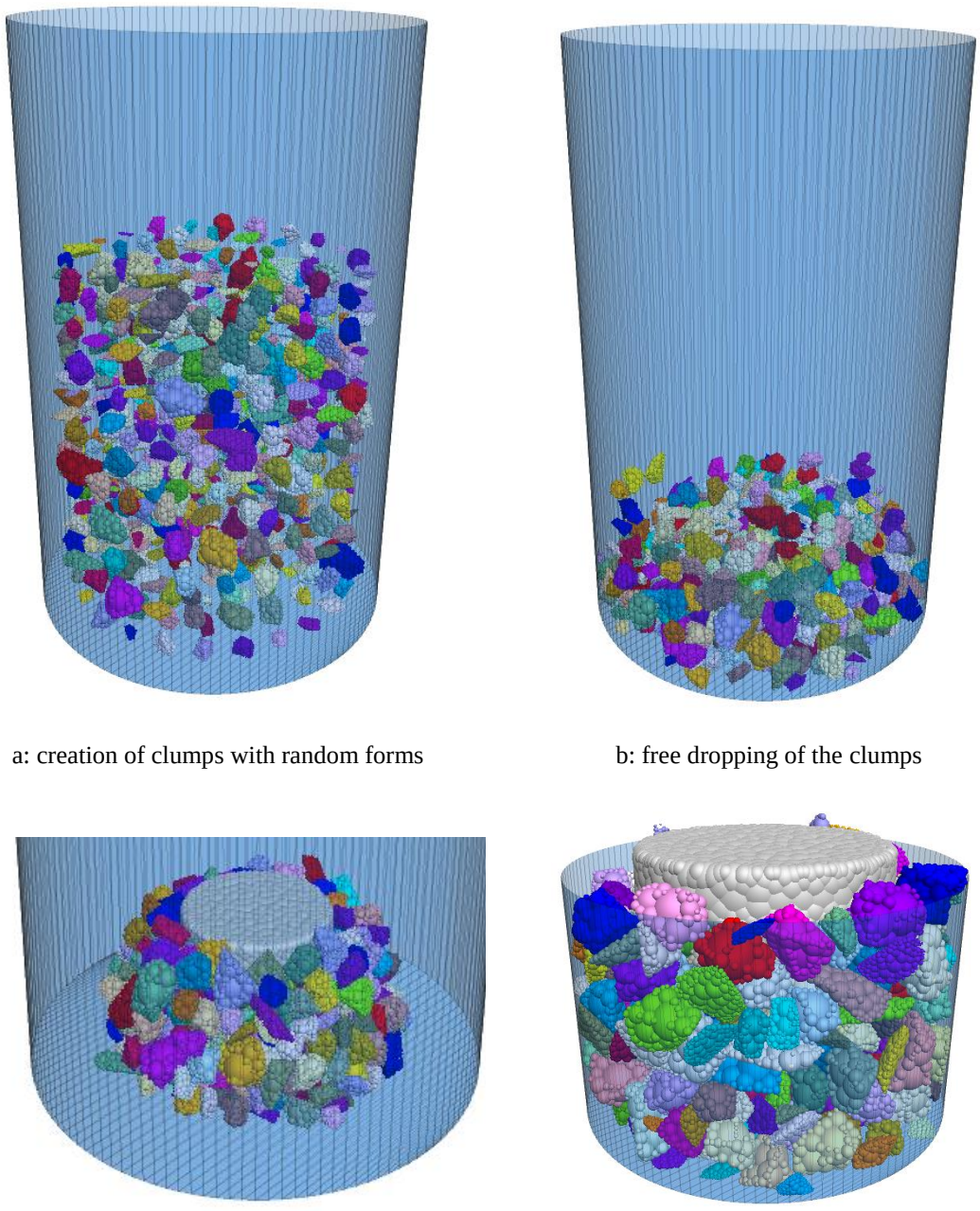

a: creation of clumps with random forms

b: free dropping of the clumps

c: tamping of the clumps

d: container reset

Appendix Fig. 6. Sub-steps of assembling the clumps in 3D

The Bubble Pack algorithm is a method for composing the pebble aggregate. It fills multiple pebbles into the pre-defined geometry shape, i.e., ballast form from the form database generated in Chapter 3. The sizes of pebbles are governed by the key parameter “ratio”, which is the ratio of the smallest to largest pebble in the clump (0 < ratio < 1). Another important parameter “distance” controls the overlap of the adjacent spheres in the clump (0 < distance < 180). By distance = 0, the adjacent spheres do not overlap, i.e., they connect only at one point; by distance = 180, two

spheres are fully overlapped. The higher the value of distance is, the more spheres there are and the smoother a ballast stone can be represented. Appendix Fig. 7 shows the different representations with different parameters of a same ballast stone.

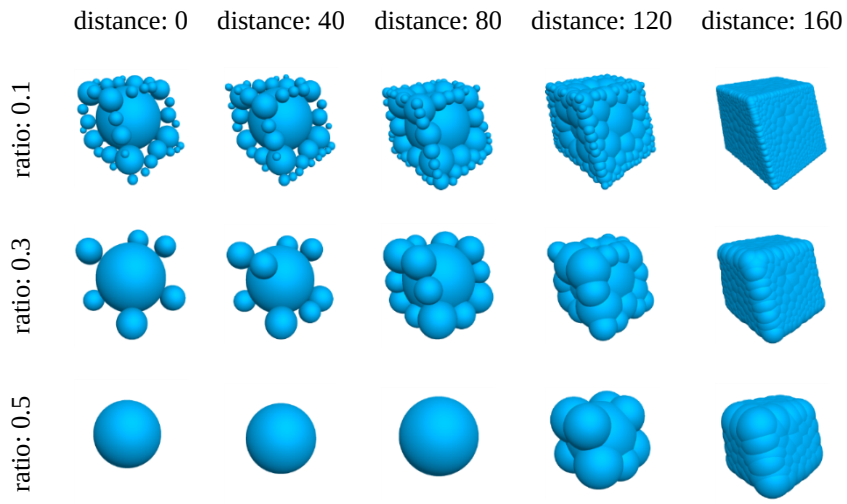

Appendix Fig. 7. Same ballast stone with different "Bubble Pack" parameter

Even though more pebbles mean more accurate representation of a ballast stone, it is necessary to control the number of the pebbles because it causes higher calculation time, simply because there are more simulative elements in the model. To simulate the angular shape of ballast, the parameter ratio should be small so that some of the spheres can be small enough to fill the edge of the shape, i.e., sharpen the shape. The other parameter distance shouldn't be too big so that the number of spheres could be minimized. In this study, ratio = 0.1 and distance = 80 are chosen (for result see Appendix Fig. 5).

Appendix Fig. 8 demonstrates the settlement curves from the box test and the simulation with unbreakable ballast stones. With the same computer used in Appendix II, whose configuration is listed in Appendix Table 1, the simulation takes two days, which is greatly reduced comparing to the duration of one simulation case with BPMs as ballast stones. It enables the running of multiple cases so that the parameters can be calibrated. As shown in the figure, the settlement curve from simulation matches not perfectly, but in great extent satisfactorily to the test result. There is no zig-zag as shown in Appendix Fig. 4, which means the modeling parameters are correctly set and the contacts between simulated ballast stones are not unrealistic rigid. Besides, the curve looks smooth, with nicely accumulated settlement. It is because the ballast model is unbreakable. The settlement is only from position rearrangement of ballast

stones under loading, but not from breakages of them, which could cause a sudden raise of the curve.

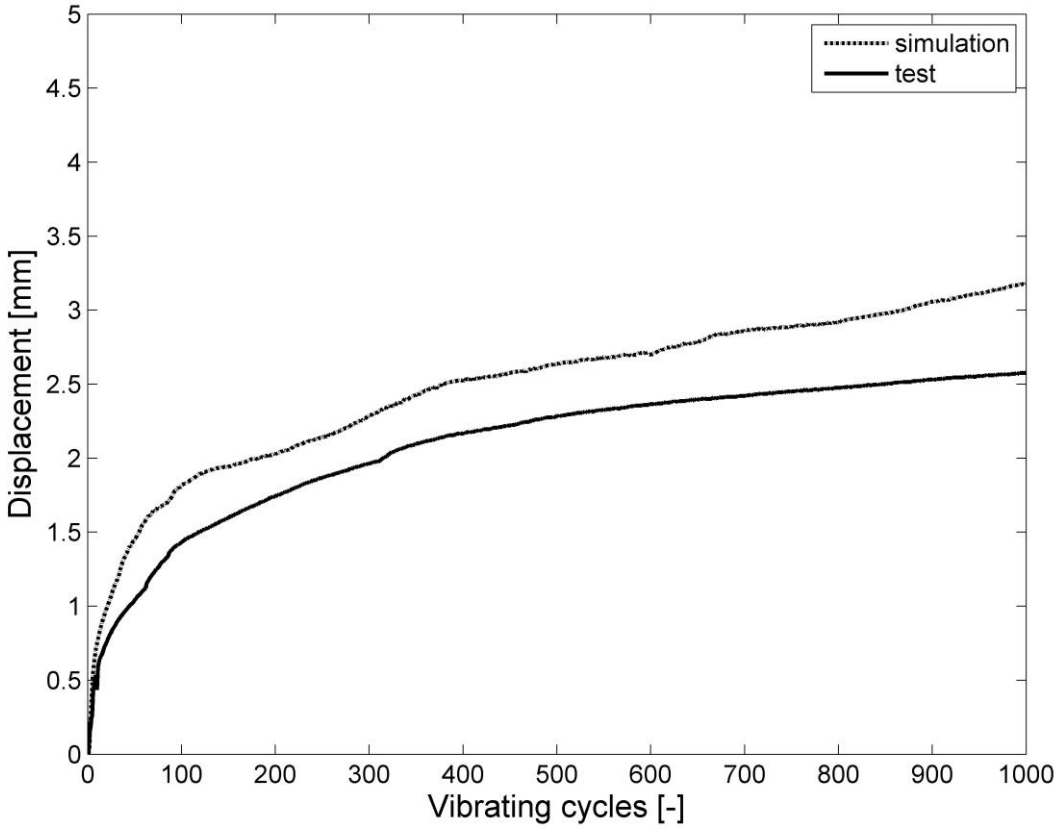

Appendix Fig. 8. Settlement curves from simulation and test

All the merits aside, the modeling with unbreakable ballast stones also has obvious disadvantages. First, breakage behavior cannot be simulated; second, even though the simulation time is reduced to two days, it is still not practical to run multiple cases. The calibration takes one month until the result shown in Appendix Fig. 8 is obtained, which is still not perfect, let along the research on the mechanical behaviors. Third, the result obtained by 3D simulation is not better than the one of 2D simulation as shown in Fig. 4-11. The advantages, which only the 3D simulation has, cannot be found in this study, and it is accompanied by great computing time expense. Therefore, 2D simulation is implemented in this dissertation.

Appendix IV: Sublayers of EA diagrams

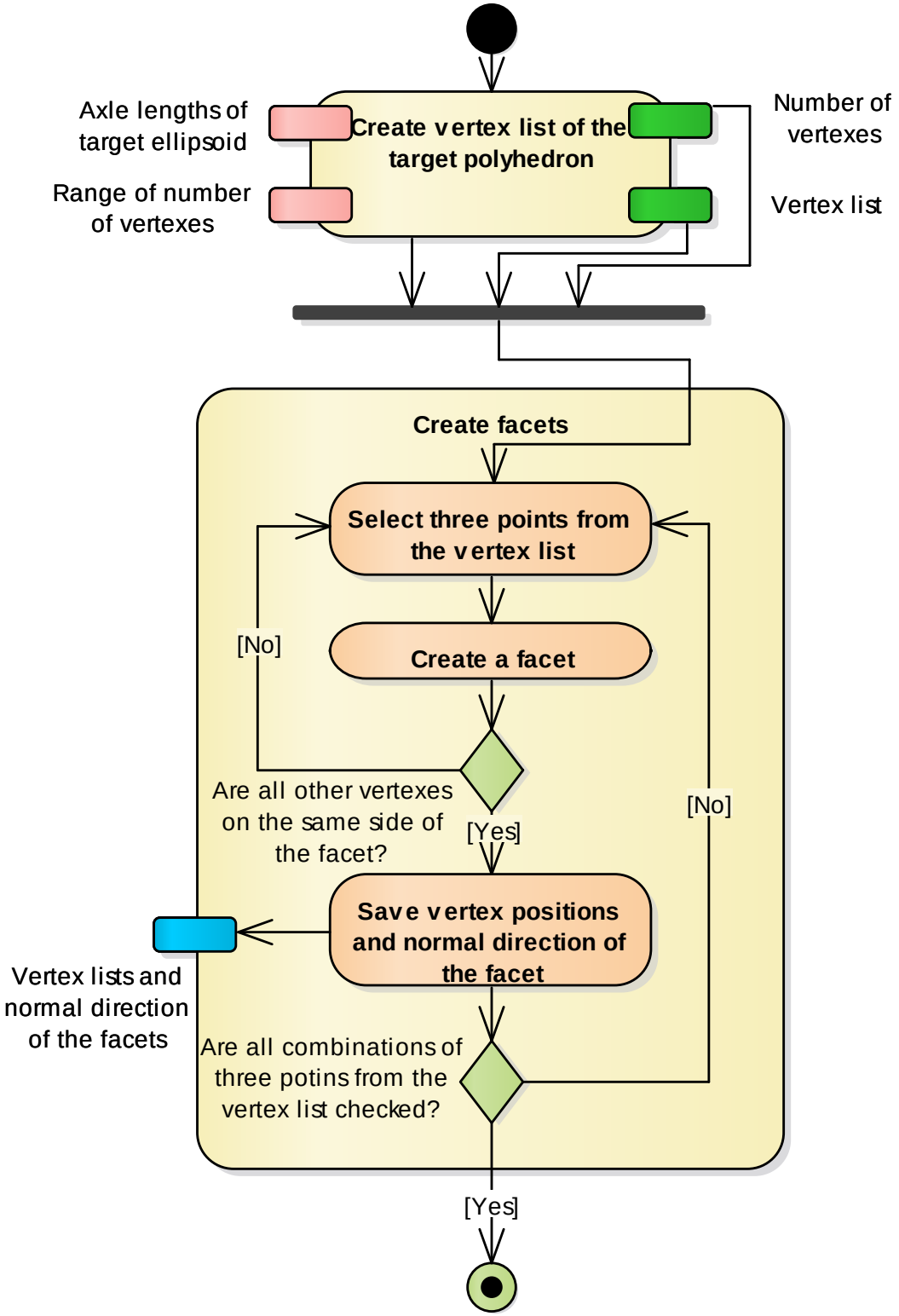

Appendix Fig. 9. Generate one ballast form

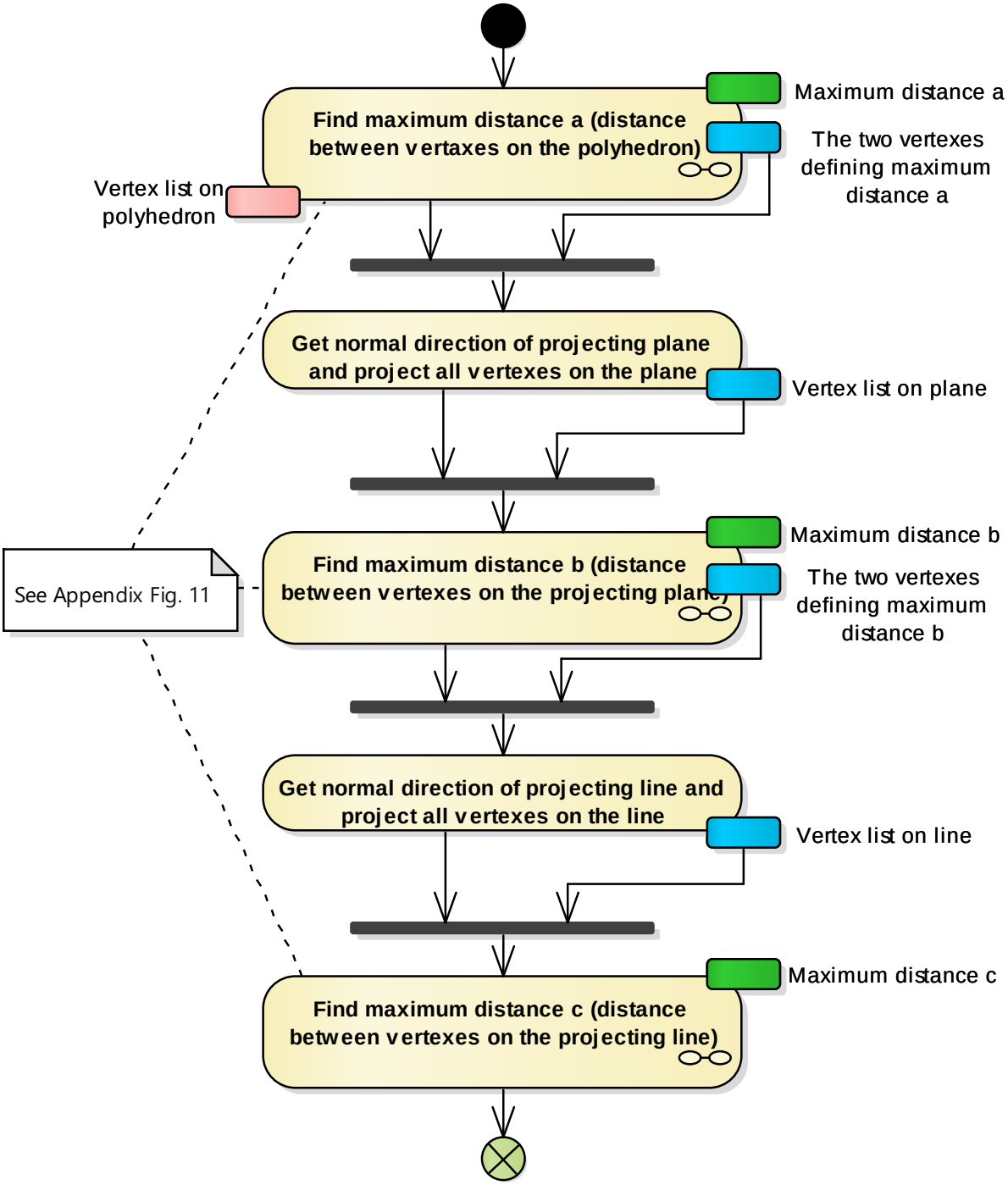

Appendix Fig. 10. Get the three orthogonal dimensions a, b and c of the form

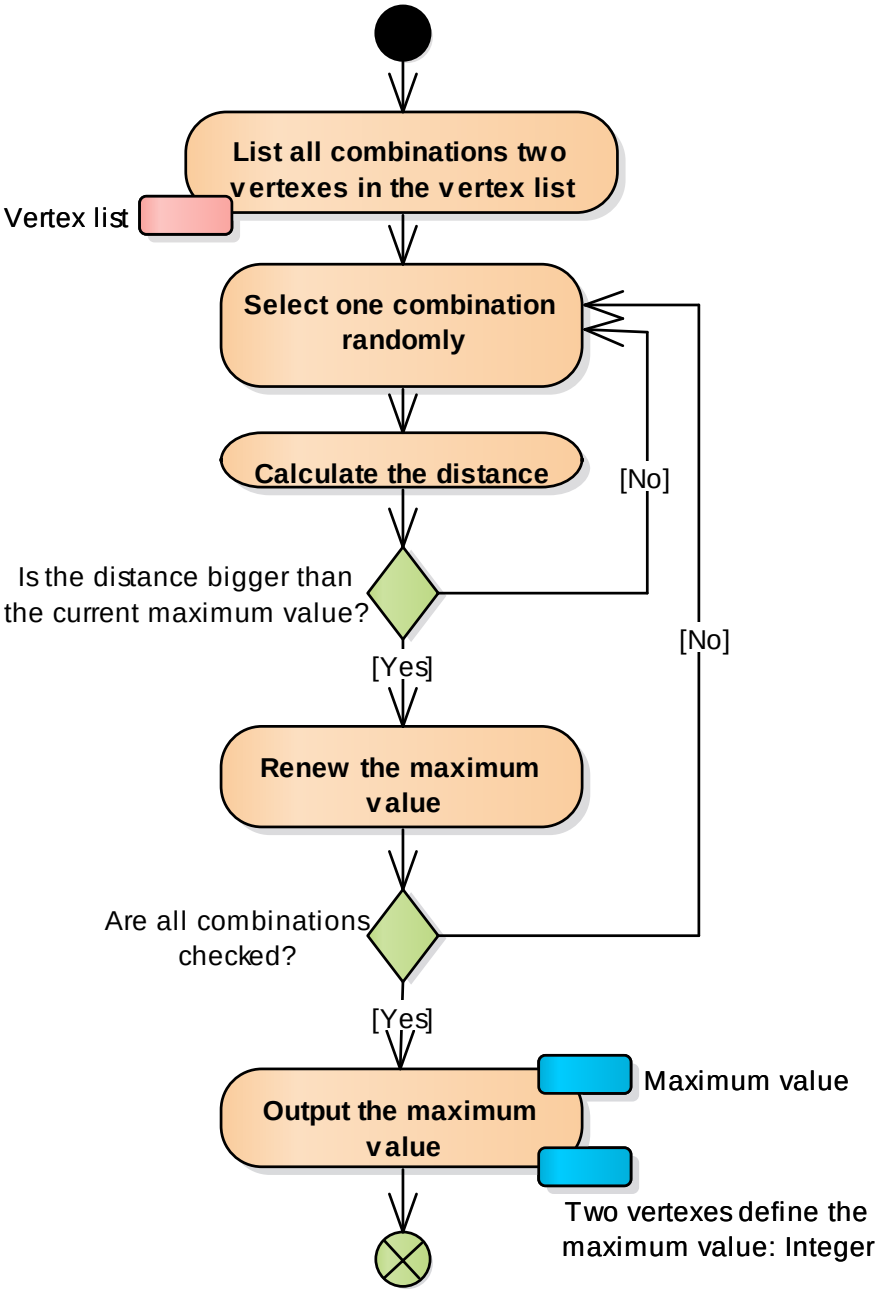

Appendix Fig. 11. Find maximum distance between two vertexes in vertex list

Appendix V: Explanation of Unified Modeling Language (UML) symbols used in Enterprise Architecture (EA)

 Activity initial	Start of an activity diagram
 Activity final	End of an activity diagram
 Flow final	End of a flow
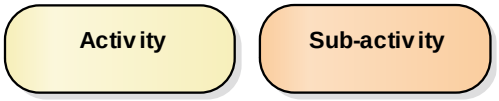	Preformed activity / sub-activity in the dissertation
	Input / output / return parameter of an activity
	Join
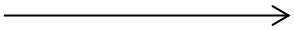	Flow from one activity to the other
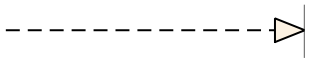	Realization
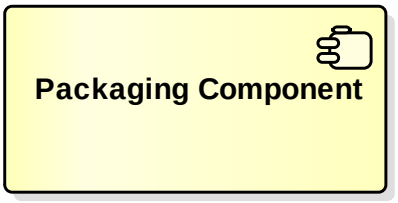	Component “This dissertation” and “Future works”
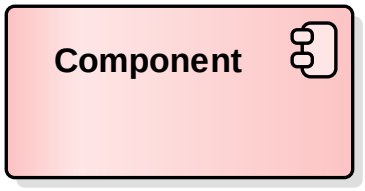	Things done in this dissertation or could be done in the future

References

[1] Lichtberger B. Handbuch Gleis: Unterbau, Oberbau, Instandhaltung, Wirtschaftlichkeit. 3rd ed. Hamburg: Eurailpress; 2010.

[2] Matthews V. Bahnbau. 8th ed. Wiesbaden: Vieweg + Teubner; 2011.

[3] Esveld C. Modern railway track. 2nd ed. Zaltbommel: Koninklijke van de Garde BV; 2001.

[4] Fendrich L. Handbuch Eisenbahninfrastruktur. 1st ed. Berlin: Springer; 2007.

[5] Suiker ASJ. The mechanical behaviour of ballasted reilway tracks. Netherlands: DUP Science; 2002.

[6] DIN EN, Deutsches Institut für Normung, Europäischen Normen. Prüfverfahren für geometrische Eigenschaften von Gesteinskörnungen - Teil 2: Bestimmung der Korngrößenverteilung Analysensiebe, Nennmaße der Sieböffnungen(DIN EN 933-2): CEN European Committee for Standardization; 00/1996.

[7] DIN EN, Deutsches Institut für Normung, Europäischen Normen. Prüfverfahren für geometrische Eigenschaften von Gesteinskörnungen - Teil 4: Bestimmung der Kornform – Kornformkennzahl(DIN EN 933-4): CEN European Committee for Standardization; 00/2015.

[8] DIN EN, Deutsches Institut für Normung, Europäischen Normen. Prüfverfahren für geometrische Eigenschaften von Gesteinskörnungen - Teil 1: Bestimmung der Korngrößenverteilung - Siebverfahren(DIN EN 933-1): CEN European Committee for Standardization; 00/2012.

[9] DIN EN, Deutsches Institut für Normung, Europäischen Normen. Prüfverfahren für geometrische Eigenschaften von Gesteinskörnungen - Teil 3: Bestimmung der Kornform - Plattigkeitskennzahl(DIN EN 933-3): CEN European Committee for Standardization; 00/2012.

[10] DIN EN, Deutsches Institut für Normung, Europäischen Normen. Gesteinskörnungen für Gleisschotter(DIN EN 13450): CEN European Committee for Standardization; 07/00/2013.

[11] Alder BJ, Wainwright TE. Phase transition for a hard sphere system. J. Chem. Phys. 1957;27(5):1208–9.

[12] Cundall PA. A computer model for simulating progressive, large-scale movements in blocky rock systems. In: Proc. Symp. Int. Rock Mech.

[13] Cundall PA, Strack ODL. A discrete numerical model for granular assemblies. Géotechnique 1979;29(1):47–65.

[14] Strack O, Cundall PA, University of Minnesota. Department of Civil and Mineral Engineering, National Science Foundation. The distinct element method as a tool for research in granular media: report to the national science foundation concerning NSF grant ENG75-20711: Department of Civil and Mineral Engineering, Institute of Technology, University of Minnesota; 1978.

[15] Walton OR. Particle-dynamics modeling of geological materials: Lawrence Livermore Laboratory; 1980.

[16] Campbell CS, Brennen CE. Computer simulation of granular shear flows. J. Fluid Mech. 1985;151(-1):167.

[17] Campbell CS, Brennen CE. Chute flows of granular material: Some Computer Simulations. J. Appl. Mech. 1985;52(1):172.

[18] Munjiza A. The combined finite-discrete element method. Chichester, UK: John Wiley & Sons, Ltd; 2004.

[19] PFC - Particle Flow Code. Minneapolis: Itasca: Itasca Consulting Group, Inc; 2014.

[20] Wang B, Martin U, Rapp S. Discrete element modeling of the single-particle crushing test for ballast stones. Computers and Geotechnics 2017;88:61–73.

[21] Cho N, Martin CD, Sego DC. A clumped particle model for rock. International Journal of Rock Mechanics and Mining Sciences 2007;44(7):997–1010.

[22] Potyondy DO. A flat-jointed bonded-particle material for hard rock. In: 46th U.S. Rock Mechanics / Geomechanics Symposium, Chicago, USA, June 24-27, 2012.

[23] Wu S, Xu X. A study of three intrinsic problems of the classic discrete element method using flat-joint model. Rock Mech Rock Eng 2016;49(5):1813–30.

[24] Xu X, Wu S, Gao Y, Xu M. Effects of micro-structure and micro-parameters on brazilian tensile strength using flat-joint model. Rock Mech Rock Eng 2016;49(9):3575–95.

[25] Vallejos JA, Salinas JM, Delonca A, Mas Ivars D. Calibration and verification of two bonded-particle models for simulation of intact rock behavior. International Journal of Geomechanics 2016:06016030.

[26] Cheng Y, Wong, Louis Ngai Yuen, Zou C. Experimental study on the formation of faults from en-echelon fractures in Carrara Marble. Engineering Geology 2015;195:312–26.

[27] Potyondy D. Material-modeling support in PFC: Explanatory notes.

[28] Lobo-Guerrero S, Vallejo LE. Discrete element method analysis of railtrack ballast degradation during cyclic loading. Granular Matter 2006;8(3-4):195–204.

[29] Popp K, Knothe K, Pöpper C. System dynamics and long-term behaviour of railway vehicles, track and subgrade: report on the DFG priority programme in Germany and subsequent research. Vehicle system dynamics 2005;43(6):485–538.

[30] Kruse H. Modellgestützte Untersuchung der Gleisdynamik und des Verhaltens von Eisenbahnschotter. Dissertation. Hannover; 2002.

[31] Huang H. Discrete element modeling of railroad ballast using imaging based aggregate morphology characterization. Dissertation. Urbana; 2010.

[32] Tutumluer E, Huang H, Hashash Y, Ghaboussi J. Discrete element modeling of railroad ballast settlement. In: AREMA Annual Conference.

[33] Tutumluer E, Huang H, Hashash Y, Ghaboussi J. Aggregate shape effects on ballast tamping and railroad track lateral stability. In: Proceedings of the AREMA Annual conference, Louisville, Kentucky.

[34] Anochie-Boateng JK, Komba JJ, Mvelase GM. Three-dimensional laser scanning technique to quantify aggregate and ballast shape properties. Construction and Building Materials 2013;43:389–98.

[35] Latham J, Munjiza A, Garcia X, Xiang J, Guises R. Three-dimensional particle shape acquisition and use of shape library for DEM and FEM/DEM simulation. Minerals Engineering 2008;21(11):797–805.

[36] Ergenzinger C, Seifried R, Eberhard P. A discrete element model predicting the strength of ballast stones. Computers and Structures 2012;108–109:3–13.

[37] Eliáš J. Simulation of railway ballast using crushable polyhedral particles. Powder Technology 2014;264:458–65.

[38] Tutumlueri E, Huang H, Hashash Y, Ghaboussi J, Emeritus. Discrete element modeling of railroad ballast settlement.

[39] Huang H, Chrismer S. Discrete element modeling of ballast settlement under trains moving at “Critical Speeds”. Construction and Building Materials 2013;38:994–1000.

[40] Bian X, Huang H, Tutumluer E, Gao Y. “Critical particle size” and ballast gradation studied by discrete element modeling. Transportation Geotechnics 2016;6:38–44.

[41] Lim, W. L., McDowell GR. Discrete element modelling of railway ballast. Granular Matter 2005;7(1):19-29.

[42] Ergenzinger C, Seifried R, Eberhard P. A discrete element model to describe failure of strong rock in uniaxial compression. Granular Matter 2011;13(4):341–64.

[43] Lobo-Guerrero S, Vallejo LE, Vesga LF. Visualization of crushing evolution in granular materials under compression using DEM. International Journal of Geomechanics 2006;6(3):195–200.

[44] Lobo-Guerrero SG, Vallejo LE. Analysis of crushing of granular material under isotropic and biaxial stress conditions. Journal of the Japanese Geotechnical Society soils and foundation 2005;45(4):79-87.

[45] Lobo-Guerrero S, Vallejo LE. Crushing a weak granular material: Experimental numerical analyses. Géotechnique 2005;55(3):245–9.

[46] Hossain Z, Indraratna B, Darve F, Thakur PK. DEM analysis of angular ballast breakage under cyclic loading. Geomechanics and Geoengineering 2007;2(3):175–81.

[47] Steiner E, Kuttelwascher C, Prager G. Druckausbreitung von belasteten Eisenbahnschwellen im Gleisschotter. ETR Austria 2012;12(1):71–5.

[48] Martin U, Wang B, Rapp S, Garrecht H, Birtel V, Lehmann F. Experimentelle und numerische Untersuchung des Bruchverhaltens von Gleisschotter. ZEVrail 2017;06+07:212–9.

[49] Martin U, Rapp S, Wang B. 11. Verkehrswissenschaftliches Fachgespräch in Stuttgart (Schottergleis – Dimensionierung und Verhalten des Schottergefüges im konventionellen Gleiskörper). EI - Der Eisenbahningenieur 2016;09(09):127–31.

[50] Lim WL. Mechanics of railway ballast behaviour. Dissertation. Nottingham; 2004.

[51] Camacho D, Le HT, Rapp S, Martin U. Light rail ballasted track geometry quality evaluation using track recording car data. In: 15th international conference on railway engineering design and operation, July 2016.